The role of the stemness factor Nanog in cell cycle regulation

Thesis

Submitted for a Doctoral Degree in Natural Sciences
(Dr. rer. nat.)

Faculty of Mathematics and Natural Sciences
Rheinische Friedrich Wilhelms Universität Bonn

Submitted by
Bernhard Münst

Bonn 2010

Prepared with the consent of the Faculty of Mathematics and Natural Sciences
Rheinische Friedrich Wilhelms Universität, Bonn.

This thesis is available online on the Hochschulschriftenserver of the ULB Bonn
http://hss.ulb.uni-bonn.de/diss_online.

Publication year: 2011

1. Reviewer: Prof. Dr. Oliver Brüstle
2. Reviewer: Prof. Dr. Hubert Schorle
Date of submission: 15/09/2010
Date of examination: 22/12/2010

Abbreviations

AFP	alpha feto-protein
AP	alkaline phosphatase
APS	ammonium persulfate
aa	amino acid
BMP	bone morphogenic protein
bp	base pair
BSA	bovine serum albumine
CDK	cyclin dependent kinase
cDNA	complementary DNA
CKI	cyclin dependent kinase inhibitor
cmc	critical micelle concentration
D-MEM	Dulbecco's Modified Eagle Medium
DMSO	dimethylsulfoxide
DNA	deoxyribonucleic acid
DTT	dithiothreitol
EB	embryoid body
EDTA	ethylenediaminetetraacetic acid
EMSA	electrophoretic mobility shift assay
EpiS	epiblast stem
ES	embryonic stem
FCS	fetal calf serum
FGF	fibroblast growth factor
g	gram
g	gravitational constant
GAPDH	glyceraldehyde 3-phosphate dehydrogenase
GSH	reduced Gluthatione
GSK3	glycogen synthase kinase 3
GSSH	oxidized Gluthatione
h	hour
HEPES	4-(2-hydroxyethyl)-1-piperazineethanesulfonic acid
HIV	human immunodeficiency virus
ICM	inner cell mass
IGF	insulin-like growth factor
iPS	induced pluripotent stem cells
ITS	Insulin / Transferrin / Selenium
JAK	Janus Kinase
kb	kilobase
kDa	kiloDalton

KPC	Kip1 ubiquitylation-promoting complex
l	liter
LB	Luria Bertani Medium
LIF	leukemia inhibitory factor
M	Mol per liter
MALDI-TOF	Matrix Assisted Laser Desorption/Ionisation - Time Of Flight
MAPK	mitogen-activated protein kinase
MEF	murine embryonic fibroblast
MEK	mitogen-activated protein kinase kinase
MES	2-(N-morpholino)ethanesulfonic acid
mg	milligram
min	minute
mL	milliliter
mM	millimolar
MWCO	molecular weight cut-off
NEAA	non-essential amino acids
ng	nanogram
Ni-NTA	Nickel-nitrilotriacetic acid
nm	nanometer
NLS	nuclear localization signal
OD	optical density
PAGE	polyacrylamid electrophoresis
PBS	phosphate buffered saline
PCR	polymerase chain reaction
PEG	polyethylene glycol
PI3K	phosphatidylinositol 3-kinase
PIPES	piperazine-N,N′-bis(2-ethanesulfonic acid)
PP1	protein phosphatase type 1
pRb	Retinoblastoma protein
PrE	primitive endoderm
PTD	protein transduction domain
Rb	Retinoblastoma
RIS	reprogramming induces senescence
RNA	ribonucleic acid
RT	room temperature *resp.* reverse transcription
s	second
SA	senescence-associated
SSEA	stage-specific embryonic antigen
SDS	sodium dodecyl sulfate
SMA	smooth muscle actin

SMAD	small mother against decapentaplegic
Stat3	signal transducer and activator of transcription 3
SV 40	simian virus 40
TAT	transactivator of transcription
TB	terrific broth
TBS	Tris buffered saline
TBS-T	Tris buffered saline supplemented with Tween
TE	trophectoderm
TEMED	tetramethylethylenediamine
TGFβ	transforming growth factor beta
Tris	tris(hydroxymethyl)aminomethane
TUJ1	neuron-specific class III beta-tubulin
UV	ultraviolet
V	volt
rpm	rounds per minute

1 Introduction 1
1.1 Embryonic Stem Cells 1
1.1.1 Embryonic development 1
1.1.2 Derivation and characteristics of ES cells 4
1.1.3 Derivatives of ES cells 5
1.2 Extrinsic signals governing pluripotency 6
1.2.1 Murine ES cells 6
1.2.1.1 LIF signaling 6
1.2.1.2 BMP signaling 7
1.2.2 Human ES cells 7
1.2.2.1 Basic FGF signaling 8
1.2.2.2 Activin A signaling 8
1.2.2.3 IGF signaling 9
1.2.3 Epiblast stem cells 9
1.3 Intrinsic stemness factors 10
1.3.1 Oct3/4 10
1.3.2 Sox2 11
1.3.3 Nanog 12
1.3.3.1 Expression and cellular activities 12
1.3.3.2 Transcriptional activities and protein interaction 12
1.3.3.3 Genetic analysis of Nanog activity 14
1.3.3.4 Analysis of stemness factors target genes 15
1.4 Cellular reprogramming 16
1.5 Cellular senescence 18
1.6 Protein transduction 18
1.7 Aim of the thesis 22

2 Materials and Methods 23
2.1 Materials 23
2.1.1 Chemicals 23
2.1.2 Equipment 23
2.1.3 Enzymes 25
2.1.4 Antibodies 26
2.1.5 Buffers, markers and medium 27
2.1.6 Bacterial strains 38
2.1.7 Cell lines 38
2.1.8 Expression vectors 39
2.1.9 Oligonucleotide primers 40

2.2 Nucleic acids 41
2.2.1 Generation of competent *E.coli* 41
2.2.2 Transformation of *E.coli* 41
2.2.3 Preparation of small amounts of DNA 41
2.2.4 Preparation of large amounts of DNA 42
2.2.5 Photometric measurement of DNA content 42
2.2.6 Cloning techniques 42
2.2.6.1 Restriction hydrolysis 42
2.2.6.2 Purification of DNA 42
2.2.6.3 Dephosporylation 43
2.2.6.4 Ligation 43
2.2.7 Polymerase chain reaction 43
2.2.8 Reverse transcriptase polymerase chain reaction 44
2.2.9 Electrophoresis in agarose gels 45
2.2.10 Retroviral infection and iPS induction 45
2.3 Proteins 46
2.3.1 Expression of recombinant fusion proteins 46
2.3.2 Imidazole gradient 46
2.3.3 Purification of recombinant fusion proteins 47
2.3.3.1 Denaturing purification 47
2.3.3.2 Native purification 47
2.3.4 Sodium dodecyl sulfate polyacrylamide gel electrophoresis 48
2.3.5 Immunoblot 49
2.3.6 Electrophoretic Mobility Shift Assay 50
2.3.7 Immunocytochemistry 51
2.4 Cell culture 52
2.4.1 General methods 52
2.4.1.1 Passaging of cells 52
2.4.1.2 Counting cells 52
2.4.1.3 Freezing and thawing cells 53
2.4.1.4 Embryoid body formation 53
2.4.2 Protein transduction 53
2.4.2.1 Oct3/4 GiP MEFs and CV1 fibroblast cells 53
2.4.2.2 MP-AF primary human dermal fibroblasts 55
2.4.2.3 Oct3/4 GiP ES cells 55
3 Results 57
3.1 Recombinant Nanog fusion proteins 57
3.1.1 Assessing purification conditions for Nanog-TAT 59

3.1.2 Denaturing purification of Nanog-TAT 61
3.1.3 An optimized purification protocol for Nanog-TAT 62
3.1.4 Assessing purification conditions for ΔNanog-TAT 66
3.1.5 Purifying ΔNanog-TAT under optimized conditions 68
3.2 Functional validation of Nanog-TAT and ΔNanog-TAT 70
3.2.1 Recombinant Nanog-TAT specifically binds to consensus sequence 70
3.2.2 Nanog-TAT as well as ΔNanog-TAT is able to translocate into mammalian cells 72
3.2.3 Direct delivery of Nanog-TAT specifically circumvents LIF dependence of murine ES cells 73
3.2.4 ΔNanog-TAT is not able to sustain pluripotency in murine ES cells 75
3.2.5 ES cells cultivated with ΔNanog-TAT show similar expression of alkaline phosphatase as control ES cells 77
3.2.6 Functional analysis of Nanog in murine somatic cells 78
3.2.7 Analysis of Nanog function in murine somatic cells on cell cycle factors 78
3.2.8 Nanog-TAT delivery results in diminished levels of $p27^{KIP1}$ expression in murine somatic cells 80
3.2.9 Nanog promotes the expression as well as the phosphorylation of Retinoblastoma protein 83
3.2.10 Analysis of Nanog function in human somatic cells 85
3.2.11 Nanog protein transduction enhances proliferation of human somatic cells 85
3.2.12 Molecular analysis of Nanog-TAT function in human somatic cells 86
3.3 The influence of Nanog on the process of reprogramming 88
3.3.1 Nanog-TAT advances reprogramming when applied 10 days *post infection* 89
3.3.2 Nanog-TAT enhances reprogramming efficiency by the factor of 3 when applied at later stages of reprogramming 91
4 Discussion 95
4.1 Expression and purification of the Nanog-TAT fusion protein and its corresponding control protein ΔNanog-TAT 95
4.2 Biological activity of Nanog-TAT and ΔNanog-TAT 97
4.3 Molecular function of Nanog-TAT in somatic cells 100
4.4 The role of Nanog in the process of reprogramming 105
4.5 Outlook 109
5 Summary 111
6 Declaration 112
7 Acknowledgment 113

8 Publications 114

9 Bibliography 115

1 Introduction

1.1 Embryonic Stem Cells

Although the derivation of embryonic stem (ES) cells was first accomplished in the mouse over 25 years ago (Evans and Kaufman, 1981; Martin, 1981) and the establishment of their human counterpart dates back over a decade (Thomson et al., 1998) ES cells have not lost their captivation and are of scientific interest more than ever, especially with regard to the very recent seminal discovery of induced pluripotent stem (iPS) cells (Takahashi and Yamanaka, 2006).

1.1.1 Embryonic development

As ES cells are generally considered a cell culture artifact it is reasonable to take a look at the embryonic development, as it appears *in vivo*. Murine embryonic development begins with the fertilization of the ovum by the spermatozoon within the oviduct. First cleavage of the zygote takes place 24 hours after fertilization; further cleavages succeed every twelve hours. As soon as the 8-cell stage is accomplished the blastomeres start compaction and become polarized (Johnson and Maro, 1985) and the compacted cells are now designated as early morula. Phenotypically this is displayed by appearance of microvilli on the apical side of the outer cells whereas inner cells remain unruffled. Outer cells will give rise to the trophectoderm (TE) and central cells will form the inner cell mass (ICM). TE will develop into extra-embryonic structures and the ICM will form the embryo proper. Further cleavages take place and fluid is accumulating within the embryo until the blastocyst stage is attained (E3.5). Thereby a cavity is formed, which separates the bigger part of the ICM from the TE. At E3.5 to E4.5 the embryo implants into the uterus and a single cell layer delaminates from the surface of the ICM facing the blastocoelic cavity and gives rise to the primitive endoderm (PrE) (Fig. 1).

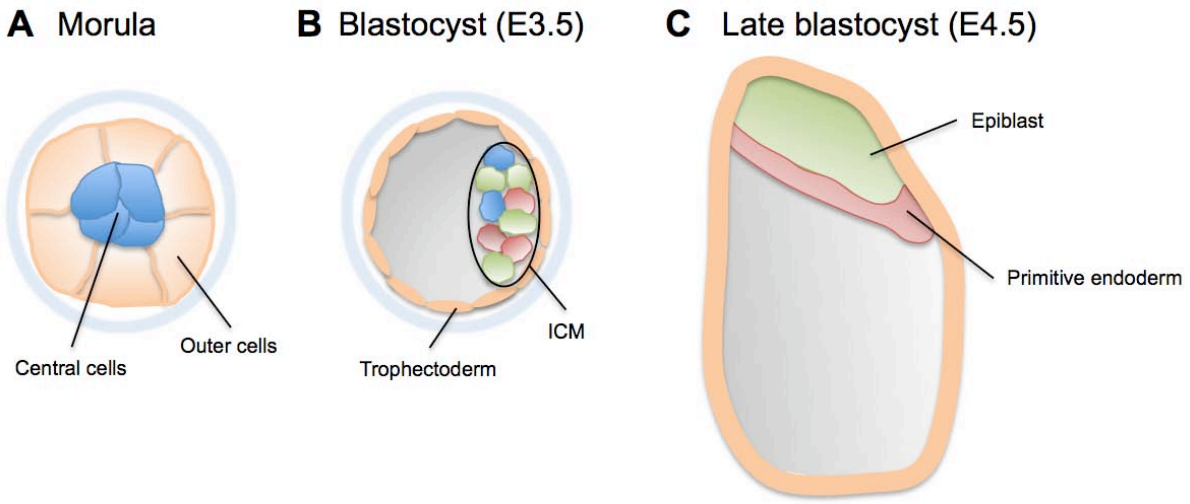

Figure 1: Embryonic development from the morula stage to the late blastocyst
(**A**) The 16-cell stage morula consists of central cells, which are surrounded by outer cells. (**B**) At E3.5 the morula has developed into the blastocyst. (**C**) Parts of the inner cell mass (ICM) will give rise to the epiblast, whereas other cells of the ICM will form the primitive endoderm in the late blastocyst at E4.5. ICM: inner cell mass (adapted from Rossant and Tam, 2009).

The PrE is involved in the formation of the extra-embryonic structures. The remaining part of the ICM forms the primitive ectoderm also called epiblast, which gives rise to the ectoderm, the mesoderm and the endoderm of the embryo. Apart from the three germ layers the epiblast is also capable to develop several extra-embryonic tissues like the umbilical cord or the yolk sac. A more detailed view of the embryonic development is shown in Figure 2. Human embryonic development slightly differs and in general it is decelerated compared to the mouse.

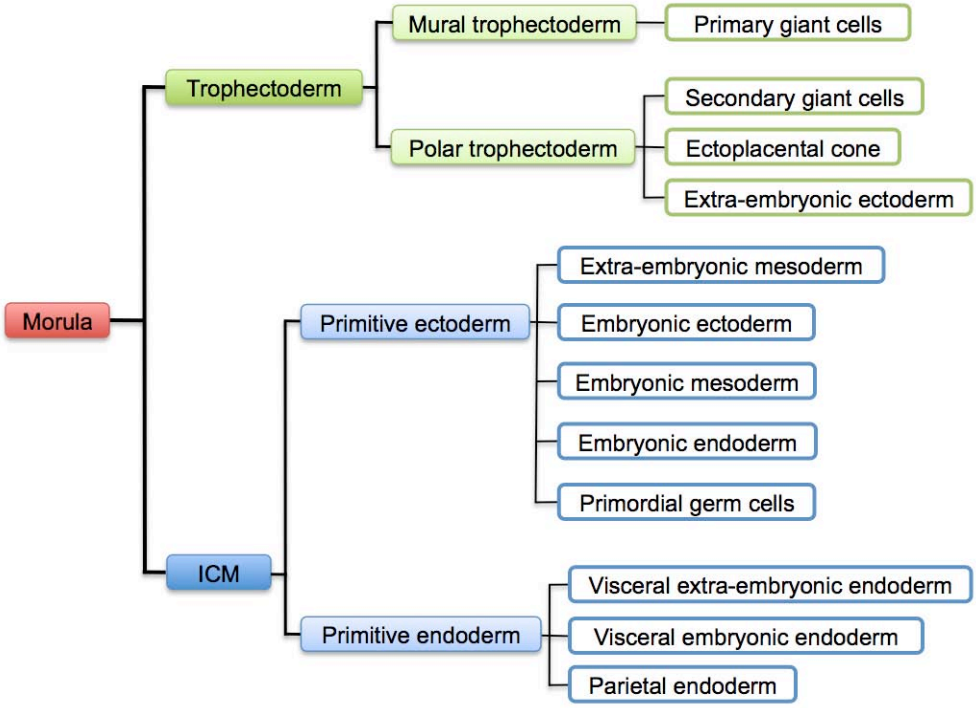

Figure 2: Schematic diagram of the embryonic development
The morula gives rise to the ICM as well as to the trophectoderm (TE). The TE will form extra-embryonic structures like giant cells, the ectoplacental cone and the extra-embryonic ectoderm. ICM splits up into primitive ectoderm comprising embryonic ectoderm, mesoderm and endoderm and primitive endoderm, which will form visceral extra-embryonic endoderm and parietal endoderm (adapted from Papaioannou and Rossant, 1977).

First lineage decisions are not only exemplified phenotypically but are made at a molecular level as well. In early blastomere and morula stage the expression of Oct3/4 is distributed evenly throughout every cell. With the formation of the blastocyst, Oct3/4 becomes down-regulated in the TE by Cdx2 through direct physical interaction and transcriptional regulation. The expression of Cdx2 in the early blastomere stage on the other hand appears to be stochastic. In the early blastocyst stage Cdx2 expression is higher in outer cells due to positive signals from the apical domain and repressive cues from the inner cells. In the long run Cdx2 expression in the blastocyst is restricted solely to the TE. The expression of Gata6 and Nanog in the early blastomere stage seems randomly distributed but is uniformly expressed when the early blastocyst stage is reached. Nanog expression in the blastocyst is restricted to the ICM by Cdx2 signaling from the TE. Grb2 signaling regulates Gata6 expression, which on one hand represses Nanog in certain cells of the ICM and on the other hand Grb2 induces the expression of Gata6 in other cells of the ICM. In the end, cells of the ICM express either Nanog or Gata6 reflecting a salt and pepper pattern (Rossant and Tam, 2009). For a schematic overview of expression patterns of Oct3/4, Cdx2 and Nanog see Figure 3.

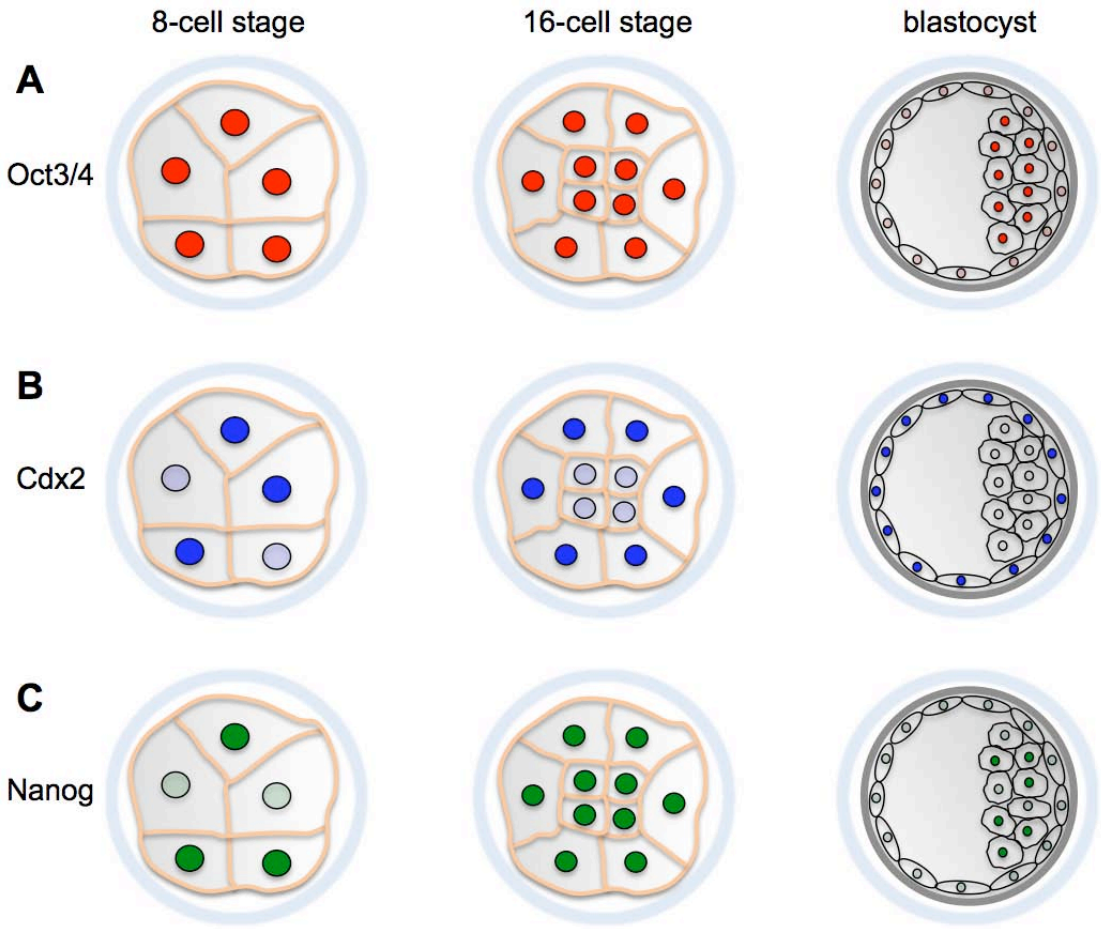

Figure 3: Expression patterns of Oct3/4, Cdx2 and Nanog during development
(**A**) Homogenous expression of Oct3/4 is observed in 8-cell and 16-cell stage embryos. In the blastocyst Oct3/4 expression is limited to the inner cell mass (ICM) as it becomes down-regulated in the trophectoderm (TE) by Cdx2. (**B**) Cdx2 expression is randomly distributed within the 8-cell stage embryo but becomes restricted to outer cells in the 16-cell stage embryo already. The expression of Cdx2 within the blastocyst is found solely in the TE. (**C**) Similar to Cdx2, Nanog expression is incidentally spread within the 8-cell stage embryo but is distributed homogeneously throughout the 16-cell stage embryo. Within the blastocyst Nanog expression displays a salt-and-pepper pattern, as it becomes down-regulated by Gata6 (adapted from Rossant and Tam, 2009).

1.1.2 Derivation and characteristics of ES cells

ES cells are derived from the ICM of the developing blastocyst at stage day 3.5, which would give rise to the epiblast *in vivo*. ES cells are characterized by two distinct properties, the first being self-renewal (Suda et al., 1987), the second feature being pluripotency. The term self-renewal is commonly referred to as the ability of cells to divide indefinitely thereby being able to maintain an undifferentiated state as well as genomic stability. This remarkable property is achieved through symmetrical cell division resulting in two identical daughter cells (Morrison and Kimble, 2006). The ES cells' ability to give rise to all three germ layers of a developing organism is termed pluripotency. In contrast to totipotent cells i.e. the zygote and early blastomeres (8 cells and less) that can give rise to every cell type of an organism, pluripotent cells are not able to form extra-embryonic tissue, e.g. trophectoderm or primitive endoderm. Besides the above-

mentioned cell types cells, which possess multi- or unipotency, such as hematopoietic stem cells or hepatocytes, exist as well. Multipotent cells are able to generate multiple cell types of a certain lineage whereas unipotent cells are restricted to form one single cell type only.

Pluripotency can be analyzed *in vitro* by applying the embryoid body (EB) differentiation paradigm. Upon withdrawal of the cytokine Leukemia inhibitory factor (LIF), murine ES cells start to differentiate spontaneously, resulting in three-dimensional aggregates designated as EBs. EBs recapitulate various aspects of development during early mammalian embryogenesis and finally give rise to cells of all three germ layers, assumed the initially used cells are pluripotent. *In vivo* pluripotency of mouse ES cells can be assessed through blastocyst injection analysis. Cells get transferred into a blastocyst via microinjection and during development of the blastocyst pluripotent cells will contribute to a wide variety of tissues. If these cells are able to form tissue of the germ line their genetic heritage can be passed on to the next generation (Bradley et al., 1984). The gold standard for analyzing pluripotency though is the tetraploid complementation assay (Nagy et al., 1990). Cells to be tested for pluripotency, get transferred into a tetraploid blastocyst and only pluripotent cells will contribute to the developing organism, as tetraploid cells are only capable of forming extra-embryonic tissue.

ES cells can be well characterized *in vivo* and *in vitro* through the expression of a wide variety of pluripotency markers such as the cell surface marker Alkaline Phosphatase (AP), the glycolipid Stage-specific embryonic antigens (SSEA) as well as the transcription factors Oct3/4, Nanog and Sox2. Moreover, ES cells, in contrast to most somatic cells, possess telomerase activity.

1.1.3 Derivatives of ES cells

Due to the capability of ES cells to give rise to cells of all three germ layers (Evans and Kaufman, 1981; Martin, 1981; Thomson et al., 1998) these cells hold great potential and could be beneficial for the treatment of several degenerative diseases where cell replacement therapy can be applied. Researchers were able to derive various cell types from murine ES cells such as cardiac muscle cells (Klug et al., 1996; Wobus et al., 2002), insulin-producing cells (Soria, 2001), and hematopoietic cells (Wiles and Keller, 1991) as well as cells of the nervous system (Brustle et al., 1999; Okabe et al., 1996). Differentiation paradigms observed in murine ES cells could be transferred to their human counterparts as well, as the derivation of multiple somatic cell types from the heart (Kehat et al., 2003), the liver (Lavon et al., 2004), the blood (Kaufman et al., 2001) and the nervous system (Reubinoff et al., 2001; Zhang et al., 2001) was feasible. Promising transplantation experiments on rats conducted by Keirstead and colleagues (Keirstead et al., 2005) may lead to the first FDA approved phase I clinical trial in the near future with human ES cell derived oligodendrocytes by the Geron Corporation.

1.2 Extrinsic signals governing pluripotency

In order to understand the state of pluripotency and to develop differentiation paradigms a profound knowledge of the signaling networks governing pluripotency is essential. The following chapter will provide an overview on signaling pathways found in murine as well as human ES cells. Finally a short paragraph will deal with a newly derived embryonic cell line established from the epiblast.

1.2.1 Murine ES cells

Pluripotency of ES cells under cell culture conditions is maintained through extrinsic as well as intrinsic key molecules. For the cultivation of murine ES cells the extrinsic cytokine LIF plays an essential role (Smith et al., 1988; Williams et al., 1988) as well as a second extrinsic factor, Bone morphogenetic protein (BMP), when cultivating cells under serum-free conditions (Ying et al., 2003a).

1.2.1.1 LIF signaling

In the presence of fetal calf serum (FCS) LIF is able to maintain pluripotency of ES cells through binding to the LIF receptor (LIFR) thereby mediating heterodimerization of the LIFR with the transmembrane protein glycoprotein-130 (gp130). The LIF signaling cascade subsequently progresses through activation of the signal transducer and activator of transcription-3 (Stat3) via phosphorylation through the Janus tyrosine kinase (JAK). Phosphorylated Stat3 molecules then form dimers and translocate into the nucleus where transcription of target genes is initiated through binding to the DNA (Fig. 4). The overexpression of Stat3 is sufficient and necessary to maintain a pluripotent phenotype in murine ES cells in the absence of LIF (Matsuda et al., 1999) whereas the inhibition of Stat3 induces differentiation (Niwa et al., 1998). Surprisingly mouse embryos lacking Stat3 are able to develop into a phase beyond ES cell derivation *in vivo* indicating that different pathways may be involved in sustaining pluripotency. A second possibility known to circumvent LIF dependence of murine ES cells is the overexpression of Nanog (Mitsui et al., 2003) but a connection between the overexpression of Stat3 and Nanog was not drawn until very recently. Niwa and colleagues described that LIF is actually regulating two different signaling pathways both responsible for the maintenance of pluripotency. On the one hand LIF is activating Klf4 via the Jak-Stat pathway, which in consequence leads to the expression of Sox2 but not Nanog. On the other hand LIF interacts with the PI3 kinase-Akt signaling cascade thereby activating Tbx3. Tbx3 subsequently induces the expression of Nanog, which in concert with Sox2 regulates Oct3/4 (Niwa et al., 2009). This triad

of key transcription factors regulates itself and other genes associated with stemness (Boyer et al., 2005; Loh et al., 2006).

1.2.1.2 BMP signaling

Ying and colleagues were the first to address the topic of culturing murine ES cells under more defined conditions than cultivation in the presence of inchoate FCS (Ying et al., 2003a). Under serum-free conditions, i.e. in N2B27 medium (Ying et al., 2003b) LIF is not capable to maintain murine ES cells in a pluripotent state, as the cells tend to take on a neuronal fate. Only when supplemented with BMP, ES cells under before mentioned conditions can be propagated in a pluripotent state, as BMP is able to suppress the neuronal differentiation through SMAD mediated expression of Inhibitor of differentiation (Id) genes. In particular BMP triggers the dimerization of two complexes of BMP receptors type I (BMPRI) and II (BMPRII). This complex of BMPRI and BMPRII phosphorylates Smad1, 5 and 8. These Smads subsequently bind co-Smad 4, and this heteromeric complex is translocated into the nucleus to drive gene expression by binding to promoter regions of BMP target genes, in this case Id genes (Fig. 4). In ES cells cultivated in N2B27 medium without LIF and BMP the sole overexpression of Nanog enables the cells to still express Id1 and Id3 indicating that Nanog influences the expression levels of Id genes (Ying et al., 2003a). Another proposed role for BMP is the inhibition of p38, which would otherwise inhibit the expression of genes sustaining with pluripotency (Qi et al., 2004).

The paradigm of dependence of murine ES cells on extrinsic stemness signals such as the above-mentioned LIF and BMP was challenged though (Ying et al., 2008). By the use of small molecules inhibiting differentiation cues initiated by Mitogen-activated protein kinase (MAPK) and Glycogen synthase kinase 3 (GSK-3) signaling, it is possible to maintain pluripotency in murine ES cells in the absence of LIF and BMP. The derivation and propagation of ES cells genetically devoid of Stat3 under these de-differentiating conditions is feasible, indicating autonomy from extrinsic LIF signaling.

1.2.2 Human ES cells

Although human ES cells and their murine equivalents share various properties, the mechanism underlying pluripotency surprisingly differs. Human ES cells as we know them do not respond to the cultivation with LIF in the absence of mouse embryonic fibroblasts (MEFs) (Thomson et al., 1998) although they express the corresponding receptor and the STAT3 signaling cascade is functional (Daheron et al., 2004; Humphrey et al., 2004). Instead human ES cells depend on basic fibroblast growth factor (bFGF) (Amit et al., 2000), Activin A - a member of the transforming

growth factor β (TGF-β) family (Beattie et al., 2005; James et al., 2005) as well as insulin-like growth factor (IGF) (Wang et al., 2007) enabling them to maintain their undifferentiated state.

1.2.2.1 Basic FGF signaling

Initially Amit and colleagues assigned a distinct role in human pluripotency to bFGF, as it is needed for prolonged undifferentiated proliferation of human ES cells (Amit et al., 2000). bFGF signaling in general is considered mainly to drive proliferation; the exact mechanism of how bFGF signaling sustains pluripotency remains poorly understood though (Fig. 4). When cultivated in medium supplemented with serum replacement and on Matrigel, a solubilized membrane preparation, which contains extracellular matrix proteins among other constituent parts, high dosage of bFGF seems to be sufficient to maintain pluripotency in human ES cells. However, bFGF is not able to sustain stemness in human ES cells when cultivated in conditioned medium without Matrigel or in the absence of Activin (Vallier et al., 2005). An additional role proposed for bFGF is the establishment of a niche in human ES cell culture. Spontaneously differentiating human ES cells give rise to fibroblast-like cells, which secrete supporting proteins such as IGF upon bFGF stimuli. IGF then triggers PI3 kinase signaling in human ES cells inhibiting differentiation cues (Bendall et al., 2007). Furthermore it has been shown that bFGF stimulates MEFs to release TGFβ, which additionally can support self-renewal of human ES cells (Greber et al., 2007).

1.2.2.2 Activin A signaling

Another key molecule to exert influence on the pluripotent status of human ES cells is Activin A. Together with BMPs, inhibins and Nodal it belongs to the TGF-β superfamily. BMP is needed to sustain pluripotency in murine ES cells (Ying et al., 2003a) but it has a contrary effect when applied to human ES cells, i.e. BMP leads to differentiation into trophectoderm (Xu et al., 2002). Activin A instead can maintain a pluripotent phenotype in human ES cells through SMAD2/3 signaling whereas SMAD1/5 initiated by BMP only is activated upon early differentiation (James et al., 2005) (Fig. 4). Besides, Activin A is also expressed and secreted by MEFs, thus pluripotency of human ES cells cultivated on feeder-layers is additionally maintained (Beattie et al., 2005). Vallier and colleagues could show an interaction between Activin A and bFGF signaling sustaining pluripotency (Vallier et al., 2005). Very recently it was shown that the transcription factor NANOG is a direct target of TGF-β/Activin A-mediated SMAD signaling in human ES cells (Xu et al., 2008), linking extrinsic stemness signals to intrinsic factors involved in pluripotency. SMAD mediated activation of NANOG consequently leads to the inhibition of BMP-induced differentiation towards endoderm (Vallier et al., 2009).

1.2.2.3 IGF signaling

IGF receptors (IGFR) are present on the cell surface of human ES cells and are susceptible to insulin. Insulin signaling is mediated via the PI3 kinase-Akt pathway resulting either in inhibition of GSK-3 signaling or activation of MAPK signaling (Fig. 4), both involved in sustaining pluripotency. Insulin is a common and very potent supplement in cell culture promoting proliferation and cell survival but a distinct role in self-renewal of human ES cells was only discovered recently. Blocking of IFGR results in reduced self-renewal and promotes differentiation of human ES cells (Wang et al., 2007).

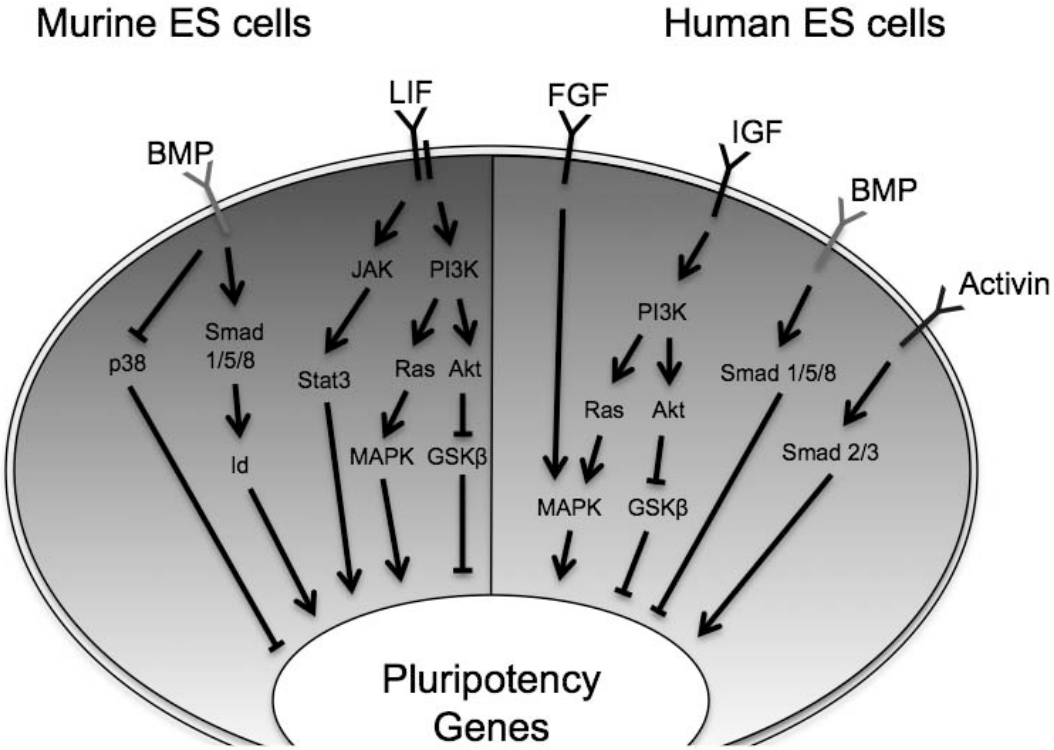

Figure 4: Signaling pathways influencing pluripotency of murine and human ES cells
Extrinsic factors operate molecular switches inside ES cells. Murine ES cells rely on LIF- and BMP signaling whereas their human counterparts depend on FGF, Activin and IGF. In contrast to murine ES cells the application of BMP leads towards differentiation in human ES cells (adapted from Ptaszek and Cowan, 2009).

1.2.3 Epiblast stem cells

The long sustained believe that the diversity of murine and human ES cells originated from species differences, was challenged by the discovery of epiblast stem (EpiS) cells. Two independent work groups accomplished the establishment of stem cells derived from the post-implantation epiblast of the mouse and the rat (Brons et al., 2007; Tesar et al., 2007). These

newly generated stem cells mirror properties of human ES cells, i.e. the morphology on the one hand and on the other hand the dependence on Activin signaling to maintain pluripotency. Additionally EpiS cells express stemness markers like SSEA-1, Nanog, Oct3/4 and Sox2 but tend to have early germ layer markers as well as epiblast markers up-regulated. By contrast these stem cells show weaker or no expression for genes characteristic for the ICM like Pecam1, or Tbx3. With this stem cell population at hand, the question is now whether the differences between murine and human ES cells might not originate from species disparity but rather both types of ES cells might represent a different developmental stage dependent of the time and mode of derivation. Interestingly, Hayashi and colleagues could show that ES cells are not a group of uniform cells, since they appear to be floating in a metastable state and shift between ES- and epiblast-like states. A variety of factors can shift this equilibrium in either way (Hayashi et al., 2008).

1.3 Intrinsic stemness factors

While describing the extrinsic factors needed to sustain pluripotency in both murine and human ES cells, intrinsic factors regulating stemness already have been mentioned. A triad of key regulators, i.e. Oct3/4, Sox2 and Nanog, mainly governs the grid of stemness.

1.3.1 Oct3/4

The Oct3/4 protein was discovered almost 20 years ago and is encoded by the Pou5f1 gene. It belongs to the POU transcription factor family (Okamoto et al., 1990; Rosner et al., 1990; Scholer et al., 1990) and is expressed in toti- and pluripotent cells passing through early embryonic development (Nichols et al., 1998; Palmieri et al., 1994; Rosner et al., 1990; Scholer et al., 1990; Yeom et al., 1996). Oct3/4 expression is restricted to the ICM as it is down-regulated in cells of the TE by Cdx2 (Niwa et al., 2005). In the artificial situation of ES cell culture this expression pattern seems to be sustained. The induction of differentiation cues leads to the down-regulation of Oct3/4. During gastrulation the expression of Oct3/4 vanishes and can only be detected in primordial germ (PG) cells (Pesce and Scholer, 2000). Apart from ES cells, Oct3/4 is expressed in embryonic carcinoma (EC) cell lines as well as in germ cell lines. The restriction of Oct3/4 to toti- and pluripotent cells assigns an important role regarding stemness to this transcription factor. Blastocysts deficient for Oct3/4 seem to develop normally but their ICM fails to give rise to ES cells (Nichols et al., 1998). Conditional knockout of Oct3/4 in PG cells leads to apoptosis (Kehler et al., 2004) and the RNAi mediated down-regulation of Oct3/4 in ES cells leads to TE differentiation (Hay et al., 2004; Hough et al., 2006). The precise level of Oct3/4 expression is essential, as ES cells exhibiting a 50% down-regulation already tend towards

differentiation into TE, whereas a 2-fold increase of Oct3/4 expression shifts ES cells towards differentiation into endo- and mesoderm (Niwa et al., 2000). Upon LIF withdrawal murine ES cells shut down Oct3/4 expression within days and the cells start to differentiate. This process cannot be reverted via inducible expression of Oct3/4, which demonstrates that Oct3/4 can only work in concert with other factors regulated by the LIF pathway.

1.3.2 Sox2

The transcription factor Sox2 belongs to the High Mobility Group (HMG) DNA-binding proteins. Depending on the homology regarding their HMG domains, proteins are combined into different groups. Within the group of SoxB1 (Uchikawa et al., 1999), which comprises Sox1, Sox2 and Sox3, the homology between the HMG reaches up to 90% (Pevny and Lovell-Badge, 1997; Wegner, 1999). The expression of Sox2 is detectable in the ICM of murine blastocysts and it is maintained until the epiblast stage is reached (Avilion et al., 2003). In contrast to Oct3/4, which seems to play an important role only during the early stages of embryonic development, Sox2 is thought to be involved in neural development (Avilion et al., 2003; Ferri et al., 2004; Graham et al., 2003; Uwanogho et al., 1995; Wood and Episkopou, 1999; Zappone et al., 2000) as well as it regulates lens development in concert with Pax6 (Kamachi et al., 2001). Analysis of Sox2 in early embryonic development suggests a tremendous influence regarding stemness, as Sox2 deletion mutants exhibit lethality. Embryos deprived of Sox2 are not able to develop into epiblast stage. Murine ES cells, which bear a Sox2 knockout, lose the potential to proliferate and cease to self-renew leading the cells towards differentiation into TE (Avilion et al., 2003). As for Oct3/4 a distinct level of expression determines proper function of the transcription factor, as a two-fold overexpression of Sox2 shifts ES cells into differentiation towards neuroectoderm, mesoderm and TE (Kopp et al., 2008). Multiple studies could confirm a direct interaction between Sox2 and Oct3/4 when it comes to binding mutual promoter regions thereby activating the expression of other stemness factors. Among these are Nanog, Fgf4, Utf1 and Fbx15 (Kuroda et al., 2005; Nishimoto et al., 1999; Rodda et al., 2005; Tokuzawa et al., 2003; Yuan et al., 1995) but the Sox2-Oct3/4 dimer also regulates its own expression (Chew et al., 2005; Okumura-Nakanishi et al., 2005; Tomioka et al., 2002). Experiments with Sox2-null mutant cells showed that the overexpression of Oct3/4 could compensate for the loss of Sox2. In addition this study revealed the dispensability of Sox2 for activation of Oct/Sox enhancer elements, indicating that other Sox proteins can probably replace the function of Sox2 (Masui et al., 2007). In conclusion, the authors suggest that Sox2 mainly sustains the expression of Oct3/4.

1.3.3 Nanog

1.3.3.1 Expression and cellular activities

A third key player of pluripotency could be identified through the functional analysis of the interaction between extrinsic and intrinsic stemness signals of ES cells. When cultivating murine ES cells LIF usually is indispensable (Smith et al., 1988; Williams et al., 1988), and several genetic studies have shown that this extrinsic signal of self-renewal is mediated intracellularly by Stat3 (Boeuf et al., 1997). Overexpression of Nanog, named after the celtic expression for 'land of the ever young', enables murine ES cells to abolish LIF-dependence (Chambers et al., 2003; Mitsui et al., 2003). The expression of Nanog can be detected in the ICM of murine blastocysts and the epiblast *in vivo* as well as *in vitro* in ES cells. With the onset of differentiation, Nanog is generally down-regulated. It is still expressed in germ cells as well as in tumorous cell lines though (Chambers et al., 2003; Hart et al., 2004). The expression of Nanog is not homogeneously distributed between ES cells. It mirrors a mosaic-like pattern in which Nanog-high populations as well as Nanog-low but Gata6-positive populations can be detected within the culture dish. This particularly depicts the situation observed in the ICM of the blastocyst at stage E3.5, where the expression of Nanog and Gata6 resembles a salt-and-pepper pattern (Singh et al., 2007). The Nanog protein encloses a homeodomain, exhibiting a structure, which it shares with members of the Nk-2 gene family in terms of the position of the homeodomain although more than half of the amino acids differ (Mitsui et al., 2003). While there is homology between its orthologs within different species, the Nanog homeoprotein seems to be unique (Pan and Thomson, 2007).

1.3.3.2 Transcriptional activities and protein interaction

Murine Nanog is a three-domain protein composed of 305 aa including the N-terminal part of the protein (aa 1–aa 95), the homeodomain which spans aa 96 to aa 155, and the C-terminal domain (aa 156– aa 305) (Chambers et al., 2003; Mitsui et al., 2003). To date, there is only few data on the transcriptional activity of Nanog. Luciferase reporter assays in HEK293, NIH3T3, and P19 as well as mouse ES cells could detect transcriptional activity in the N-terminal as well as the C-terminal part, albeit the C-terminal domain being about 7 times more active (Pan and Pei, 2003). In more detail, the C-terminal domain contains two distinct parts exhibiting strong activation capability. These domains were named CD1 (aa 150–aa 197) and CD2 (aa 248–aa 305). A repetitive sequence in which every fifth residue represents a tryptophan, therefore called tryptophan repeat (WR), was assigned to lay between aa 198 and aa 247, thus encircled by CD1 and CD2 (Pan and Pei, 2005). Figure 5 schematically illustrates the structure of the murine Nanog transcription factor.

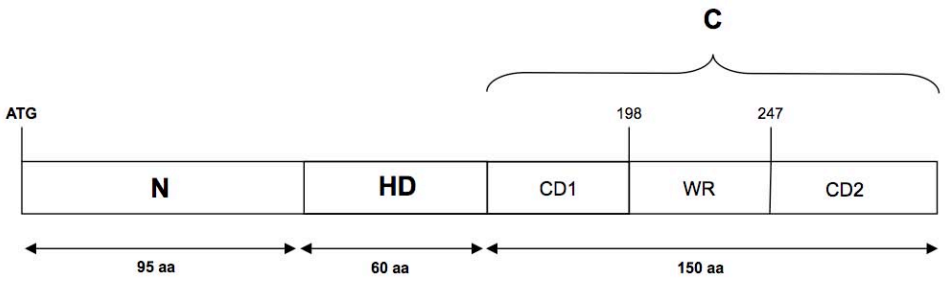

Figure 5: Schematic overview of the murine stemness factor Nanog
The Nanog transcription factor is a three-domain protein consisting of an N-terminal part, a homeodomain and a C-terminal domain. The C-terminal part itself is composed of the three subdomains CD1, CD2 and a tryptophan-rich repeat termed WR. N: N-terminal domain; HD: homeodomain; C: C-terminal domain; CD: C-terminal subdomain exhibiting strong activation capability; WR: tryptophan repeat; aa: amino acid.

Recent research by Wang et al. shed light on potential co-activators or Nanog-protein interactors. Various binding partners of Nanog, such as Oct4, Nac1, Rif1, Dax1, and Zfp281, could be identified by co-immunoprecipitation (Wang et al., 2006). Torres and Watt provided first indications of a presumable homodimerization of Nanog as they could observe Nanog–Nanog interaction via GST pull-down experiments. Moreover, they reported that Nanog is able to bind NFkB, which leads to the inhibition of pro-differentiation activities and consequently maintains pluripotency (Torres and Watt, 2008). Lately the exact position of the dimerization site within the Nanog protein was identified. The results stand to reason that Nanog self-association takes place within the WR (Mullin et al., 2008). This finding was confirmed by another study (Wang et al., 2008b) where the authors performed size chromatography of ES cell nuclear extracts that revealed putative Nanog dimers. The use of various truncated Nanog versions for co-immunoprecipitation allocated the position of the dimerization domain to the WR. A mutant Nanog protein, incapable to selfdimerize, did not confer LIF-independent selfrenewal to murine ES cells as judged by colony formation assay. In contrast the forced expression of a functional but artificial Nanog dimer was able to keep the ES cells self-renewing independent of LIF, whereas overexpression of the mutant non-dimerizing Nanog protein did result in differentiation. Upon cultivation with LIF, the Nanog dimer as well as the monomeric variant did increase the percentage of undifferentiated colonies though, indicating enhanced self-renewal. In order to be able to interact with other stemness proteins, as shown for Zfp281, Sall4, Dax1, and Zfp198, Nanog should be available in its dimeric form as judged by co-immunoprecipitation experiments (Wang et al., 2008b). Beyond that, Nanog has been reported to physically interact with Smad1 thereby blocking BMP-induced mesoderm differentiation of murine ES cells (Suzuki et al., 2006). In addition Nanog operates as a direct activator of transcription for the Rex-1 promoter in conjunction with Sox2 (Shi et al., 2006). Another factor purified within a protein complex together with Nanog was Sall4. Within this complex Nanog positively controls its expression as well as that of Sall4 (Wu et al., 2006). In order to limit steady-state levels of Nanog

mRNA, protein and promoter activity within murine ES cells Tcf3 activity is needed (Pereira et al., 2006). Furthermore, Nanog in concert with Oct3/4 is able to recruit a complex called NODE (Nanog and Oct4 associated deacetylase). Through this interaction Nanog and Oct3/4 are able to mediate repressive influence to the chromatin remodeling machinery, as NODE possesses histone deacetylase (HDAC) activity (Liang et al., 2008). In human ES cells NANOG promoter activity seems to be positively regulated via SMAD2/3 mediated signaling, which is governed by TGFβ. Interestingly the overexpression of NANOG can bypass the requirement for TGFβ/Activin and bFGF (Xu et al., 2008) under defined conditions.

1.3.3.3 Genetic analysis of Nanog activity

As mentioned before, the overexpression of Nanog empowers murine ES cells to self renew in the absence of the cytokine LIF. The ability of two known reagents to induce differentiation, i.e. retinoic acid and 3-methoxybenzamide, is reduced in Nanog-overexpressing cells. Differentiation cues mediated during EB formation are hampered as well in those cells. Restoration of wild-type expression levels of Nanog lead to full differentiation potential in those cells, which was analyzed by blastocyst injection (Chambers et al., 2003). Since different signaling pathways are active in murine and human ES cells only few data is indicating that the function of Nanog could be conserved (Daheron et al., 2004). As the enhanced expression of NANOG in human ES cells enables them to feeder-free growth in unconditioned medium, an important role is assigned to NANOG in the human system as well (Darr et al., 2006). The influence of enhanced expression of Nanog in non-ES cells is analyzed only insufficiently. Cell fusion experiments as well as the iPS cell generation assign Nanog a role in the induction of pluripotency in somatic cells though. Increased expression of Nanog is able to promote transfer of pluripotency to the somatic cell genome in the cell fusion paradigm (Silva et al., 2006). Moreover Nanog seems to influence the process of reprogramming of human somatic cells (Ebert et al., 2009; Liao et al., 2008; Yu et al., 2007) although Nanog is expendable and is likely to have only a promoting effect. A potential role of Nanog in cellular reprogramming might be disclosed by experiments of ectopic Nanog expression in stem cells as well as in somatic cells. Studies by Zhang and colleagues indicated a possible role of NANOG in cell cycle regulation, as the authors observed that NANOG is able to influence S-phase entry in human ES cells by transcriptional regulation of CDK6 and CDC25A, two prominent cell cycle mediators (Zhang et al., 2009). Ablation of Nanog leads to decelerated cell growth of murine ES cells, supporting the idea of Nanog influencing the cell cycle (Mitsui et al., 2003). Ectopic expression of Nanog in NIH 3T3 cells leads to increased proliferation by promoting the entry into S phase of the cell cycle (Zhang et al., 2005). Additionally Piestun et al. observed an increased growth rate in NIH 3T3 cells overexpressing Nanog. Furthermore, the ectopic expression of Nanog resulted in a

transformed phenotype as judged by cell foci formation (Piestun et al., 2006). Loss-of-function studies revealed additional insights into the role of Nanog. Ablation of Nanog leads to the loss of pluripotency accompanied by an induction of extraembryonic marker gene expression, namely Gata6 (Mitsui et al., 2003) as well as an up-regulation of CDX2, a trophectodermal marker (Hyslop et al., 2005). The down-regulation of Nanog via RNAi induces the expression of markers for mesoderm, ectoderm and neural crest cells (Ivanova et al., 2006). While Nanog, Oct3/4 and Sox2 share a high percentage in their target genes, Nanog appears to fulfill a distinct function within the stem cell machinery. As stated before Nanog exhibits a heterogeneous expression pattern in the morula during development (Dietrich and Hiiragi, 2007). The same expression pattern is found in ES cells. Murine ES cells expressing high levels of Nanog also express other pluripotency markers such as Oct4, whereas Nanog-low cells also exhibit marker expression for primitive endoderm (Singh et al., 2007). The fluctuative expression pattern of Nanog in ES cells may indicate varying subsets of the pluripotency state. A clue to the distinct role of Nanog in the stem cell machinery was reported by Chambers et al., who could show that Nanog-null ES cells still possess the ability to self renew, although these cells are more likely to be prone to differentiation. After aggregation of $Nanog^{-/-}$ cells with wild-type morulae, Nanog-deficient cells are still able to give rise to post-natal chimeras. The developmental potential of Nanog-null ES cells was further assessed as the authors analyzed the persistence of Nanog-null cells during PG cell development. Nanog-deficient cells could be detected in the soma of the genital ridge until stage E11.5 of murine embryogenesis. Therefore, Nanog seems to be required for PG development beyond E11.5 (Chambers et al., 2007). In conclusion, these data indicates that Nanog is dispensable for the maintenance of pluripotency but does play a distinct role in the establishment and construction of the ICM as well as germ cell development. While Oct3/4 and Sox2 are needed to mediate stemness, Nanog seems to be expendable for the housekeeping machinery of pluripotency.

1.3.3.4 Analysis of stemness factors target genes

Applying genome-wide location analysis, a multitude of target genes for OCT3/4, SOX2 and NANOG could be identified in the human genome (Boyer et al., 2005). These three transcription factors co-occupy a substantial amount of target genes. In an autoregulatory manner the core transcription factors regulate their own expression. A feedforward mechanism additionally initiates events corresponding to the maintenance of stemness, like proliferation, activation of transcription factors and chromatin modifiers as well as stemness signaling. Furthermore, factors involved in the process of differentiation get down-regulated, thereby inhibiting ES cells to adopt an ectodermal, mesodermal or endodermal fate. A similar interplay and share of target genes of Oct3/4 and Nanog could be observed in murine ES cells. A multitude of pathways

governing pluripotency via REST, self-renewal like in the case of nMyc, genome surveillance as for Trp53, as well as cell fate determination seem to be controlled by Nanog and Oct3/4 (Loh et al., 2006). Additionally the polycomb group (PcG) proteins could be identified as transcriptional repressors in murine ES cells (Boyer et al., 2006).

For a schematic overview on the influence of changes in Oct3/4, Sox2 and Nanog expression levels on cellular fate, see Figure 6.

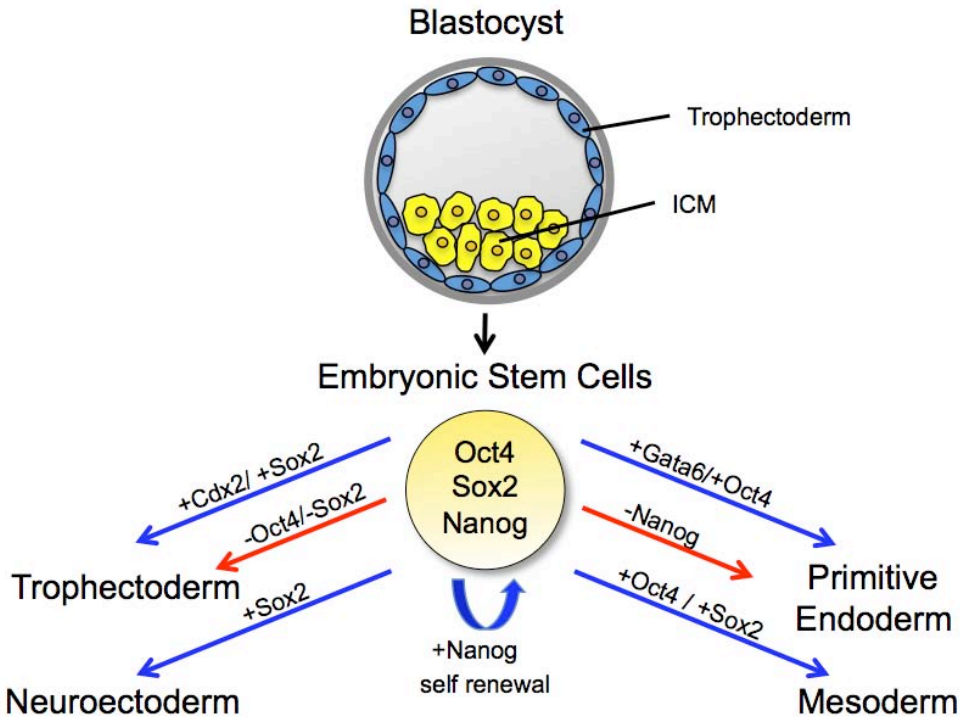

Figure 6: Oct3/4, Sox2 and Nanog intrinsically govern embryonic stem (ES) cell properties
ES cells are derived from the inner cell mass (ICM) of the blastocyst. The triad of stemness factors, namely Oct3/4, Sox2 and Nanog, controls pluripotency within ES cells. An alteration of expression levels of these transcription factors leads to differentiation (loss-of-function indicated by red arrows, gain-of-function indicated by blue arrows) towards specific lineages (adapted from Bosnali et al., 2009).

1.4 Cellular reprogramming

For a long time scientists from all around the globe had the vision of turning back the wheels of time cell biologically spoken. The experiments performed by John Gurdon in 1962 (Gurdon, 1962) firstly indicated the feasibility to reprogram and smoothened the way for upcoming nuclear transfer experiments, which led to the well-known sheep Dolly in 1997 (Wilmut et al., 1997). Since then, the technique of somatic cell nuclear transfer (SCNT) was successfully adapted to many different species, including mice (Wakayama et al., 1998) as well as calves (Kato et al., 1998). Another paradigm applied in order to reprogram is cell fusion. ES cells, when fused to somatic cells are able to revert the cellular memory thereof albeit resulting in tetraploid

hybrid cells (Tada et al., 2001). Additionally Silva and colleagues could show that an elevated level of Nanog turns out to be beneficial for the reprogramming process of cell fusion (Silva et al., 2006). The two above-mentioned techniques to reprogram cells harbor certain moral and therapeutic regards though. The groundbreaking experiment by Takahashi and Yamanaka in 2006 opened up a new way to reprogram cells thereby overcoming concerns associated with SCNT and cell fusion. Through the retroviral introduction of 4 transcription factors, namely Oct3/4, Sox2, Klf4 and c-myc into murine fibroblasts the researchers were able to induce a pluripotent state in somatic cells (Takahashi and Yamanaka, 2006). Those cells were termed iPS cells. Since then it was not only possible to reprogram various cells with fewer factors (Huangfu et al., 2008; Kim et al., 2009b; Kim et al., 2008; Nakagawa et al., 2008) but the technique could also be applied to human cells (Takahashi et al., 2007; Yu et al., 2007). Interestingly Thomson and colleagues could induce pluripotency in human cells with a slightly different combination of transcriptions factors than Takahashi and Yamanaka. They made use of Oct3/4, Sox2, Nanog and Lin-28 (Yu et al., 2007). Up to now, many laboratories successfully reprogrammed cells with this combination of factors (Ebert et al., 2009; Liao et al., 2008). It seems to be of great importance regarding the efficiency of cellular reprogramming, which type of cell is actually used for this purpose (Eminli et al., 2009). The more differentiated a cell is, the harder this cell is to revert into a pluripotent state. As the retroviral transduction leads to an altered host genome, researchers are still eager to find a way to circumvent this obstacle. The use of non-integrating genetic techniques to reprogram cells (Kaji et al., 2009; Soldner et al., 2009; Stadtfeld et al., 2008b; Woltjen et al., 2009; Yu et al., 2009) was a first step towards iPS cells, which could eventually be of use in cell replacement therapies one day. Another step towards safe iPS cells was made by the application of small molecules (Lyssiotis et al., 2009; Shi et al., 2008) on the one hand or recombinant proteins (Kim et al., 2009a; Zhou et al., 2009) on the other hand to partially or even completely replace virally transduced reprogramming factors. In a very recent publication Ichida and colleagues could identify a small compound, i.e. a TGFβ inhibitor named RepSox, able to replace Sox2 and c-myc during the reprogramming process of murine fibroblasts. The TGFβ inhibitor initiates expression of endogenous Nanog when applied 11 days post viral transduction with Oct3/4, Klf4 and c-myc (Ichida et al., 2009). Multiple publications could show that manipulating the cell cycle via down-regulation of key molecules like the tumor suppressor p53 (Hong et al., 2009; Kawamura et al., 2009; Marion et al., 2009) significantly enhances reprogramming efficiency, although likely resulting in chromosomal aberrations of the target cells. Cultivation of cells under hypoxic conditions, which basically also affects proliferation of cells showed similar results (Yoshida et al., 2009). Nevertheless, the process of cellular reprogramming is still inefficient and not well understood at a molecular level.

1.5 Cellular senescence

Leonard Hayflick, who could show that somatic cells can only be cultivated for a distinct period of time before they stop proliferating, initially observed cellular senescence. Although the cells did not divide anymore they were still viable for a prolonged period of time (Hayflick, 1965). This phenomenon was termed Hayflicks' limit and is also known as replicative senescence. Due to the fact that many carcinogenic cell lines are able to proliferate indefinitely, senescence can be regarded as a tumor-suppressor mechanism on the one hand. On the other hand, senescence may be seen as an artificial form of ageing *in vitro* as the ability for tissue regeneration declines over time *in vivo*. Senescence is characterized by various indications. The most prominent hallmark is the inability of senescent cells to proceed through the cell cycle, i.e. growth arrest. These cells exhibit DNA content typical for G1 phase while still displaying an active metabolism (Di Leonardo et al., 1994; Herbig et al., 2004; Ogryzko et al., 1996; Serrano et al., 1997). Another feature of senescent cells is a resistance towards some apoptotic cues. Human fibroblasts for example can withstand apoptotic signals caused by removal of growth factors and oxidative stress but will undergo apoptosis mediated by the Fas death receptor (Chen et al., 2000; Tepper et al., 2000). Moreover senescent cells exhibit tremendous changes in gene expression (Shelton et al., 1999; Trougakos et al., 2006; Yoon et al., 2004). A marker widely used to identify senescent cells is senescence-associated (SA) β-galactosidase (Dimri et al., 1995). SA β-Galactosidase marker expression allows distinguishing between senescent and quiescent cells, which is not possible when using for instance 5-bromodeoxyuridine (BrdU) in order to check for DNA replication. SA β-Galactosidase expression is induced as well by prolonged confluent cell culture conditions though, so other markers are required. $p16^{INK4a}$ expression can serve as another marker for senescence (Krishnamurthy et al., 2004), although it is not expressed in all cells exhibiting a senescent phenotype (Itahana et al., 2003). Various signals can shift a cell towards senescence like dysfunctional telomeres (Martens et al., 2000), damage to the DNA per se (Di Leonardo et al., 1994), disorganization of chromatin (Ogryzko et al., 1996) or oncogene activity (Zhu et al., 1998). These signals get mediated either via the $p16^{INK4a}$-Retinoblastoma protein (pRb) pathway or the p53 pathway. Still there are few instances of senescence that seem to be independent of these two pathways (Michaloglou et al., 2005; Olsen et al., 2002).

1.6 Protein transduction

In order to genetically modify cells, thereby analyzing the function of proteins in a 'gain-of-function' scenario, several conventional methods are available nowadays. Transfection, i.e. lipofection or electroporation as well as microinjection and viral transduction of nucleic acids represent the techniques most commonly used. These methods suffer from certain limitations

though, as primary cells tend to be hard to transfect, hampering the overall transfection efficiency. Additionally toxic side effects can occur, and maybe the biggest limitation is posed by the risk of insertional mutagenesis. Although the protein transduction paradigm may still be in its infancy, it represents a promising alternative approach, which is able to overcome several of the above-mentioned limitations. The protein-of-interest is thereby fused to a protein transduction domain (PTD) enabling the cellular uptake. Since now, transducible proteins have been widely used to analyze gene function as shown for example for Oct3/4, Sox2, HoxB1 as well as $p27^{KIP1}$ and other proteins (Bosnali and Edenhofer, 2008; Elliott and O'Hare, 1999; Ezhevsky et al., 1997; Hall et al., 1996; Nagahara et al., 1998). Moreover, it seems like cellular reprogramming could be achievable applying the transducible reprogramming factors Oct3/4, Sox2, Klf4 and c-myc (Kim et al., 2009a; Zhou et al., 2009) although the results published have to be reproduced.

To confer the ability of translocation to proteins-of-interest mainly three different PTDs, otherwise also called cell-penetrating peptides (CPP) are employed, i.e. a 16 aa polypetide derived from the third helix of the Antennapedia (Antp) homeodomain (Derossi et al., 1994), a basic 34 aa peptide emerging from VP22 herpes simplex virus type 1 (HSV-1) tegument protein (Elliott and O'Hare, 1997) and an 11 aa polypeptide originating from the human immunodeficiency virus (HIV) transactivator of transcription (TAT) domain (Frankel and Pabo, 1988; Green and Loewenstein, 1988). In this thesis the TAT-PTD is used to generate transducible fusion proteins since the work on a transducible variant of the site-specific recombinase Cre and Flp harboring TAT-PTD has led to convincing results in our workgroup (Haupt et al., 2007; Nolden et al., 2006; Patsch et al., 2010; Peitz et al., 2007; Peitz et al., 2002). Moreover the multitude of transducible proteins makes use of the TAT-PTD (Dietz and Bahr, 2004).

The exact molecular mechanism is still not completely elucidated but basic events during protein transduction have been unraveled (for review see (Patsch and Edenhofer, 2007). Wender and colleagues could show that the guanidinium groups of the arginins found within the TAT-PTD play an important role in facilitating cellular uptake through electrostatic interaction as they possess a high charge at physiological pH (Wender et al., 2000). In addition the TAT-PTD requires the expression of negatively charged glycosaminoglycans, i.e. heparan sulfate proteoglycans on the target cells to initiate binding to the cell surface (Console et al., 2003; Tyagi et al., 2001). As these glycosaminoglycans are expressed on the majority of mammalian cellular surfaces most cells are susceptible to protein transduction. Through a process called macropinocytosis, a subtype of endocytosis, TAT fusion proteins were shown to internalize. Macropinocytosis is a rapid, lipid raft-dependent but receptor-independent process, which requires macropinosomes, i.e. actin membrane bulges enclosing the PTD-fused cargo thereby

forming vesicles (Wadia et al., 2004). The process of uptake seems to be energy-dependent and the PTD fusion proteins entering the cell accumulate around the nucleus, but do not co-localize with the nucleus (Caron et al., 2004). This observation of sole perinuclear sequestration suggests that the main factor limiting protein transduction efficiency is posed by endosomal escape of the PTD fusion protein. Nevertheless, as up to 99% of PTD-fused cargo molecules are trapped in endosomes (Kaplan et al., 2005), as little as 1% thereof is able to exert functionality as demonstrated by the transducible Cre recombinase (Jo et al., 2001; Peitz et al., 2002).

Overcoming this obstacle seems to be possible by the application of sucrose or chloroquine to increase delivery of PTD fusion proteins (Caron et al., 2004). The same effect was observed upon addition of TAT-HA, a pH-sensitive, fusogenic peptide capable of disrupting the endosome integrity (Wadia et al., 2004). Additionally photo release can be used to set PTD-fused cargo molecules free from the endosomes (Matsushita et al., 2004).

In conclusion, three steps are needed during the process of protein transduction. First the PTD-fused cargo hast to bind to the cell surface. Subsequently the cargo has to be internalized before it can finally be released from the endosome (Figure 7).

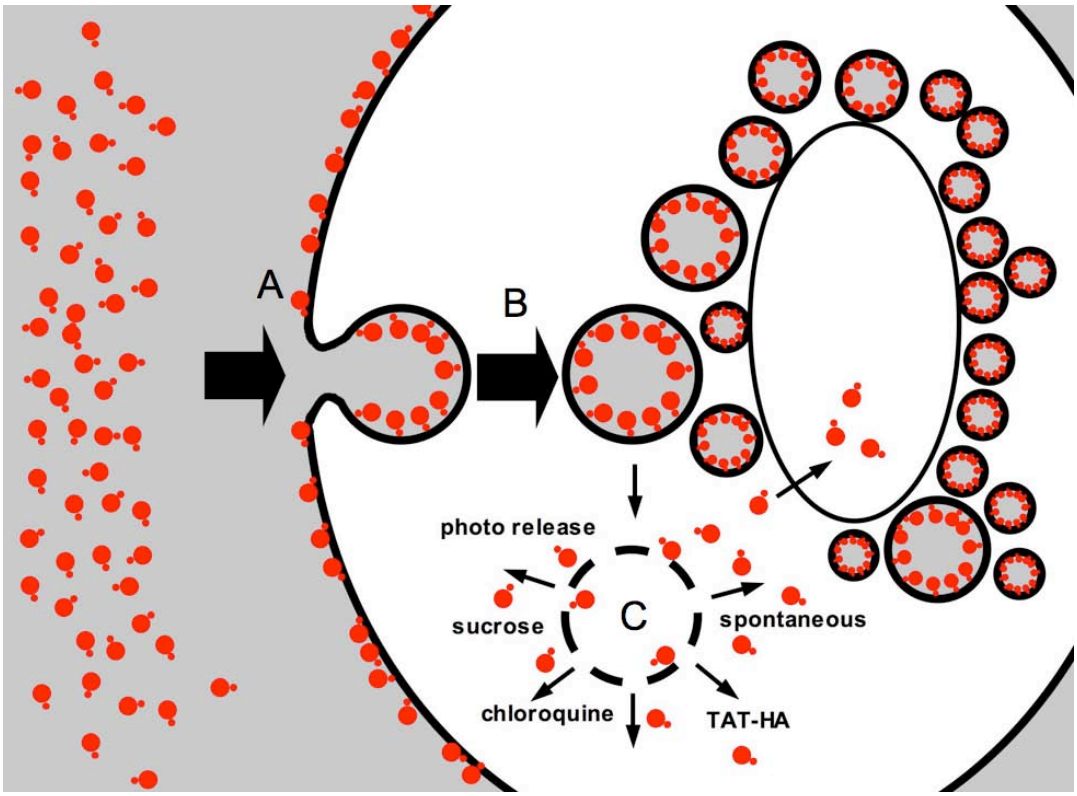

Figure 7: Illustration of the process of protein transduction
(**A**) Proteins fused to a cell penetrating peptide (CPP) bind to heparan sulfate proteoglycans on the surface of the target cell. (**B**) Through electrostatic interactions the protein becomes internalized to the endosomes. Endosomes accumulate around the nucleus in a perinuclear pattern. (**C**) Release of the CPP-fused protein from the endosomes occurs spontaneously but can be mediated by different cues facilitating endosomal escape as well (adapted from Patsch and Edenhofer, 2007).

Initial experiments in our workgroup with a transducible version of the murine stemness factor Nanog were performed with a construct harboring a nuclear localization signal, the sequence encoding for the murine Nanog as well as the PTD TAT and a Histidin-Tag. This construct was termed Nanog-TAT. During these first studies the application of Nanog-TAT onto murine ES cells deprived of the cytokine LIF could sustain pluripotency over several passages, as judged by activity of the Oct3/4 promoter region, immunohistochemical analysis of stemness markers as well as differentiation potential of those cells. Moreover, murine Nanog-TAT could partially inhibit differentiation cues when applied onto human ES cells (Peitz, 2007). Additional studies in our workgroup assigned a role to Nanog in somatic cells as well. Therein Nanog-TAT was applied onto NIH 3T3 cells and primary MEFs. In the presence of Nanog-TAT, NIH 3T3 cells lost contact inhibition, which led to foci formation. Upon cultivation of MEFs with Nanog-TAT, cells showed an enhanced proliferation rate and seemed to bypass senescence, while maintaining a stable set of chromosomes (Winnemöller, 2007).

1.7 Aim of the thesis

For detailed analysis of the Nanog function, especially in somatic cells, the cell permeable version of Nanog shall be applied in further cell culture paradigms. In order to assess the specificity of Nanog protein transduction in ES and somatic cells, a control protein shall be designed and purified. This control fusion protein should mirror Nanog-TAT, but lacking the homeodomain of the full-length Nanog fusion protein, representing an essential functional part of the protein (ΔNanog-TAT). An optimized purification protocol for both recombinant Nanog proteins has to be developed applying an imidazole gradient, which shall be analyzed by immunoblot and SDS-PAGE indicating for optimal purification conditions. The recombinant Nanog fusion proteins shall be further examined for their biochemical properties, i.e. the ability to recognize and bind to a Nanog consensus sequence as well as the proteins' capability to translocate into mammalian cells.

The phenomenon of enhanced proliferation of primary murine cells upon Nanog-TAT cultivation shall be analyzed at a molecular level to link this phenotypical observation to molecular changes inside the cell. Furthermore, Nanog-TAT shall be applied onto human primary cells to assess in more detail the protein's partial trans-species function observed upon treatment of human ES cells with Nanog-TAT. Underlying molecular events shall be elucidated by whole genome expression analysis. Finally, a potential influence of Nanog-TAT on the process of cellular reprogramming shall be analyzed.

2 Materials and Methods

2.1 Materials

2.1.1 Chemicals

All chemicals were obtained from Sigma-Aldrich, Fluka and Carl Roth GmbH. Any case of exception is mentioned.

2.1.2 Equipment

Incubator used for expression of bacteria

innova 44; New Brunswick (Nürtingen, Germany)
innova 4300; New Brunswick (Nürtingen, Germany)
EB KS-15; Johanna Otto GmbH (Hechingen, Germany)
TH 15 incubator hood; Johanna Otto GmbH (Hechingen, Germany)

Chemiluminescence detection

Chemidoc XRS; Biorad (Munich, Germany)

Thermocycler

T3 Thermocycler; Biometra (Göttingen, Germany)

Electrophoresis

Standard PowerPack P25; Biometra (Göttingen, Germany)
Powerpack 200; Biorad (Munich, Germany)
Agagel Mini; Biometra (Göttingen, Germany)
Agagel Midi-Wide; Biometra (Göttingen, Germany)
Agagel Maxi; Biometra (Göttingen, Germany)
ProteanIII MiniGel System; Biorad (Munich, Germany)

Incubators for cell culture

Heracell; Heraeus (Hanau, Germany)

Microscope

Axiovert 25; Zeiss (Göttingen, Germany)
Axiovert 135; Zeiss (Göttingen, Germany)

pH-meter

CG840; Schott (Mainz, Germany)

Photometer

BioPhotometer; Eppendorf (Hamburg, Germany)
NanoDrop; Peqlab (Erlangen, Germany)

Shaker

Roto-Shake Genie; Scientific Industries (New York, USA)
Vortex-2 Genie; Scientific Industries (New York, USA)

Sonicator

Sonoplus HD 2070; Bandelin electronics (Berlin, Germany)

Sterile workbenches

Herasafe; Heraeus (Hanau, Germany)

Plasticware

Cell culture dish 15 cm	TPP (Trasadingen, Switzerland)
Cell culture dish 10 cm	BD Falcon (Bedford, USA)
Cell culture dish 6 cm	BD Falcon (Bedford, USA)
Cell culture dish 3.5 cm	BD Falcon (Bedford, USA)
6 well cell culture plate	Nunc (Roskilde, Denmark)
12 well cell culture plate	Nunc (Roskilde, Denmark)
24 well cell culture plate	Costar (Corning, USA)
Petri dish 10 cm	BD Falcon (Bedford, USA)
15mL centrifuge tubes	Greiner Bio (Frickenhausen, Germany)
50mL centrifuge tubes	Greiner Bio (Frickenhausen, Germany)

cryo vials	Nunc (Roskilde, Denmark)
Cell scraper	Costar (Corning, USA)
Plastic pipets (1mL – 25mL)	Costar (Corning, USA)
Sterile filter (0,2µm)	Whatman (Dassel, Germany)

UV transilluminators

GelVue GVM20; Syngene (Cambridge, UK)
GelDoc EQ; Biorad (Munich, Germany)

Scales

LA310S; Sattorius (Göttingen, Germany)
BL610; Sattorius (Göttingen, Germany)

Centrifuges

5416 R; Eppendorf (Hamburg, Germany)
5415 D; Eppendorf (Hamburg, Germany)
Biofuge pico; Heraeus (Hanau, Germany)
Megafuge 1.0R; Heraeus (Hanau, Germany)
RC5B plus; Thermo (Waltham, USA)
RC26 plus; Thermo (Waltham, USA)
RC6 plus; Thermo (Waltham, USA)

2.1.3 Enzymes

Restricion endonucleases; NEB (Frankfurt, Germany)
GoTaq polymerase; Promega (Mannheim, Germany)
Phusion polymerase; NEB (Frankfurt, Germany)
iScript Reverse Transcriptase; Biorad (Munich, Germany)
Benzonase; Novagen (Darmstadt, Germany)
Lysozyme; Sigma-Aldrich (Munich, Germany)
T4 DNA Ligase; NEB (Frankfurt, Germany)
Shrimp alkaline phosphatase; Roche (Mannheim, Germany)

2.1.4 Antibodies

Immunocytochemistry

α-SSEA-1; mouse IgG; 1:80; NEB (Frankfurt, Germany)

α-Nanog; rabbit IgG; 1:1300; Chemicon (Schwalbach/Taunus, Germany)

α-smooth muscle actin (SMA); mouse IgG; 1:200; DAKO

α-alpha-1-fetoprotein (AFP); rabbit; 1:100; DAKO

α-β(III)tubulin (TUJ1); mouse IgG; 1:1000; Covance

Secondary Antibodies

Alexa Fluor 488 labeled anti-rabbit IgG; 1:600; Invitrogen (Karlsruhe, Germany)

Alexa Flour 555 labeled anti-mouse IgG; 1:800; Invitrogen (Karlsruhe, Germany)

Alexa Fluor 555 labeled anti-rabbit IgG; 1:800; Invitrogen (Karlsruhe, Germany)

Western Blots

α-Nanog; rabbit IgG; 1:3000 for recombinant proteins; 1:1000 for cell lysates; Chemicon (Frankfurt, Germany)

α-β-actin; mouse IgG; 1:2000, NEB (Frankfurt, Germany)

α-Cyclin D1; mouse IgG; 1:200; BD Pharmingen (Heidelberg, Germany)

α-Histidin, conjugated to HRP, 1:1000, Qiagen (Hilden, Germany)

α-$p21^{CIP/WAF}$; mouse IgG; 1:200, BD Pharmingen (Heidelberg, Germany)

α-$p27^{KIP1}$; mouse IgG; 1:200; BD Pharmingen (Heidelberg, Germany)

α-p53; mouse IgG; 1:1000; Cell Signaling Technology (Frankfurt, Germany)

α-Retinoblastom protein; mouse IgG; 1:1000; abcam (Cambridge, UK)

α-α-tubulin; rabbit IgG; 1:1000; Cell Signaling (Frankfurt, Germany)

Secondary Antibodies

HRP-conjugated anti-mouse IgG; 1:1000; Cell Signaling Technology (Frankfurt, Germany)

HRP-conjugated anti-rabbit IgG; 1:5000; Cell Signaling Technology (Frankfurt, Germany)

2.1.5 Buffers, markers and medium

Denaturing purification buffers

Washing buffer

0.5%	Triton-X100 [v/v]
50mM	Tris-HCl, pH 8.0
100mM	NaCl
0.1%	sodium azid

Resuspension buffer

50mM	Tris-HCl, pH 8.0
100mM	NaCl

Solubilization buffer

6M	Guanidine HCl
50mM	Tris-HCl, pH 8.0
100mM	NaCl
10mM	EDTA
10mM	DTT

Refolding buffer 1

50mM	MES, pH 6.0
9.6 mM	NaCl
0.4mM	KCl
2mM	$MgCl_2$
2mM	$CaCl_2$
0.75M	Guanidine HCl
0.5%	Triton-X100 [v/v]
1mM	DTT

Refolding buffer 2

50mM	MES, pH 6.0
9.6 mM	NaCl
0.4mM	KCl
2mM	$MgCl_2$
2mM	$CaCl_2$
0.5M	Arginine
0.05%	PEG 3550
1mM	GSH
0.1mM	GSSH

Refolding buffer 3

50mM	MES, pH 6.0
9.6 mM	NaCl
0.4mM	KCl
1mM	EDTA
0.4M	Sucrose
0.75M	Guanidine HCl
0.5%	Triton-X100 [v/v]
0.05%	PEG 3550
1mM	DTT

Refolding buffer 4

50mM	MES, pH 6.0
240mM	NaCl
10mM	KCl
2mM	$MgCl_2$
2mM	$CaCl_2$
0.5M	Arginine
0.5%	Triton-X100 [v/v]
1mM	GSH
0.1mM	GSSH

Refolding buffer 5

50mM	MES, pH 6.0
240mM	NaCl
10mM	KCl
1mM	EDTA
0.4M	Sucrose
0.75M	Guanidine HCl
1mM	DTT

Refolding buffer 6

50mM	MES, pH 6.0
240mM	NaCl
10mM	KCl
1mM	EDTA
0.5M	Arginine
0.4M	Sucrose
0.5%	Triton-X100 [v/v]
0.05%	PEG 3550
1mM	GSH
0.1mM	GSSH

Refolding buffer 7

50mM	MES, pH 6.0
240mM	NaCl
10mM	KCl
2mM	$MgCl_2$
2mM	$CaCl_2$
0.75M	Guanidine HCl
0.05%	PEG 3550
1mM	DTT

Refolding buffer 8

50mM	Tris-HCl, pH 8.5
9.6 mM	NaCl
0.4mM	KCl
2mM	$MgCl_2$
2mM	$CaCl_2$
0.4M	Sucrose
0.5%	Triton-X100 [v/v]
0.05%	PEG 3550
1mM	GSH
0.1mM	GSSH

Refolding buffer 9

50mM	Tris-HCl, pH 8.5
9.6 mM	NaCl
0.4mM	KCl
1mM	EDTA
0.5M	Arginine
0.75M	Guanidine HCl
0.05%	PEG 3550
1mM	DTT

Refolding buffer 10

50mM	Tris-HCl, pH 8.5
9.6 mM	NaCl
0.4mM	KCl
2mM	$MgCl_2$
2mM	$CaCl_2$
0.5M	Arginine
0.4M	Sucrose
0.75M	Guanidine HCl
1mM	GSH
0.1mM	GSSH

Refolding buffer 11

50mM	Tris-HCl, pH 8.5
9.6 mM	NaCl
0.4mM	KCl
1mM	EDTA
0.5%	Triton-X100 [v/v]
1mM	DTT

Refolding buffer 12

50mM	Tris-HCl, pH 8.5
240mM	NaCl
10mM	KCl
1mM	EDTA
0.05%	PEG 3550
1mM	GSH
0.1mM	GSSH

Refolding buffer 13

50mM	Tris-HCl, pH 8.5
240mM	NaCl
10mM	KCl
1mM	EDTA
0.5M	Arginine
0.75M	Guanidine HCl
0.5%	Triton-X100 [v/v]
1mM	DTT

Refolding buffer 14

50mM	Tris-HCl, pH 8.5
240mM	NaCl
10mM	KCl
2mM	$MgCl_2$
2mM	$CaCl_2$
0.5M	Arginine
0.4M	Sucrose
0.75M	Guanidine HCl
0.5%	Triton-X100 [v/v]
0.05%	PEG 3550
1mM	GSH
0.1mM	GSSH

Refolding buffer 15

50mM	Tris-HCl, pH 8.5
240mM	NaCl
10mM	KCl
2mM	$MgCl_2$
2mM	$CaCl_2$
0.4M	Sucrose
1mM	DTT

Native purification buffers

Lysis buffer for Nanog-TAT and ΔNanog-TAT

500mM	NaCl
2mM	Imidazole
1x	PTB
pH 8.0	

Washing buffer for Nanog-TAT

500mM	NaCl
30mM	Imidazole
1x	PTB
pH 8.0	

Washing buffer for ΔNanog-TAT

500mM	NaCl
100mM	Imidazole
1x	PTB
pH 8.0	

Elution buffer for Nanog-TAT and ΔNanog-TAT

500mM	NaCl
250mM	Imidazole
1x	PTB
pH 8.0	

Nanog-TAT glycerol buffer

50%	Glycerin [v/v]
1M	NaCl
1mM	DTT
1mM	EDTA
20mM	HEPES

TBS (Tris Buffered Saline) buffer

50mM	Tris-HCl, pH 7.4
150mM	NaCl

TBS-T buffer

50mM	Tris-HCl, pH 7.4
150mM	NaCl
0.05%	Tween 20 [v/v]

TBS-TT buffer

50mM	Tris-HCl, pH 7.4
150mM	NaCl
0.05%	Tween 20 [v/v]
0.2%	Triton X-100 [v/v]

LB medium

For 1L of LB medium prepare the following

10g	Tryptone/Peptone
5g	Yeast extract
10g	NaCl

Solve ingredients in 800mL dH_2O and adjust pH to 7.5 with NaOH. Thereafter fill up to 1L with dH_2O and sterilize by autoclaving.

TB medium

For 1L of TB medium prepare two solutions:

Solution 1

12g	Tryptone/Peptone
24g	Yeast Extract
4mL	Glycerol

Solve ingredients in 900mL of dH_2O.

Solution 2

2.31g	KH_2PO_4
12.54g	K_2HPO_4

Solve ingredients in 100mL of dH_2O.

Combine both solutions after autoclaving.

SOB medium

0.5%	Yeast extract
2%	Tryptone/Peptone
10mM	NaCl
2.5mM	KCl
10mM	$MgCl_2$
10mM	$MgSO_4$

Dissolve in nanopure water and autoclave.

TB buffer

10mM	PIPES
15mM	$CaCl_2$
250mM	KCl

Dissolve in nanopure water and adjust the pH to 6.7 before adding $MnCl_2$ to a final concentration of 55mM. Afterwards TB buffer is sterilized by filtration with a 0.45µm filter and stored at 4°C.

Protein Marker

Prestained Protein Marker; NEB (Frankfurt, Germany)

Color Plus Protein Prestained Marker; NEB (Frankfurt, Germany)

Perfect Protein Marker; Novagen (Darmstadt, Germany)

6x His Ladder; Qiagen (Hilden, Germany)

DNA ladders

1kb ladder; NEB (Frankfurt, Germany)

100bp ladder; NEB (Frankfurt, Germany)

TAE (Tris-acetate-EDTA) buffer

40mM	Tris
20mM	Acetic acid
1mM	EDTA

pH of 50xTAE has to be adjusted to 8.4

TBE (Tris-borate-EDTA) buffer

89mM	Tris
89mM	Boric acid
2mM	EDTA

pH of 10xTBE has to be adjusted to 8.3

Agarose gel loading buffer

30% Glycerin
Spatula tip of bromophenol blue
Spatula tip of xylenxyanol

5x SDS-PAGE loading buffer

250mM	Tris-Cl, pH 6.8
10%	SDS [w/v]
50%	glycerol [w/v]
0.02%	bromphenol blue [w/v]

Add 10% [v/v] β-mercaptoethanol prior to use.

10x SDS-PAGE electrophoresis buffer

0.25M	Tris
1.92M	Glycine
1.0%	SDS, pH 8.3

4 x Tris/SDS buffer pH 8.8:

1.5M	Tris-Cl, pH 8.8
0.4%	SDS

4 x Tris/SDS buffer pH 6.8:

0.5M	Tris-Cl, pH 6.8
0.4%	SDS

SDS-PAGE stacking gel (for 5mL):

2.85mL	H_2O
0.83mL	30%/0.8% acrylamide/bis-acrylamide
1.25mL	4x Tris/SDS buffer, pH 6.8
0.075mL	10% APS [w/v]
0.0015mL	TEMED

SDS-PAGE separating gel (for 10mL exhibiting 10%):

4.1mL	H_2O
3.33mL	30%/0.8% acrylamide/bis-acrylamide
2.5mL	4x Tris/SDS buffer, pH 8.8
0.075mL	10% APS [w/v]
0.0015mL	TEMED

Native Gel (for 30mL exhibiting 5%)

3mL	10xTBE buffer
5mL	acrylamide/bisacrylamide
22mL	H_2O
125µL	10% APS
17µL	TEMED

Immunoblot (wet) transfer buffer

25mM	Tris
192mM	Glycin
20%	Methanol

Stripping buffer for immunoblot:

2%	SDS
100mM	β-mercaptoethanol
50mM	Tris-Cl, pH 6.8

Cell culture stock solutions

L-Glutamin	200mM; Gibco (Karlsruhe, Germany) catalogue number 25030-024
Non-Essential Amino Acids (NEAA)	100x; Gibco (Karlsruhe, Germany) catalogue number 11140-035
β-mercaptoethanol	50mM; Gibco (Karlsruhe, Germany) catalogue number 31350-010
Insulin Transferin Selenin G (ITS)	100x ; Gibco (Karlsruhe, Germany) catalogue number 41400-045
D-MEM	Gibco (Karlsruhe, Germany) catalogue number 41966-029 supplemented with L-Glutamine, 110mg/L sodium pyruvat and 4500mg/L D-glucose
KnockOut D-MEM	Gibco (Karlsruhe, Germany) catalogue number 10829-018 supplemented with L-Glutamine, 110mg/L sodium pyruvat and 4500mg/L D-glucose

Advanced D-MEM	Gibco (Karlsruhe, Germany) catalogue number 12491-015 supplemented with 110mg/L sodium pyruvat and 4500mg/L D-glucose
FCS used for ES cells	PAN (Aidenbach, Germany) catalogue number 3302-P260719
FCS used for MEFs	Gibco (Karlsruhe, Germany) catalogue number 10270-106
Puromycin [1mg/mL]	Gibco (Karlsruhe, Germany)

MEF cell culture medium

88mL	D-MEM (final concentration 88%)
10mL	FCS for MEFs (final concentration 10%)
1mL	L-Glutamine (final concentration 2mM)
1mL	NEAA (final concentration 1x)
200µL	β-mercaptoethanol (final concentration 100µM)

ES cell culture medium

85mL	KnockOut D-MEM (final concentration 85%)
15mL	FCS for ES cells (final concentration 15%)
1mL	L-Glutamine (final concentration 2mM)
1mL	NEAA (final concentration 1x)
200µL	β-mercaptoethanol (final concentration 100µM)
100µL	Puromycin if needed (final concentration 1µg/mL)

ESGRO LIF from Millipore (Schwalbach/Taunus, Germany) is added at a dilution of 1:10.000 if required. The same applies for LIF inhibitor (LI), which is used at a dilution of 1:500 (according to functional analysis performed by Dr. Michael Peitz). Prior to all experiments, Oct3/4 GiP ES cells were cultivated in the presence of puromycin, diluted 1:1000 (stock solution 1mg/mL) to ensure a stringent pluripotent ES cell population.

Advanced medium

94mL	Advanced D-MEM (final concentration 94%)
5mL	FCS for ES cells (final concentration 5%)
1mL	L-Glutamine (final concentration 2mM)
0,5mL	ITS (final concentration 1x)
200µL	β-mercaptoethanol (final concentration 100µM)

2x Advanced medium

94mL	Advanced D-MEM (final concentration 94%)
2mL	FCS for ES cells (final concentration 2%)
2mL	L-Glutamine (final concentration 2mM)
1mL	NEAA (final concentration 1x)
1mL	ITS (final concentration 1x)
200µL	β-mercaptoethanol (final concentration 100µM)

2x Freezing medium for ES cells

20%	DMSO (final concentration 10%)
40%	FCS for ES cells
40%	ES cell culture medium (supplemented with LIF)

2x Freezing medium for somatic cells

20%	DMSO (final concentration 10%)
40%	FCS for MEFs
40%	MEF medium

4%PFA (Paraformaldehyde)

In order to assemble 500mL of 4%PFA heat 200mL of nanopure water to 80°C and place on a stir plate inside a hood. While stirring add 20g of PFA and drop-wise add 1N NaOH until PFA crystals are dissolved. Subsequently add 210mL of 0.2M sodium dibasic phosphate buffer and 40mL of 0.2M sodium monobasic phosphate buffer. Adjust pH to 7.4 and fill up the volume to 500mL with nanopure water. Finally 4%PFA is filtered and can be stored at -20°C.

Mounting Medium 1:

Solve 2.4g Moviol in 4.8mL glycerol. Then add 6mL H_2O and stir overnight. Moviol mounting medium can be stored at -20°C.

Mounting Medium 2:

Vectashield fluorescence mounting medium; Vector Laboratories (Burlingame, USA)

2.1.6 Bacterial strains

DH5α (Gibco BRL, Karlsruhe, Germany)

Used for cloning purposes.

DH5α bacteria cells possess high transformation efficiency. By the endA1 mutation internal nucleases are inactivated. The hsdR17 mutation leads to the elimination of another endonuclease. Mutation in recA1 prevents homologous recombination.

Genotype: *E.coli* F^- endA1 glnV44 thi-1 recA1 relA1 gyrA96 deoR nupG Φ80d*lacZ*ΔM15 Δ(*lacZYA-argF*)U169, hsdR17(r_K^- m_K^+), λ–

BL21(DE3) GOLD (Agilent Technologies, Waldbronn, Germany)

Used for the expression of all constructs.

BL21(DE3) GOLD bacteria cells are improved derivates of BL21 competent cells. The major advancement of these cells is increased transformation efficiency, i.e. >1 x 10^8 cfu/µg of pUC18 DNA through the presence of Hte phenotype. High expression levels are achieved by utilizing the T7 RNA polymerase promoter. Furthermore these bacteria cells lack the Lon protease as well as a second protease, namely OmpT.

Genotype: *E. coli* B F– *ompT hsdS*(rB– mB–) *dcm*+ Tetr *gal* λ(DE3) *endA* Hte

2.1.7 Cell lines

Somatic cell lines

CV1 (Jensen et al., 1964)

This fibroblasts cell line is derived from the kidney of the vervet monkey (Cercopithecus Aethiops). These cells were used to assess the translocation ability of the recombinant proteins Nanog-TAT and ΔNanog-TAT since fibroblasts exhibit beneficial properties regarding the protein transduction technique, i.e. big cell surface.

Oct3/4 GiP Mouse Embryonic Fibroblasts (Yeom et al., 1996)

This heterozygous primary MEF cell line was established from fetuses derived from breeding of Oct3/4 GiP mice with C57BL/6J (Black6) mice (Jackson Laboratory, Main, USA). As these cells carry the transgene encoding for GFP and a gen conveying resistance to puromycin under the regulatory sequence of the murine Oct3/4 promoter, these cells were preferentially employed for reprogramming experiments, as they will turn on transgene expression upon dedifferentiation. These cells were used for cell cycle analysis as well.

MP-AF (Peitz 2007; lab stock)

This cell line is a wild type human dermal fibroblast line. The cells were derived from a 34-year-old healthy male. A skin biopsy taken from the patient was cultivated in MEF medium and dermal fibroblasts started to migrate out of the biopsy patch. Cells were then trypsinized, subsequently expanded and cryopreserved at an early passage number (passage 5). These cells were used in order to investigate the functionality of Nanog-TAT on human cells.

ES cell lines

Oct3/4 GiP (Ying et al., 2002)

This hybrid murine ES cell line (129 X MF1) carries a transgene encoding for GFP linked to a resistance gene to puromycin via an internal ribosomal entry site (IRES) under the regulatory sequence of the murine Oct3/4 promoter. Pluripotent cells therefore will exhibit GFP fluorescence and are resistant to puromycin.

2.1.8 Expression vectors

Nanog-TAT – This vector, employing the pTriEx1 vector from Novagen (Darmstadt, Germany) as a backbone, harbors the genetic information for a NLS, the murine Nanog, the TAT PTD as well as an 8xHistidin tag (Nanog-TAT). The vector can be used to express recombinant protein in *E.coli*, as well as in insect cells or mammalian cells. The plasmid was verified by sequencing (Peitz, 2007).

ΔNanog-TAT – This vector, employing the pTriEx1 vector from Novagen (Darmstadt, Germany) as a backbone, harbors the genetic information for murine Nanog lacking its homeodomain. The insert for ΔNanog-TAT (without NLS, PTD-TAT and Histidin-Tag) was amplified using a construct already present in the workgroup (Münst, 2005). The vector can be used to express recombinant proteins in *E.coli*, as well as in insect cells or mammalian cells.

2.1.9 Oligonucleotide primers

Table 1: Primers used for sequencing

pTriEx-F	5'-TAA TCC GGG ACC TTT AAT TC
pTriEx-R	5'-GC TCA AGG GGC TTC ATG ATG

Table 2: Primers used for cloning

Nanog-F	5'-GGC CTA GGA GTG TGG GTC TTC CTG GTC C
Nanog-R	5'-GTG CTA GCT ATT TCA CCT GGT GGA GTC AC
ΔNanog-TAT-F	5'-CTG AAC CAT GGG CGC TAA AAA AAA GAG GAA AGT GAG TGT GGG TCT TCC TGG TC
ΔNanog-TAT-R	5'-CAT GCT CGA GTT AGT GAT GGT GAT GGT GAT GAC CGC CAG GCG GAC GCG ACG TTG GCG ACG TTT CTT GCG TAT TTC ACC TGG TGG AGT CAC

Table 3: RT-PCR primers

GAPDH-F	5'-GCA CAG TCA AGG CCG AGAAT
GAPDH-R	5'-GCC TTC TCC ATG GTG GTG AA
$p16^{INK4a}$-F	5'-GCT GCA GAC AGA CTG GCC A
$p16^{INK4a}$-R	5'-GTC CTC GCA GTT CGA ATC TG
$p21^{CIP/WAF}$-F	5'-CTG AGG ATG AAC AGT AAC AAC CG
$p21^{CIP/WAF}$-R	5'-CTG GGA AGA TAG AGC GAA GCC
$p27^{KIP1}$-F	5'-TCT CTT CGG CCC GGT CAA T
$p27^{KIP1}$-R	5'-GGG GCT TAT GAT TCT GAA AGT CG
p53-F	5'-TGA AAC GCC GAC CTA TCC TTA
p53-R	5'-GGC ACA AAC ACG AAC CTC AAA
FGF-receptor 1-F	5'-GGT GCT TCA TCT ACG GAA TGT C
FGF-receptor 1-R	5'-TGA TGG GAG AGT CCG ATA GAG T

Table 4: Primer for silencing and re-activation of pluripotency markers

tg-Oct3/4-F	5'-CCC CAC TTC ACC ACA CTC TAC
tg-Oct3/4-R	5'-TTT ATC GTC GAC CAC TGT GC
tg-Sox2-F	5'-GCC CAG TAG ACT GCA CAT GG
tg-Sox2-R	5'-CCC CCT TTT TCT GGA GAC TA
tg-c-myc-F	5'-CAG AGG AGG AAC GAG CTG AAG CGC (Takahashi and Yamanaka, 2006)
tg-c-myc-R	5'-CTT GTA CAA GAA AGC TGG GT
tg-Klf4-F	5'-AGG CAC TAC CGC AAA CAC AC
tg-Klf4-R	5'-TTT ATC GTC GAC CAC TGT GC
endo-Oct3/4-F	5'-TCT TTC CAC CAG GCC CCC GGC TC (Takahashi and Yamanaka, 2006)
endo-Oct3/4-R	5'-TGC GGG CGG ACA TGG GGA GAT CC (Takahashi and Yamanaka, 2006)
endo-Sox2-F	5'-TAG AGC TAG ACT CCG GGC GAT GA (Takahashi and Yamanaka, 2006)
endo-Sox2-R	5'-TTG CCT TAA ACA AGA CCA CGA AA (Takahashi and Yamanaka, 2006)
endo-Nanog-F	5'-CAG GTG TTT GAG GGT AGC TC (Takahashi and Yamanaka, 2006)
endo-Nanog-R	5'-CGG TTC ATC ATG GTA CAG TC (Takahashi and Yamanaka, 2006)

2.2 Nucleic acids

2.2.1 Generation of competent *E.coli*

Pipettes and tubes used should be pre-chilled at -20°C.

E.coli bacteria cells can be made competent following an adapted protocol from Inoue and colleagues (Inoue et al., 1990). First, bacteria cells were cultivated on a LB-agar plate without antibiotics at 37°C over night. Then a dozen of the emerging colonies were picked from the plate and 250mL of SOB medium were inoculated with those bacteria cells. Cells were grown over night at 18 to 20°C until they reach an OD_{600} of 0.5. The beaker containing the bacteria culture was then put on ice for 10 minutes. Subsequently cells were centrifuged at 4000rpm for 10 minutes at 4°C. The bacteria pellet was gently re-suspended in 80mL of ice-cold TB buffer and stored again on ice for 10 minutes. The cells were pelletized again applying 4000rpm for 10 minutes at 4°C. Thereafter the bacteria pellet was re-suspended in 20mL of ice-cold TB buffer and 1.4mL of DMSO was added drop-wise to the solution. The competent cells finally were aliquoted in a volume of 100µL and shock frozen using liquid nitrogen. Competent cells could then be put on -80°C for long-term storage. The transformation efficiency i.e. competency of the cells can be calculated using the following equation:

colonies on plate/ng of DNA plated x 1000ng/µg

2.2.2 Transformation of *E.coli*

100µL of competent *E.coli* cells were taken from -80°C and thawed on ice for 10 minutes. For protein expression cultures, BL21(DE3) GOLD were used, whereas DH5α cells were used for cloning purposes. Subsequently 100ng of the desired plasmid was added to the competent bacteria cells. In case of transforming ligation assays 5µL thereof were used. Mixing of the solution was accomplished by tipping the Eppendorf tube. Bacteria cells were then incubated on ice for 20 minutes. Thereafter cells were put on 42°C for 40 seconds using a water bath. The cells were then directly incubated on ice for 2 minutes. 900µL of SOC medium was added and the cells were grown at 37°C for 45 minutes.

2.2.3 Preparation of small amounts of DNA

Colonies cultivated on a LB-agar plate supplemented with the appropriate antibiotic were used to inoculate a volume of 3mL of LB medium supplemented with the appropriate antibiotic as well. These small cultures were grown over night at a temperature of 37°C and 100rpm. The next day bacterial cells were pelletized and subjected to the PureLink Quick Plasmid Miniprep Kit from Invitrogen (Karlsruhe, Germany) according to the manufacturer's protocol.

2.2.4 Preparation of large amounts of DNA

Either colonies growing on a LB-agar plate supplemented with the appropriate antibiotic or freshly prepared transformation assays were used to inoculate 100mL of over night culture consisting of LB and the appropriate antibiotics. Cells were grown over night at 37°C and 120rpm. The next day bacteria cells were harvested via centrifugation and subjected to either the PureLink HiPure Plasmid Maxiprep Kit from Invitrogen (Karlsruhe, Germany) or the NucleoBond Xtra Maxi Kit from Machery-Nagel (Düren, Germany).

2.2.5 Photometric measurement of DNA content

For the measurement of DNA content two different systems were used. When using the Eppendorf Biophotometer 50µL of DNA samples were subjected to UV-cuvettes from Eppendorf (Hamburg, Germany) for instant measurement. If the amount of DNA was limited, the NanoDrop system from peqlab (Erlangen, Germany) was used. Here only 1µL is needed for measurement of DNA content, as this system is independent of cuvettes. In general the DNA concentration was determined measuring at a wavelength of 260nm as nucleic acids possess their maximum absorption at this wavelength. Additionally a measurement at a wavelength of 280nm was done to analyze for protein contaminations as aromatic amino acids absorb light the most at this wavelength. The ratio of $OD_{260/280}$ therefore defines the purity of the DNA solution where a ratio >1,8 is regarded as pure.

2.2.6 Cloning techniques

2.2.6.1 Restriction hydrolysis

For digesting of plasmids, PCR fragments, etc. restriction endonucleases were used at a concentration of 2 to 5 unites of enzyme per µg of DNA. All reactions were performed in the appropriate NEB buffer supplemented with 1% of BSA if needed at the temperatures recommended by the manufacturer. For analytical purposes digestion reactions were performed for 1 to 2 hours. This time frame was extended up to 16 hours for preparative approaches.

2.2.6.2 Purification of DNA

For purifying DNA from restriction hydrolysis analyzed in agarose gel or PCR reactions the Wizard SV Gel and PCR Clean-Up Kit purchased from Promega (Mannheim, Germany) was used. The ability of DNA to bind to silica membranes in the presence of chaotropic salts is utilized in this procedure. Contaminations, which were not able to bind to the membrane, were washed off.

Finally, DNA was eluted using either water or 10mM of Tris-Cl pH 8.5 and could be used for downstream applications.

2.2.6.3 Dephosporylation

Recirculation of plasmid DNA can be suppressed by removing 5'phosphates of both ends of the linearized DNA. To this end 1U of Shrimp Alkaline Phosphatase (SAP) was employed to dephosphorylate 1pmol of linear DNA at 37°C for 20 minutes. After inactivation of the SAP for 15 minutes at 65°C the plasmid DNA was directly subjected to ligation reaction, in which DNA fragments with 5'terminal phosphates could be effectively ligated to dephosphorylated DNA.

2.2.6.4 Ligation

Ligase catalyzes the formation of phosphodiester bonds between juxtaposed 5'phosphate and 3'hydroxyl termini of DNA. In order to introduce DNA fragments into linearized DNA T4 ligase is used. For blunt end ligation reactions were performed for 2 hours at RT, whereas cohesive end ligation was conducted for 10 minutes. T4 ligase activity was heat inactivated through incubation at 65°C for 10 minutes. Afterwards, the ligation reaction was directly used in a transformation assay.

2.2.7 Polymerase chain reaction

In order to amplify DNA fragments polymerase chain reaction (PCR) is commonly used. In an initial step double stranded DNA is denatured applying high temperatures. Subsequently the temperature gets lowered allowing the oligonucleotide primers to anneal to the now single stranded DNA. Next, temperature is raised to 72°C, which represents the optimal temperature for DNA polymerase to exhibit functionality. Primers, which do anneal to the single DNA strand, get elongated until an exact match of the template DNA is amplified. These steps are repeated in cycles until an abundant amount of DNA is produced.

Conditions for the PCR performed in a Thermocycler were as follows:

I. Initial denaturation at 98°C for 30 sec

II. Denaturation at 98°C for 7 sec

III. Annealing at 45°C to 72°C for 20 sec

IV. Extension at 72°C for 25 sec (repetition of step II. to IV. for 30 cycles)

V. Final extension at 72°C for 8 min

VI. Hold at 4°C

2.2.8 Reverse transcriptase polymerase chain reaction

Reverse transcriptase (RT)-PCR is a technique in which DNA is amplified from mRNA, which initially was isolated from cells (see 2.4.2). This allows a transcriptional analysis of the cells. The RNA is used as a template to derive complementary DNA (cDNA). This reverse transcription was conducted using a modified enzyme called reverse transcriptase from the Moloney Murine Leukemia Virus, i.e. iScript from Biorad (Munich, Germany). Random primers with a length of 6 to 10 bases were used for the synthesis of the cDNA.

Conditions for the reverse transcription performed in a Thermocycler were as follows:

I. 25°C for 5min

II. 42°C for 42min

III. 85°C for 5min

IV. Hold at 4°C

The synthesized cDNA was then used as a template for the PCR reaction. Corresponding gene-specific primers (see Table 3) were used for the transcriptional analysis. cDNA was diluted to a final concentration of 200ng. Subsequently, 1µL of cDNA was subjected to the PCR reaction.

Conditions for the PCR performed in a Thermocycler were as follows:

I. Initial denaturation 95°C

II. Denaturation 95°C

III. Annealing 55°C

IV. Extension 72°C

V.Final extension at 72°C for 8min

VI. Hold at 4°C

For the amplification of GAPDH 25 cycles were used. All other factors were amplified using 30 cycles.

2.2.9 Electrophoresis in agarose gels

DNA fragments can be separated according to their size applying an electric current to an agarose gel harboring the DNA. As the phosphate backbone of the DNA is negatively charged, DNA will move towards the anode within the electrical field. Thereby the speed of the movement is inversely proportional to the logarithm of the molecular weight of the DNA fragment. Applying an intercalating dye, namely ethidium bromide, the DNA can be visualized within the gel using UV light exhibiting a wavelength of 254nm. For this purpose agarose was dissolved in boiling 1xTAE buffer. Depending on the size of the DNA fragments different percentages of agarose ranging from 0.5% to 2% [m/v] were used. After cooling of the agarose solution, ethidium bromide was added in a ratio of 1:10.000 (c=10mg/mL) and subsequently poured into a gel chamber with slot combs. After loading of the samples diluted with an agarose gel loading buffer in a ratio of 1:10 first, and a DNA ladder that served as a migration standard an electric current was applied. For analysis the gel was put on a UV table or into the GelDoc system from Biorad (Munich, Germany).

2.2.10 Retroviral infection and iPS induction

Plasmids of pMXs-Oct3/4, pMXs-Sox2, pMXs-c-myc and pMXs-Klf4 were obtained from ADDGENE. Retroviruses were generated using Plat-E packaging cells as previously described (Takahashi et al., 2007). Plat-E cells were seeded at a density of $1x10^5$ cells per well in a six-well plates. 24 hours after transfection, the supernatant containing the viruses encoding for the reprogramming factors, was collected and filtered using a 0.45µm cellulose acetate filter. Oct3/4, Sox2, Klf4 and c-Myc viruses were combined in equal shares and supplemented with

polybrene at a final concentration of 4µg/mL. Oct3/4-GiP MEFs were incubated with the viruses encoding for OKSM for 16 hours. Then the supernatant containing the viruses was removed. After 5 days cells were splitted onto irradiated feeder cells. The experiments were stopped at indicated time points and the cells were fixed applying 4% PFA and subsequently analyzed by fluorescence microscopy. These experiments were performed in collaboration with M. Thier. For analysis of silencing of transgenes genomic DNA of generated iPS cell lines was harvested employing the DNeasy Blood and Tissue Kit from Qiagen (Hilden, Germany) according to the manufacturer's instruction.

2.3 Proteins

2.3.1 Expression of recombinant fusion proteins

After transformation of the various expression vectors into the bacterial expression strain the transformation was used to inoculate an overnight culture, consisting of LB medium, supplemented with glucose at a final concentration of 0.5% [v/v] and carbenicillin at a final concentration of 50µg/mL. The next day, the densely grown overnight culture (OD_{600} >2.0) was centrifuged and the bacteria pellet is re-suspended in fresh LB medium in order to remove β-lactamase otherwise dissolving the antibiotics used. Afterwards, these bacteria cells were used to inoculate the expression culture. The expression culture consisted of TB medium supplemented with glucose at a final concentration of 0.5% [v/v] and ampicillin at a final concentration of 100µg/mL. Measuring OD_{600} monitors the growth of the expression culture. As soon as an OD_{600} of 1.5 was reached, expression became induced through the application of IPTG at a final concentration of 0.5mM. After 1 hour bacteria cells were harvested using a SLA3000 rotor running at 5000rpm (≈ 4.200g) with a temperature of 4°C for 10 minutes. Bacteria cell pellets were then frozen until purification of the recombinant fusion proteins. A general overview of the expression of recombinant protein can be seen in this video protocol (Munst et al., 2009).

2.3.2 Imidazole gradient

In order to analyze a fusion protein for its optimal washing conditions an imidazole gradient was applied. A bacteria pellet corresponding to 1L of expression culture was lysed in 20mL of lysis buffer. After treatment of the solution with lysozyme and benzonase (see 2.3.3) the solution was centrifuged in a SS34 rotor at 15000rpm (≈ 26.900g) running at 4°C. The supernatant was collected, 1mL of 50% Ni-NTA slurry was added and the solution was incubated for 1 hour on an over-head rotor at 4°C. This allowed for binding of the His-Tag of the fusion protein to the Nickel ions. Afterwards the solution was applied onto an Econo Pac column from Biorad (Munich,

Germany) and allowed to run through by gravity flow. 1mL of 50% Ni-NTA results in a bed volume of 0.5mL. Subsequently 0.5mL, i.e. 1 bed volume of buffers containing 1x PTB, 500mM NaCl and a step-wise increasing concentration of imidazole were applied. The imidazole concentration had a range of 10mM to 240mM, increasing by 10mM of imidazole each step. Throughout the imidazole gradient samples for SDS-PAGE and immunoblot analysis were collected.

2.3.3 Purification of recombinant fusion proteins

2.3.3.1 Denaturing purification

A bacteria cell pellet corresponding to 1L of expression was resuspended in 15mL PBS and sonicated on ice to lyse the cells. The crude inclusion bodies were pelleted at 12.000g for 30 minutes and the supernatant was discarded. The pellet was resuspended in 15mL of washing buffer. The inclusion bodies were centrifuged at 25.000g for 10 minutes. The last two steps were repeated 4 to 5 times until the pellet step-wise exhibited a slightly whiter color. In a final washing step the pellet was resuspended in resuspension buffer containing no Triton-X100. The purified inclusion bodies were dissolved in solubilization buffer, i.e. the pellet was broken up using a pipette tip and was then put on an over-head shaker at 4°C over night. Once the inclusion bodies were fully dissolved, the solution was centrifuged at 25.000g for 20 minutes. The supernatant was carefully transferred into a fresh 15mL tube and applied to a rapid dilution refolding approach. 15 different buffer conditions were tested. 50µL of the supernatant obtained were diluted drop-wise into 950µL of the corresponding refolding buffer while gently shaking the solution. Functional refolding buffers were buffer 6, 8 and 11. Refolded protein was then subjected to Ni-affinity chromatography and the recombinant protein was displaced from the column employing native lysis buffer. Subsequently buffer exchange was performed using PD10 desalting columns from GE Healthcare (Freiburg, Germany).

2.3.3.2 Native purification

A temperature of 4°C is essential while purifying all fusion proteins analyzed in this work. A bacteria pellet corresponding to 1L of expression culture was lysed for 20 minutes using 20mL of lysis buffer. Afterwards 1mg/mL of lysozyme was added and incubated for 20 minutes. Subsequently 25U/mL of benzonase were added for another 20 minutes. Samples of the crude lysate as well as of the pellet fraction for SDS-PAGE were taken. The crude lysate was then centrifuged for 30 minutes at 15.000rpm (≈ 26.900g) in a Sorvall SS34 rotor from Thermo Scientific (Bonn, Germany) running at 4°C. A sample of the supernatant was taken for SDS-PAGE analysis. The supernatant was transferred into clean 50mL centrifuge tubes. 1mL of 50%

Ni-NTA slurry from Invitrogen (Karlsruhe, Germany) or Qiagen (Hilden, Germany) per 20mL of supernatant was added and incubated for 1 hour. 1mL Ni-NTA results in 0.5mL column bed. The suspension was then poured onto an Econo pac column and allowed to run through by gravity flow. Washing buffer was applied one time with a volume of 10 times the column bed-volume. Elution was carried out applying 5 times the column bed volume.

The eluate fraction was dialysed 2 times for 1 hour against PBS at 4°C. Subsequently dialysis over night at 4°C against KnockOut D-MEM medium from Invitrogen (Karlsruhe, Germany) was conducted. Netx, dialysate was centrifuged for 30 minutes at 6000rpm (≈ 6.240g) at 4°C. Concentration was then assessed via Bradford.

In the case of ΔNanog-TAT the exchange of medium was conducted via a PD10 desalting column. Briefly, the column was washed with 25mL of PBS and was equilibrated with 25mL of KnockOut D-MEM medium thereafter. Subsequently 2.5mL of eluate fraction were applied onto the column. The protein was dissolved from the PD-10 desalting column with 3.5mL of KnockOut D-MEM medium.

Dialysate fraction was then sterile-filtrated. Afterwards it was diluted with 2x Advanced Medium in a ratio of 1:1. Thereafter the solution was put on 37°C for 2 hours for pre-incubation to force proteins prone to precipitate under cell culture conditions to do so beforehand. The medium containing the fusion protein was then centrifuged for 30 minutes at 6000rpm (≈ 6.240g) at 4°C. After sterile-filtration, the medium was supplemented with the missing 4% of FCS from PAN (Aidenbach, Germany) to reach a final concentration of 5% of FCS. The fusion protein could now be applied in cell culture experiments.

2.3.4 Sodium dodecyl sulfate polyacrylamide gel electrophoresis

Sodium dodecyl sulfate polyacrylamide gel electrophoresis (SDS-PAGE) allows the separation of proteins according to their size. This process is enabled by the fact that sodium dodecyl sulfate acts as a strong anionic detergent and denatures the secondary and tertiary structure of proteins and at the same time charges the proteins negatively according to their size. Disulfide bonds are reduced by β-mercaptoethanol. Two polyacrylamide gel parts with varying pH-values are stacked when performing discontinuous SDS-PAGE. The upper part, called stacking gel exhibits bigger pore sizes due to the low amount of (bis)acrylamide used, and all proteins concentrate in a small part of the stacking gel before uniformly entering the separating gel. Because of the high amount of (bis)acrylamide the separating gel possesses smaller pores, which leads to a separation of the proteins according to their molecular mass.

The separating gel was poured into a tightly assembled gel chamber first, and after polymerization of the separating gel the stacking gel was stratified on top. A comb was inserted

into the stacking gel. For SDS-PAGE the gel was transferred into a gel chamber containing 1x SDS-PAGE running buffer. The SDS-PAGE samples were heated at 95°C for 5 minutes and subsequently centrifuged before loading into the gel slots. 5µL were used per sample of recombinant proteins, for whole protein lysates obtained from cell culture the amount corresponding to 50 µg was loaded. Additionally at least one slot was loaded with (Color) Prestained Protein Marker, a defined marker ranging from a molecular mass of 175 to 7. Electrophoresis was carried out at 200V for 45 minutes. After completion of the gel run, the gel was washed 3 times for 5 minutes in H_2O before it was incubated with Imperial Protein Stain Solution from Perbio (Bonn, Germany) for 5 minutes up to 16 hours. This coomassie R-250 based staining solution offers high sensitivity, since 6ng of protein per lane can be detected. Afterwards the gel was decolorized with H_2O for 15 minutes to 16 hours. The longer this process lasts, the less background staining remains.

2.3.5 Immunoblot

In order to doubtlessly identify a protein of interest, immunoblot is the method of choice. A soon as SDS-PAGE was finished the gel became transferred into immunoblot (wet) transfer buffer and incubated for 10 minutes. Thereafter the immunoblot was assembled. The cassette was placed on a clean surface with the black side down. One pre-wetted - also incubated in immunoblot (wet) transfer buffer - fiber pad was put on the black side of the cassette, followed by 2 Whatman filter papers. Next the equilibrated gel was put on top followed by a pre-wetted - in immunoblot (wet) transfer buffer as well - nitrocellulose membrane from Carl Roth GmbH (Karlsruhe, Germany). The assembly was completed by 2 additional filter papers and another pre-wetted fiber pad. The assembly was then closed and put into the Mini Trans-Blot buffer tank together with a Bio-Ice cooling unit. The buffer tank was filled with immunoblot (wet) transfer buffer and an electrical current of 100V was applied for 1 hour. Alternatively, the blotting can be performed at 30V for 16 hours. After the blotting procedure was completed the blot was disassembled. Staining of the membrane was performed with Ponceau S from Sigma-Aldrich (Munich, Germany), which is able to stain all proteins transferred onto the nitrocellulose membrane. Thereby equal loading of all protein samples could be evaluated. Destaining of Ponceau S was performed by application of PBS to the membrane for 3 times for 5 minutes. The nitrocellulose membrane was then incubated in TBS for 10 minutes before the membrane was subjected to a suitable blocking solution, according to the instructions of the manufacturer of the antibody used. After blocking of the immunoblot the membrane was washed 3 times for 10 minutes in TBS-T. Subsequently the membrane was transferred to the primary antibody solution for different durations according to the manufacturer of the antibody. 3 washing steps with TBS-T lasting for 10 minutes were performed thereafter. The membrane was then incubated

with the secondary antibody solution for different durations according to the manufacturer of the antibody. A final washing of the membrane was performed for 3 times 10 minutes in TBS-TT. Subsequently the immunoblot could be analyzed by the application of a substrate solution. For recombinant proteins SuperSignalWest Pico Substrate from Perbio (Bonn, Germany) was used, for the detection of proteins extracted from cells SuperSignal West Femto Substrate from Perbio (Bonn, Germany) was employed, as it possesses a higher sensitivity than the before-mentioned substrate. The actual detection was carried out using the ChemiDoc XRS system from Biorad (Munich, Germany), which harbors a CCD camera able to detect the emerging chemiluminescence.

Immunoblot stripping protocol

In order to use a nitrocellulose membrane for the detection of another protein of interest with a different primary and secondary antibody, the primary antibodies initially used can be removed, i.e. stripped off the membrane. To this end the nitrocellulose membrane was incubated with pre-warmed stripping buffer for 30 minutes at 50°C in a hybridization oven. Heat combined with strong detergents strips antibodies off the blot. Afterwards the blot was rinsed with TBS for several times. Successful stripping of the membrane could be checked through the application of chemiluminescent substrate. No signal should be detectable. The immunoblot could then be treated as a freshly blotted membrane.

2.3.6 Electrophoretic Mobility Shift Assay

An electrophoretic mobility shift assay (EMSA) allows investigating whether a protein, i.e. in this special case a transcription factor is able to bind to a specific DNA or RNA sequence. In order to analyze the biological activity of the purified recombinant fusion proteins Nanog-TAT and ΔNanog-TAT, a shift assay was performed. Briefly, the protein to be analyzed was incubated with a specific DNA sequence, mostly a promoter or enhancer regulatory element, which is known to be bound by the transcription factor Nanog. Complexes of Protein and DNA migrate slower through a polyacrylamide gel than free DNA. This phenomenon is termed shift.

The oligo sequences (Pan and Pei, 2005) chosen for the EMSA were as follows:

5’-TCGACACCCTTCGCCGATTAAGTACTTAAG (sense)

5’-TCGACTTAAGTACTTAATCGGCGAAGGGTG (antisense)

EMSA was performed with the Lightshift Chemiluminescent EMSA Kit from Thermofisher Scientific (Bonn, Germany) according to the given instructions. Binding of 100ng of recombinant proteins and 0.5ng of biotinylated or non-biotinylated oligonucleotides was performed in 20µL

binding buffer (10mM Tris, 50mM KCl, 1mM DTT, 2.5% glycerol, 5mM MgCl2, 1µg poly(dI-dC), 0.05% NP-40). Binding reactions were separated by native PAGE and subsequently blotted on a positively charged nylon membrane from Roche (Mannheim, Germany). Streptavidin-labeled horseradish peroxidase was then used for detection purpose. Signals were detected with the CCD camera of a ChemiDoc XRS documentation system from Biorad (Munich, Germany).

All materials used were washed thoroughly beforehand to ensure complete absence of SDS, which would consequently lead to the denaturation of the proteins to be analyzed.

Prior to loading of the binding reactions the gels was allowed to pre-run for 1 hour at 100V.

2.3.7 Immunocytochemistry

In order to detect proteins inside or on the surface of cells, immunocytochemistry (ICC) was conducted. Cells were fixed and subsequently stained for the expression of the protein of interest. Briefly, the cell culture medium was aspired and cells were washed twice with PBS from Gibco (Karlsruhe, Germany). Subsequently cells were fixed with 4% PFA for 10 minutes at RT. PFA cross-links proteins via formaldehyde. Thereafter, cells were washed 3 times for 10 minutes with PBS to remove the remaining PFA. All of these steps were performed under a fume hood. Cells were then either stored at 4°C or directly subjected to ICC. In order to block free binding sites, a blocking solution consisting of 5% FCS diluted in PBS was applied onto the cells for 60 minutes. Subsequently a washing step with PBS was performed before the primary antibody was applied over night at 4°C. The next day unbound antibody was washed off with PBS 3 times for 60min at RT. Subsequently the second antibody, diluted in 5% FCS/PBS, was applied for 2 hours at RT in darkness. Cells were finally washed 3 times with PBS for 10 minutes. DAPI was applied for 5 minutes prior to covering cells with a microscope glass slide. Either Moviol or Vectashield mounting medium was used to preserve the cells. Cells were then analyzed by fluorescence microscopy. Afterwards cells were stored at 4°C in darkness to prevent fading of the staining.

Alkaline Phosphatase staining of cells was performed with the Alkaline Phosphatase Kit III from Vector Laboratories (Burlingame, USA). At a glance, staining solution was composed as specified by the manufacturer. Staining solution was applied onto fixed cells and staining procedure was conducted for 30 minutes. Staining solution was then aspirated and cells were stored in PBS.

Senescence-associated β-Galactosidase staining was performed as follows. After fixation of the cells, fibroblast cells were incubated with freshly prepared SA β-Galactosidase staining solution for a maximal time period of 16 hours at 37°C without CO_2. The staining solution consisted of 1mg of 5-bromo-4-chloro-3-indolyl β-D-galactoside (X-Gal) per mL/40mM citric acid/sodium phosphate, pH 6.0/5mM potassium ferrocyanide/5mM potassium ferricyanide/150mM

NaCl/2mM $MgCl_2$. Staining solution was aspired and cells were washed with PBS. Subsequently analysis was performed.

2.4 Cell culture

2.4.1 General methods

2.4.1.1 Passaging of cells

Fibroblast as well as ES cells were passaged according to their confluency. Briefly, culture medium was aspirated from the cells and the cells were washed once with pre-warmed PBS. Subsequently, a sufficient amount of TrypLE Express from Gibco (Karlsruhe, Germany) to cover the bottom of the dish was added to the cells and the cell culture dish was incubated at 37°C for at least 5 minutes. If 5 minutes had not been sufficient to dissolve all cells from the bottom of the culture dish, another 5 minutes of incubation at 37°C were conducted. Dissolved cells were then carefully re-suspended to obtain a single cell solution allowing to count them. Thereafter cells were transferred into a 15mL centrifuge tube and centrifuged at 1000rpm (≈ 170g) for 3 minutes at 4°C. The supernatant was aspirated and the cells were re-suspended in fresh cell culture medium and seeded onto the corresponding plates. ES cells were seeded onto gelatin-coated dishes; fibroblasts were seeded onto untreated dishes. In order to coat cell culture dishes with gelatin, 0.1% gelatin solved in PBS was applied for 20 minutes at 37°C.

2.4.1.2 Counting cells

A cell suspension was prepared directly from the cell culture and depending on the density this suspension was further diluted. 10µL of the suspension were mixed thoroughly with 10µL of 0.4% trypan blue from Gibco (Karlsruhe, Germany). Living cells will not take up trypan blue, whereas dead cells will. So living cells will appear in bright light within the counting chamber under the binocular, dead cells stain blue instead. Approximately 15µL of the solution were transferred to the Fuchs-Rosenthal chamber sheeted with a cover plate and the solution was allowed to fill in by capillary forces. Using a binocular, viable cells were counted. A Fuchs Rosenthal chamber contains 16 big squares, each further subdivided into 16 small squares. Cells within two big squares were counted, average value thereof was determined and the cell number according to the following equation was calculated. If too few or too many cells were present, the cell suspension was diluted accordingly.

cells/mL = average cell count per square x dilution factor x 10^4

total cells = cells/mL x original volume of fluid from which cell sample was removed

2.4.1.3 Freezing and thawing cells

Using cryovials, 1.2 x 10^6 to 3.0 x 10^6 ES cells were cryopreserved in 500µL of ES cell culture medium and 500µL of 2x-freezing medium as well as LIF if needed. It is important to (I) slowly add the ice-cold 2x-freezing medium to the ES cells and to (II) take care not to re-suspend the cells more than once after that. After that cryovials were stored at -80°C in a Cryo 1°C Freezing container from Nalgene (Roskilde, Denmark) filled with isopropanol guaranteeing slow and gentle freezing of the cells. The next day cells were transferred into liquid nitrogen. For somatic cells the protocol was basically the same, except the cells were frozen in 500µL of MEF medium supplemented with 500µL of 2x freezing medium.

In order to thaw cells, a cryovial was taken from the liquid nitrogen and put on 37°C using a water bath. Gentle agitation of the vial was performed until only a small ice crystal in the middle of the cryovial remained. Cells were then transferred from the cryovial into a 15mL centrifuge tube containing pre-warmed cell culture medium. Cells were centrifuged at 800rpm (≈ 110g) for 3 minutes at 4°C. Supernatant was aspirated and the cells were carefully resuspended and finally seeded on the appropriate cell culture dish.

2.4.1.4 Embryoid body formation

iPS cells generated in the presence of Nanog-TAT were cultivated employing mouse ES medium supplemented with LIF for 15 to 25 passages on irradiated MEFs. Cells were splitted and replated on gelatine-coated dishes for 2 days in the same medium. On the third day, cells were carefully trypsinized and transferred onto 10cm petri dishes in mouse ES media without LIF. The suspension cultures were kept for several days until EBs formed. EBs were plated and cultivated for additional 3 to 7 days. Staining for the three germ-layers was conducted after fixation of the plated EBs.

2.4.2 Protein transduction

2.4.2.1 Oct3/4 GiP MEFs and CV1 fibroblast cells

For maintenance cultures of MEFs resp. CV1 cells, cells were cultivated in MEF medium on 10cm dishes and cells were splitted using TrypLE Express from Gibco (Karlsruhe, Germany) every 3 to 4 days prior to becoming confluent. Change of medium was conducted every other day. For cell

cycle analysis of MEFs cultivated with Nanog-TAT, ΔNanog-TAT or control medium via immunoblot, 750.000 cells exhibiting passage number 5 were seeded on a 10cm dish. In order to synchronize the fibroblasts, cells were first put under serum starvation, i.e. a concentration of 0.2% FCS, for 48 hours. This led to an accumulation of cells in G0 phase of the cell cycle. Subsequently MEFs were cultivated in MEF medium supplemented with 4µg/mL aphidicolin for another 16 hours to finally synchronize cells in S phase of the cell cycle, since aphidicolin efficiently inhibits DNA polymerase α. Afterwards MEFs were washed twice with PBS and cultivated with 100nM of Nanog-TAT, 50nM of ΔNanog-TAT or control medium for the indicated time points. Cells were then washed once with ice-cold PBS and thereafter - in the presence of 7mL of ice-cold PBS - scratched from the dish using a cell scraper. Cells were transferred into a 15mL centrifuge tube and the tube was put on ice. Additional 3mL of ice-cold PBS were used to wash remaining cells from the dish and these cells were transferred into the 15mL centrifuge tube already harboring the 7mL of cell suspension. Cells were then centrifuged at 4000rpm (≈ 2.770g) for 10 minutes at 4°C. PBS was aspirated and cells were resuspended in ice-cold RIPA buffer supplemented with HALT protease inhibitors from Thermo Fisher Scientific (Bonn, Germany). The solution was transferred into an Eppendorf tube and put on an over-head rotator for 30 minutes at 4°C. Thereafter the solution was centrifuged at 13.000rpm at 4°C for 30 minutes. The supernatant, i.e. the whole protein lysate, was transferred into a new Eppendorf tube and the protein concentration was determined via Bradford assay. The volume accounting for a total of 50µg of protein was diluted with the appropriate amount of 5x SDS-PAGE buffer and was then heated up at 96°C for 5 minutes. Samples were then ready to be applied onto SDS-PAGE followed by immunoblot analysis.

For harvesting RNA of MEFs, 250.000 cells were seeded onto a 6cm dish and the cells were synchronized as described above. Thereafter MEFs were washed twice with PBS and cultivated with 100nM of Nanog-TAT, 50nM of ΔNanog-TAT or control medium for indicated periods of time. Cells were then washed again with PBS and trypsinized using TrypLE Express and centrifuged at 4°C for 5 minutes at 1000rpm (≈ 170g). MEFs were then directly applied to RNA purification with the RNeasy Mini Kit from Qiagen (Hilden, Germany) according to manufacturer's instructions.

For protein transduction of CV1 fibroblast cells, $1x10^4$ cells were seeded per 12 well dish and protein transduction medium containing either 100nM of Nanog-TAT or 50nM of ΔNanog-TAT was applied. After 5 hours cells were washed 3 times with 0.5mg/mL of Heparin at 37°C to strip off recombinant proteins attached to the cellular surface. Thereafter cells were fixed and subjected to ICC.

In order to analyze for nuclear translocation of the recombinant protein, CV1 cells cultivated with 50nM of ΔNanog-TAT for 2 days were harvested and nuclear extracts were prepared. To

this end, cells were put directly on ice and subsequently washed twice with ice-cold PBS. Cells were harvested using a cell scraper and transferred into a 15mL centrifuge tube. Cells were centrifuged for 5 minutes at 4°C at 1000rpm (≈ 170g). The supernatant was discarded. Cell debris is resuspended in buffer A (10mM Tris, pH 7.8; 1.5mM $MgCl_2$, 10mM KCl) by vortexing. Cell suspension is transferred into a new 1.5mL centrifuge tube and incubated on ice for 15 minutes. Cell suspension was centrifuged again at 6000rpm (≈ 3220g) at 4°C for 5 minutes and the supernatant was again discarded. To transfer nuclear proteins into aqueous solution 150µL of high molecular buffer C (20mM Tris, pH 7.8; 420mM KCl; 1.5mM $MgCl_2$; 20% glycerol [v/v]) was added. The pellet was resuspended and incubated on ice for 30 minutes. Afterwards the nuclei were centrifuged down and the solution containing the nuclear proteins was subjected to immunoblot analysis.

2.4.2.2 MP-AF primary human dermal fibroblasts

For maintenance culture of human dermal fibroblasts, cells were cultivated with MEF medium. Cells were splitted every 2 to 3 days prior to confluency using TrypLE Express. Change of medium was conducted every other day. For growth curve analysis, 250.000 cells exhibiting passage number 6 were seeded on a 6cm dish. As soon as cells reached 90% confluency, the cells were splitted and again 250.000 cells were seeded. Cell numbers were accessed and to finally analyze growth properties, cumulative cell numbers were determined. For the analysis of SA β-Galactosidase expression, cells at passage 16, already cultivated with 100nM of Nanog-TAT for 2 weeks were seeded at a density of 250.000 cells. The next day, cells were fixed and stained for SA β-Galactosidase in order to prevent the cells from becoming confluent and thereby eventually distorting SA-βGalactosidase expression. For the assessment of whole genome RNA expression, cells were treated as described for growth curve analysis. The starting cell population exhibited passage number 9. After 5 passages, cells were trypsinized and subjected to RNA extraction using the RNeasy Mini Kit from Qiagen (Hilden, Germany). RNA was then processed with the Illumina TotalPrep-96 RNA Amplification Kit from Ambion (Darmstadt, Germany) according to the manufacturer's instruction. Subsequently the labeled RNA was loaded onto Illumina Whole Genome Expression Chips and processed as described by the manufacturer.

2.4.2.3 Oct3/4 GiP ES cells

Murine ES cells were cultivated on gelatine-coated dishes or plates. Prior to all experiments involving Oct3/4 GiP ES cells, cells were cultivated in the presence of puromycin for one week to obtain stringent pluripotent ES cell populations. 5000 cells were seeded per well of a 6-well plate and cultivated with control medium or medium containing ΔNanog-TAT - either in the

presence or absence of the cytokine LIF. For cells cultivated in the absence of LIF the medium additionally contained LIF inhibitor to exclude LIF signaling. For analysis of pluripotency, cells were fixed and stained for AP.

3 Results

The technique of protein transduction offers an attractive alternative to manipulate cellular fate by non-genetic means in contrast to conventional methods employing transfection or viral transduction for example. The transducible protein has to fulfill distinct requirements though in order to be successfully transferred into cell culture paradigms. Already at the very beginning of the production of a transducible protein one has to focus on several potentially limiting parameters. In case the fusion protein should exhibit toxic side effects, affecting the condition of the expression system a suitable expression host has to be chosen. Especially in the beforehand mentioned case the basal expression of the recombinant protein before induction has to be minimized as well. The expression of the protein of interest then has to be inducible and one should carefully check for the stability of the desired fusion protein during the phase of induction. A protocol for the optimized purification of a Histidin-tagged fusion protein can be established best when applying an imidazole gradient analyzed by SDS-PAGE and immunoblot, which will indicate the adequate washing conditions in order to obtain recombinant protein of high purity. The transfer of the fusion protein into physiological conditions then is a pivotal step during the process of protein purification as the protein-of-interest may precipitate. For the analysis of biological activity of the recombinant fusion proteins several assays can be performed. So as to investigate the translocation capability of the recombinant protein cells transduced therewith can be analyzed immunocytochemically. Nuclear extracts of cells transduced with the recombinant protein can be explored via immunoblot. Moreover, an electrophoretic mobility shift assay can indicate binding of the fusion protein, i.e. a transcription factor, to a specific consensus sequence. Only if the recombinant fusion protein fulfills these preconditions, experiments in cell culture should be conducted.

3.1 Recombinant Nanog fusion proteins

Initial studies in our workgroup employing recombinant Nanog protein fused to peptides like Thioredoxin (LaVallie et al. 1993), Maltose Binding Protein (Bedouelle and Duplay, 1988) or NusA (Davis et al., 1999) failed for the proper expression of Nanog (Peitz, 2007). Expression of the full-length Nanog fusion protein could be achieved though by using a construct, where the protein exhibits an NLS at the N-terminus, followed by the genetic information for murine Nanog. Then the TAT protein transduction domain and the Histidin-Tag are attached to the C-terminus of the protein (Fig. 8A). This recombinant protein was named Nanog-TAT (Peitz, 2007). It is highly desirable to have pure protein at hand when working in cell culture, since this would for example allow for the labeling of the fusion protein with fluorescent dyes. This, in consequence, would enable the analysis of living cells transduced with the labeled protein, in

order to investigate the cellular uptake since fixation of cells may lead to artificial distribution of the recombinant protein. Furthermore, the specificity of the potentially observed effect could be linked more easily to the recombinant fusion protein than to any contaminations. Hence, the need for optimizing the purification process of the Nanog-TAT fusion protein was accentuated. A bacterial expression system was chosen for Nanog-TAT. For expression purposes the plasmid encoding for Nanog-TAT was transformed into *E.coli*.. Bacteria cells containing the plasmid were grown over night and used to inoculate the expression culture, which was induced via IPTG. As Nanog-TAT became degraded over prolonged time of induction (data not shown) the bacteria cells were harvested 1 hour after induction.

As for a proper experimental setup a control protein was missing, a variant of Nanog-TAT lacking its homeodomain was generated, since up to now no point mutation leading to a loss of Nanog functionality is known.

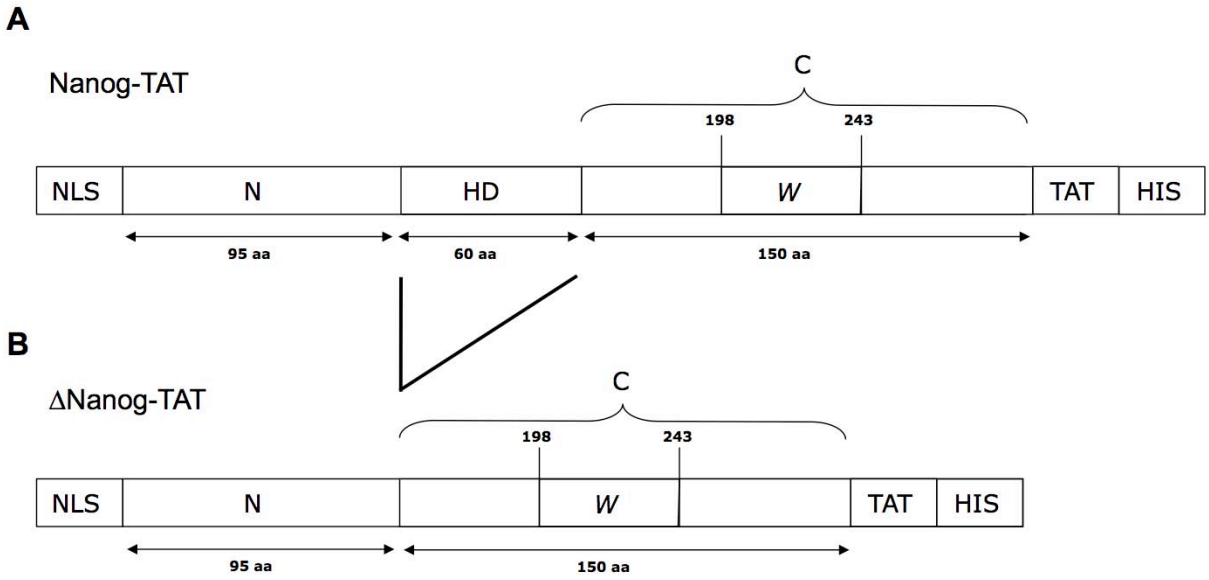

Figure 8: Schematic overview of Nanog fusion proteins
(**A**) Cellular uptake of the full-length Nanog protein is expected through the addition of TAT to the recombinant stemness factor. For enhanced nuclear translocalization a Simian Virus 40 NLS is added. The Histidin-Tag enables Ni-affinity chromatography. (**B**) Nanog control protein consists of two domains. The ommitance of the 65 aa long homeodomain should disable binding of the deletion mutant to the DNA, i.e. ΔNanog-TAT should not exhibit functionality. Cellular uptake of the protein is assured through the addition of TAT to the recombinant control protein. The Histidin-Tag enables Ni-affinity chromatography. aa: amino acids; NLS: nuclear localization sequence; N: N-terminal domain; W: tryptophan repeat; C: C-terminal domain; TAT: transactivator of transcription domain; HIS: Histidin-Tag

The mutant Nanog control protein, named ΔNanog-TAT, comprises a NLS at the N-terminus, a truncated variant of the murine Nanog, as well as a TAT PTD and the Histidin-Tag at the C-terminus. Comparably to Nanog-TAT a bacterial expression system was chosen for ΔNanog-TAT as well. For expression purposes the plasmid encoding for ΔNanog-TAT was

transformed into the same *E.coli* strain used for Nanog-TAT. Bacteria cells harboring the genetic information for ΔNanog-TAT were grown over night and used to inoculate the expression culture, which was induced via addition of IPTG. As ΔNanog-TAT became degraded over prolonged times of induction as well (data not shown) the bacteria cells were harvested via centrifugation after 1 hour of induction. Although the control protein ΔNanog-TAT is only lacking the homeodomain of murine Nanog (Fig. 8B), purification protocols applied for Nanog-TAT could not simply be transferred onto ΔNanog-TAT. Even the rearrangement of the additional tags, i.e. Histidin-Tag, TAT PTD and NLS, can have major influence on solubility and biochemical properties of a newly designed fusion protein. Optimal conditions for the purification of the control protein had to be established as well, since the criteria applying for Nanog-TAT are also valid for ΔNanog-TAT.

3.1.1 Assessing purification conditions for Nanog-TAT

In order to assess purification conditions for Nanog-TAT, a bacteria pellet was processed as described in the material and methods part. The soluble fraction was incubated with Ni-NTA slurry and subjected onto a gravity flow column. Subsequently an imidazole gradient exhibiting a stepwise increase of concentration of imidazole from 10 to 240mM was applied. Throughout the purification process, fractions were collected, diluted with SDS-PAGE sample buffer and loaded onto SDS-PAGE for analysis.

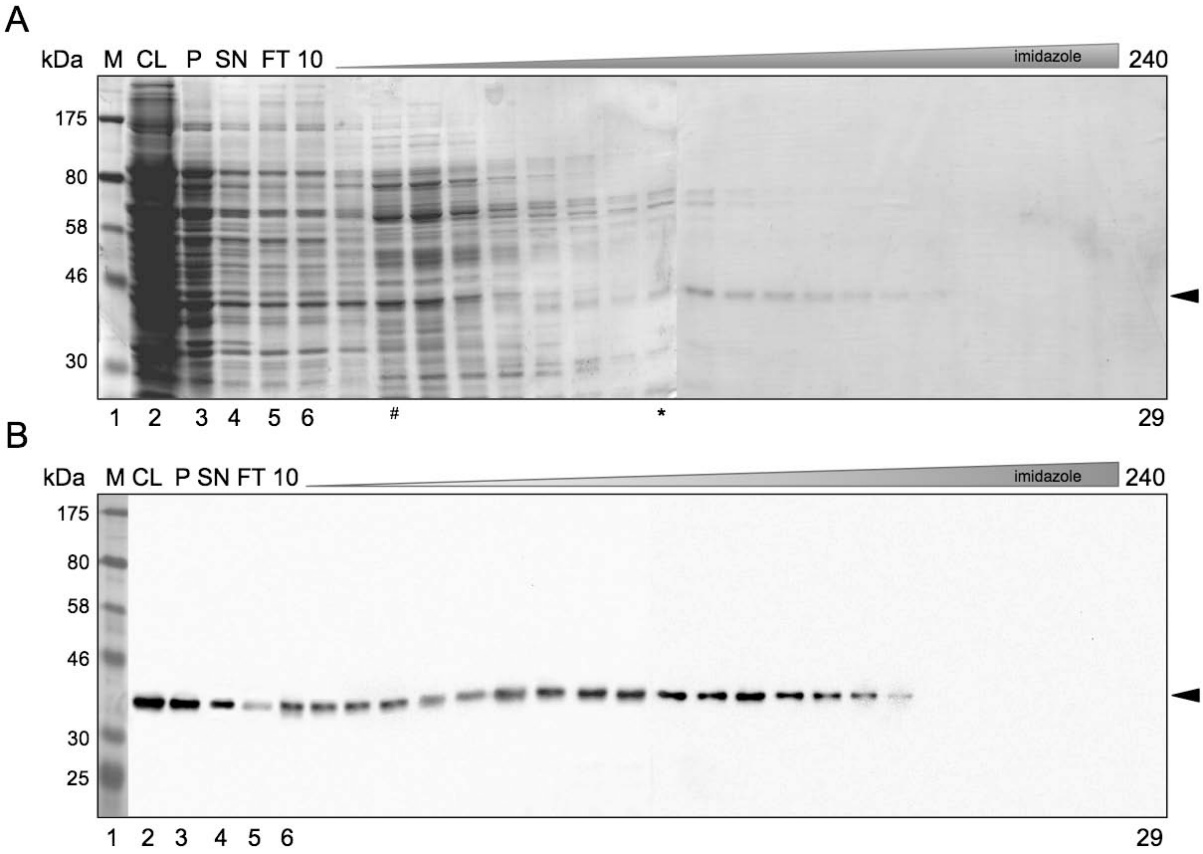

Figure 9: Analysis of Nanog-TAT expression and imidazole gradient
(**A**) SDS-PAGE analysis reveals expression of recombinant Nanog-TAT. During washing steps the fusion protein can be enriched (black arrowhead). Upon application of washing buffer containing 100mM (indicated by *) of imidazole Nanog-TAT shows least contaminating bands. Black arrowhead shows the recombinant protein. (**B**) Immunoblot analysis employing α-Nanog antibody indicates expression of recombinant Nanog-TAT in the CL fraction. A major part of Nanog-TAT is detected in the insoluble fraction. Throughout the washing fractions Nanog-TAT detection is visible up to concentrations of 170mM of imidazole. Black arrowhead shows the recombinant protein. SDS-PAGE and immunoblot were performed with a gel exhibiting a concentration of 10% (bis)acrylamide. M: marker; CL: crude lysate; P: pellet; SN: supernatant; FT: flow through; 10-240: increasing concentrations of imidazole in mM; *: 100mM of imidazole; #: 30mM of imidazole

The crude lysate (Fig. 9A - lane 2) fraction shows an induction of expression of Nanog-TAT at a molecular mass of approximately 43. The calculated molecular weight for Nanog-TAT is 38kDa. Most of the fusion protein is insoluble (Fig. 9A - lane 3) and seems to be trapped within inclusion bodies. A minor part of the protein remains in the soluble fraction (Fig. 9A - lane 4) though. Although a small amount of the Nanog-TAT fusion protein gets washed off, a major part of the contaminations accompanying Nanog-TAT can be eliminated through washing with buffers containing concentrations of up to 100mM of imidazole (Fig. 9A - lanes 6 to 15). Washing with buffers containing more than 100mM of imidazole results in a relatively pure fusion protein containing almost only very few high-molecular contaminations (Fig. 9A - lane 16). In order to identify the Nanog-TAT fusion protein the samples of the imidazole gradient were also subjected to SDS-PAGE followed by immunoblot analysis. Via immunoblot analysis applying a α-Nanog

antibody, Nanog-TAT can be identified in the crude lysate (Fig. 9B - lane 2). Like in the SDS-PAGE Nanog-TAT exhibits a molecular mass of around 43. The major part of the fusion protein is likely to be accumulated within inclusion bodies (Fig. 9B - lane 3) though. A strong signal indicating Nanog-TAT in the supernatant could be observed (Fig. 9B - lane 4). A negligible part of Nanog-TAT was depleted within the flow through fraction (Fig. 9B - lane 5). Upon increasing concentrations of imidazole Nanog-TAT was detectable up to concentrations of 170mM of imidazole within the buffer (Fig. 9B - lanes 6 to 22). No fusion protein could be detected in later fractions, indicating that Nanog-TAT was completely displaced from the column by imidazole. This assumption was further strengthened since no tailing effect of the fusion protein could be observed within the immunoblot. The tailing effect normally occurs when not all of the protein can be eluted in one step, mostly due to the small volume of buffer applied on the column when performing an imidazole gradient. Tailing of the proteins analyzed by imidazole gradient sometimes has to be taken into consideration when defining optimal washing buffer conditions.

3.1.2 Denaturing purification of Nanog-TAT

The observation that Nanog-TAT was highly enriched within the insoluble fraction, indicating formation of inclusion bodies, strongly suggested protein purification under denaturing conditions. Thus, Nanog-TAT purification under denaturing conditions from the insoluble fraction and refolding in a rapid dilution paradigm was assessed. Judged by SDS-PAGE analysis, Nanog-TAT exhibited high purity after 3 out of 15 refolding conditions (Fig. 10A). Immunoblot identified Nanog-TAT (Fig. 10B). Buffer exchange could be conducted using PD10 desalting columns and Nanog-TAT was still detectable (Fig.10C). The buffer conditions were incompatible with cell culture conditions though, as Triton-X100, one component of the refolding buffers analyzed, could not be eliminated via dialysis. Consequently cells transduced with Nanog-TAT from denaturing purification possibly underwent apoptosis, since Triton-X100 is able to disrupt the cellular membrane.

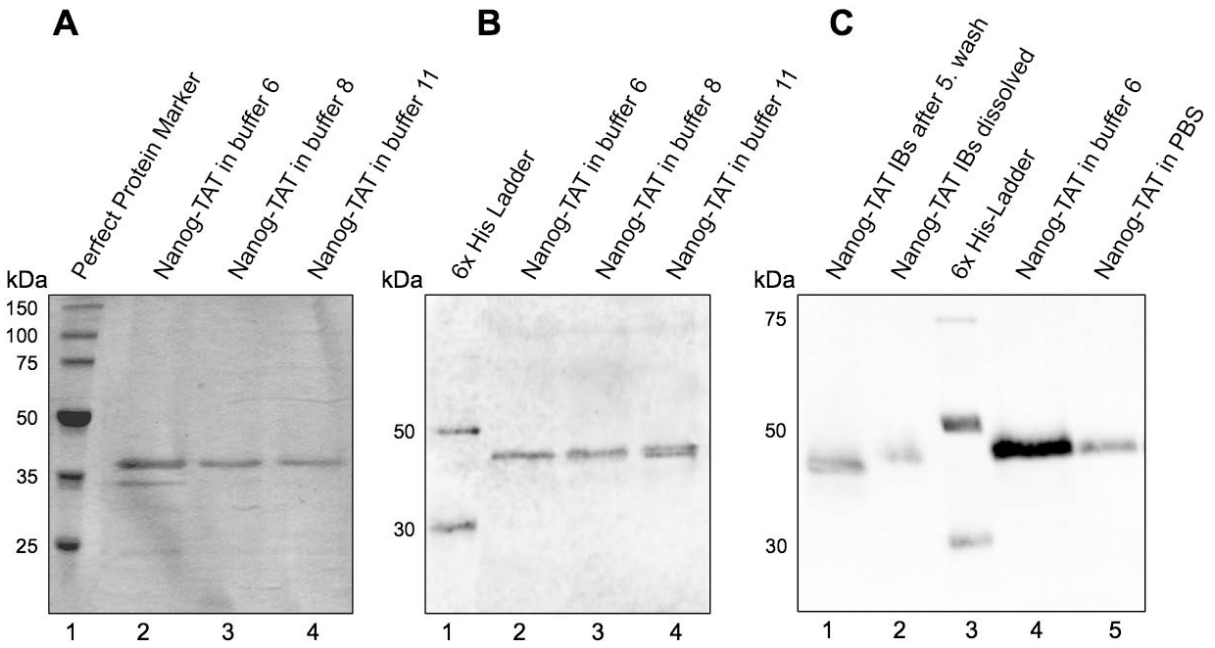

Figure 10: SDS-PAGE and immunoblot analysis of denaturing purification
(**A**) SDS-PAGE. Inclusion bodies were purified and subsequently subjected to a refolding paradigm using a rapid dilution approach. Buffer conditions were analyzed via SDS-PAGE. 3 out of 15 refolding conditions showed highly pure Nanog fusion protein. (**B**) The same samples were analyzed via immunoblot applying a α-His antibody in order to identify the recombinant fusion protein. (**C**) Chronologically gained samples from denaturing purification, refolding and dialysis were analyzed via immunoblot employing a α-His antibody. SDS-PAGE and immunoblot were performed with a gel exhibiting a concentration of 10% (bis)acrylamide. IB: inclusion bodies

3.1.3 An optimized purification protocol for Nanog-TAT

Based on these results a native protocol for the purification of Nanog-TAT had to be established (Fig. 11). Lysis of the bacteria cells was performed in the presence of low concentrations of imidazole in order to guarantee proper binding of Nanog-TAT to the Nickel ions. The washing buffer exhibited a concentration of 100mM of imidazole, since this condition showed least contaminations within the SDS-PAGE of the imidazole gradient (Figure 9A *). This enabled enrichment of a highly pure Nanog-TAT fusion protein, although a great proportion of the protein-of-interest was washed off (Fig. 11 – lane 4). On the other hand though, all contaminating proteins could be eliminated as judged by SDS-PAGE. Therefore the washing procedure with 100mM of imidazole seemed to be the optimal purification condition. The protein was finally eluted with a buffer containing 250mM of imidazole to ensure complete displacement of Nanog-TAT by imidazole. SDS-PAGE analysis shows a pure fusion protein (Fig. 11 – lane 5). The recombinant Nanog-TAT could be identified by immunoblot applying a α-Nanog antibody (Fig. 11 – lane 6).

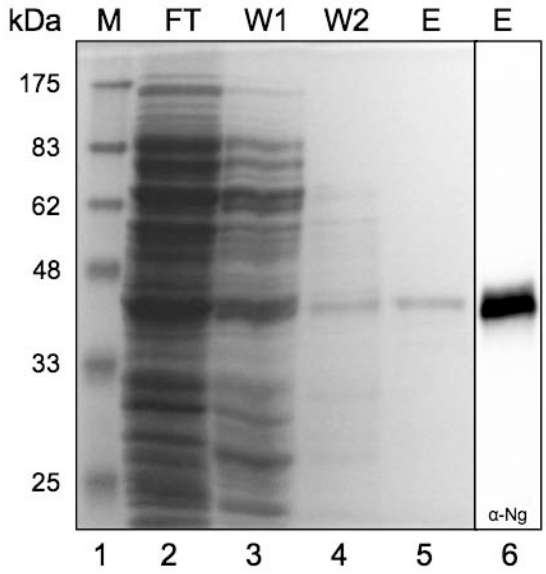

Figure 11: SDS-PAGE and immunoblot analysis of optimized native purification conditions
Washing with 5x column bed volumes of buffer containing 100mM of imidazole led to a highly pure Nanog fusion protein, which could be identified by immunoblot analysis applying α-Nanog antibody. SDS-PAGE and immunoblot were performed with a gel exhibiting a concentration of 10% (bis)acrylamide. M: marker; FT: flow through; W: washing; E: eluate

Dialysis against a glycerol-based buffer and the use of vivaspin columns further concentrated Nanog-TAT judged by SDS-PAGE from 130µg/mL up to over 1mg/mL measured via Bradford assay (Fig. 12A – lane 2). The concentration by vivaspin columns revealed some minor contaminating protein bands within the glycerol stock analyzed by SDS-PAGE, which were not visible in Figure 11 due to the low concentration of protein. The Nanog-TAT fusion protein could then be stored at -20°C for prolonged periods of time. Interestingly, upon dilution in cell culture medium, i.e. physiological conditions, the Nanog-TAT fusion protein almost completely precipitated as analyzed by immunoblot performed with α-Nanog antibody (Fig. 12B – lane 3).

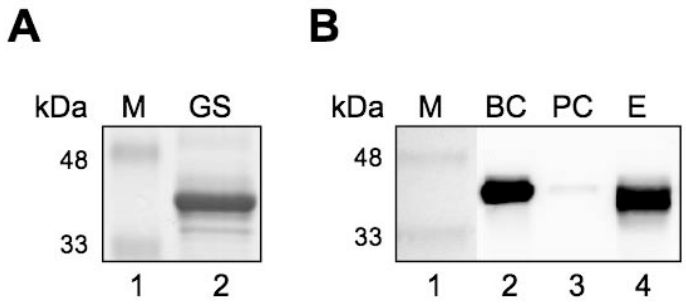

Figure 12: SDS-PAGE and immunoblot indicate that highly pure Nanog-TAT is not stable under physiological conditions
(**A**) SDS-PAGE. The eluate fraction can be concentrated via dialysis and vivaspin columns up to over 1mg/mL. Dialysis of the eluate fraction against a glycerol buffer leads to a 6-fold concentration of Nanog-TAT. Subsequent centrifugation of the glycerol stock solution using a vivaspin column leads to a final concentration of 1mg/mL of recombinant fusion protein (**B**) Immunoblot. When diluting an amount of Nanog-TAT - corresponding to the amount available after elution - from the glycerol stock into readily supplemented cell culture medium the protein almost completely precipitates. SDS-PAGE and immunoblot were performed with a gel exhibiting a concentration of 10% (bis)acrylamide. M: marker; GS: glycerol stock; BC: before centrifugation; PC: post centrifugation; E: eluate fraction

Given the low solubility of Nanog-TAT in the medium after dilution from the glycerol stock, an adapted protocol for the purification of Nanog-TAT had to be established. To enable Nanog-TAT to efficiently bind to the Ni-NTA matrix a low concentration of imidazole within the lysis buffer was chosen. The concentration of imidazole within the washing buffer was lowered compared to the protocol mentioned above, as some of the contaminations could exhibit a stabilizing effect on the Nanog-TAT fusion protein and therefore prevent precipitation after transfer of Nanog-TAT in physiological conditions.

Bacteria pellets were lysed in a buffer containing 5mM of imidazole. Washing steps were performed with a buffer containing 30mM of imidazole. 250mM of imidazole was used to entirely dissociate Nanog-TAT fusion protein from the Ni-NTA matrix.

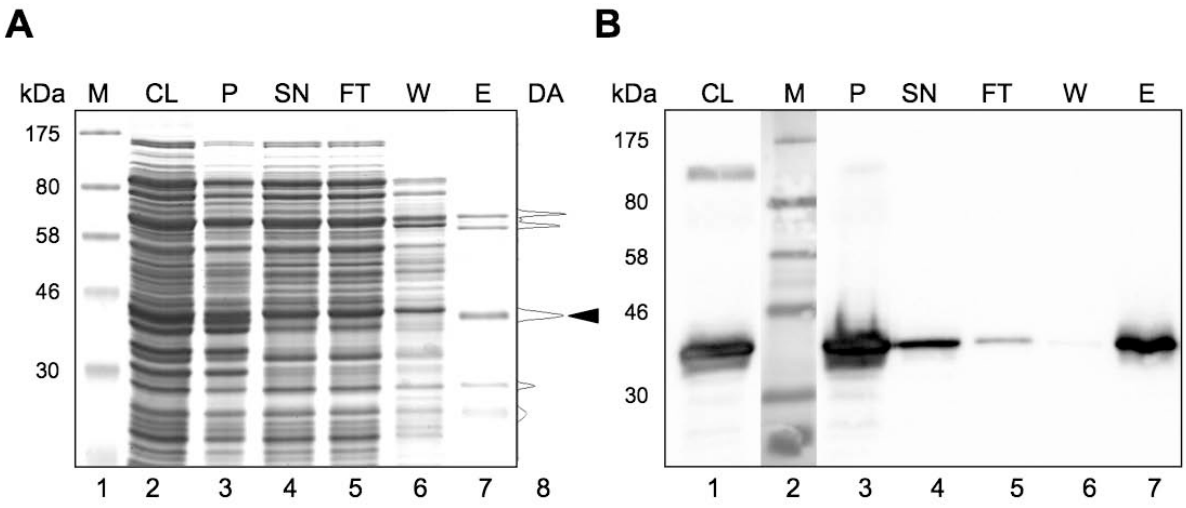

Figure 13: Adapted purification protocol for Nanog-TAT
(**A**) SDS-PAGE. A chronological loading of samples taken during the process of purification of Nanog-TAT under optimized conditions is shown. Washing with 10x column bed volume of buffer containing 30mM of imidazole results in a relatively pure Nanog-TAT fusion protein that can be enriched in the eluate fraction (black arrowhead). (**B**) Immunoblot analysis applying anti-Nanog antibody identifies Nanog-TAT and confirms the results obtained in SDS-PAGE analysis. SDS-PAGE and immunoblot were performed with a gel exhibiting a concentration of 10% (bis)acrylamide. M: marker; CL: cleared lysate; P: pellet; SN: supernatant; FT: flow through; W: washing; E: eluate; DA: densitometric analysis

With the adapted purification protocol Nanog-TAT can be enriched in the eluate fraction as shown in the SDS-PAGE. The amount of Nanog-TAT fusion protein lost during washing of the column is minimized (Fig. 13B – lane 5) compared to washing steps performed with 100mM of imidazole (Fig. 11 – lanes 3 and 4). In addition to the Nanog-TAT fusion protein, 2 high molecular contaminations are detectable within the eluate fraction at a molecular mass of 60 to 70. Furthermore, 2 low molecular contaminations stain in the SDS-PAGE at a molecular mass of around 25 (Fig. 13A – lane 7). None of these contaminations are detected in the corresponding immunoblot (Fig. 13B – lane 7). Densitometric analysis reveals a share of 39.8% of Nanog-TAT within the eluate fraction (Fig. 13A – lane 8). An additional weak band is seen on the immunoblot within the crude lysate at a molecular mass of 130 (Fig. 13B – lane 1). This additional band results from unspecific binding of the antibody, as the appearance of the band is stated in the datasheet provided by the manufacturer of the antibody. A minor amount of the Nanog-TAT fusion protein is lost in the flow through fraction, as shown in the immunoblot (Fig. 13B – lane 5). If the concentration of imidazole within the lysis buffer is further lowered, in order to avoid loss of Nanog-TAT in the flow through fraction, additional contaminating bands appear in the eluate fraction analyzed by SDS-PAGE (data not shown).

The Nanog-TAT fusion protein is then dialyzed at 4°C against physiological buffer to get rid of the imidazole exhibiting toxicity and to provide salt concentrations necessary for the cultivation of mammalian cells. A part of the fusion protein is lost during dialysis. Adjustment of the

temperature to 37°C further diminishes the amount of Nanog-TAT fusion protein as only one fifth of the remaining Nanog-TAT originating from the dialysis is soluble then. Nanog-TAT is relatively stable under cell culture conditions, i.e. cell culture medium consisting of Advanced DMEM supplemented with 5% FCS at 37°C, if pre-incubated at 37°C for 2 hours before usage in cell culture experiments. Dot blot analysis revealed that Nanog-TAT exhibited a concentration of 100nM. After 48 hours *in vitro* only around 50% of the Nanog-TAT fusion protein could be detected via immunoblot compared to 0 hours. Co-incubation of the fusion protein with CV1 fibroblasts for 24 hours led to a reduction of the Nanog-TAT signal to 50% as well (Fig. 14). Therefore a change of medium was conducted every 24 hours in all experiments performed with the Nanog-TAT fusion protein.

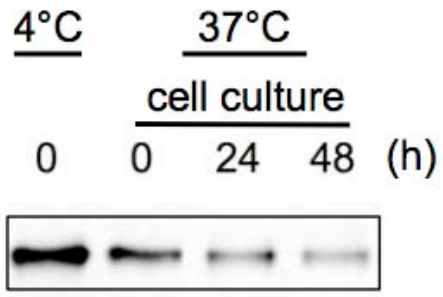

Figure 14: Stability of Nanog-TAT under cell culture conditions is 24h
Nanog-TAT was applied onto fibroblast cells. After indicated time points samples for immunoblot analysis were taken and analyzed applying α-Nanog antibody. After 24h the intensity of the Nanog band is diminished to approximately 50%. Immunoblot was performed with a gel exhibiting 10% (bis)acrylamide (in collaboration with M. Peitz, unpublished data).

In conclusion, Nanog-TAT could be reproducibly expressed in and purified from *E.coli* and could be brought to physiological conditions at a final concentration of 100nM. These optimized conditions represent a robust basis to perform experiments with Nanog-TAT in cell culture.

3.1.4 Assessing purification conditions for ΔNanog-TAT

Assessment of optimal conditions for the purification of ΔNanog-TAT was achieved by means of an imidazole gradient. A bacteria pellet was subjected to lysis and the soluble fraction was incubated with Ni-NTA slurry and subjected onto a gravity flow column. Subsequently an imidazole gradient exhibiting a stepwise increase of concentration of imidazole from 10 to 240mM was applied. Samples from every fraction throughout the purification process were taken, transferred into SDS-PAGE sample buffer and subjected onto SDS-PAGE for analysis.

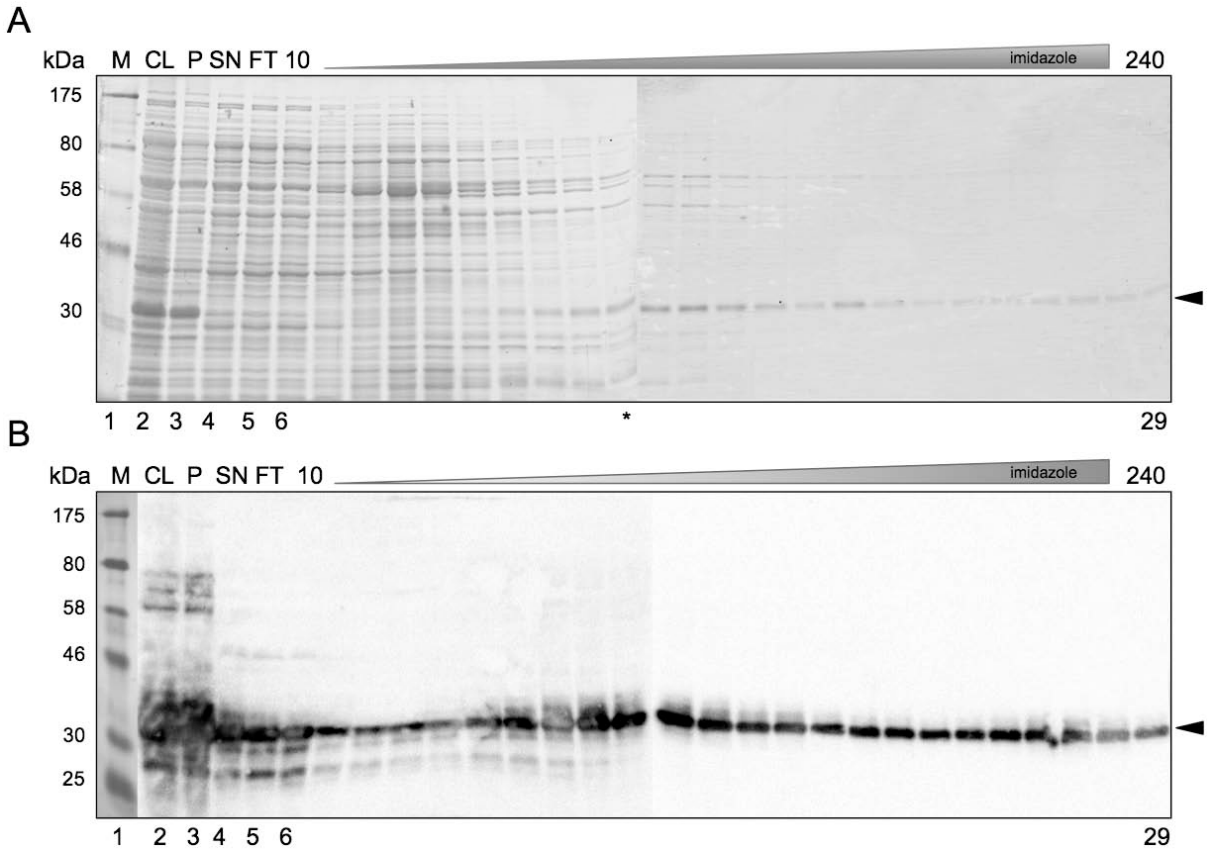

Figure 15: SDS-PAGE analysis of ΔNanog-TAT subjected to an imidazole gradient
(**A**) The expression of recombinant ΔNanog-TAT can be detected in the fraction of the crude lysate within the SDS-PAGE. Approximately 50% of the protein is found within the pellet fraction. Increasing concentrations of imidazole in the washing buffer enriches the fusion protein. Upon application of washing buffer containing 100mM (marked by *) of imidazole, ΔNanog-TAT shows least contamination bands. A relatively pure protein band indicating for ΔNanog-TAT can be detected in buffers containing concentrations of 110 to 240mM of imidazole. Black arrowhead shows the recombinant protein. (**B**) Induction of expression of recombinant ΔNanog-TAT can be detected in the CL fraction via immunoblot. A major part of ΔNanog-TAT is detected within the insoluble fraction as well as in the flow through. ΔNanog-TAT detection is visible throughout all fractions of the imidazole gradient. Black arrowhead shows the recombinant protein. Immunoblot was performed with a gel exhibiting a concentration of 10% (bis)acrylamide. M: marker; CL: crude lysate; P: pellet; SN: supernatant; FT: flow through; 10-240: increasing concentrations of imidazole in mM

A strong expression of ΔNanog-TAT can be detected within the crude lysate (Fig. 15A - lane 2). Around half of the control protein is found in the pellet fraction, i.e. the insoluble part of the fusion protein (Fig. 15A - lane 3), which is likely to be trapped in inclusion bodies. Still a high amount of ΔNanog-TAT remains in the soluble fraction (Fig. 15A - lane 4). Only a small amount of the ΔNanog-TAT fusion protein gets washed off, as great parts of the contaminations accompanying ΔNanog-TAT can be eliminated through washing with buffers containing concentrations of up to 70mM of imidazole (Fig. 15A - lanes 6 to 12). Washing with buffers containing more than 100mM of imidazole results in a relatively pure fusion protein containing only few high-molecular contaminations. In contrast to the full-length protein, a band indicating

ΔNanog-TAT is detectable throughout all late fractions of the imidazole gradient (Fig. 15A - lanes 16 to 29).

In order to identify the ΔNanog-TAT fusion protein the samples of the imidazole gradient were subjected to SDS-PAGE followed by immunoblot analysis performed with an α-Nanog antibody.

ΔNanog-TAT can be identified through the α-Nanog antibody exhibiting a molecular mass of around 33. The calculated molecular weight of the protein is 30.2kDa. The expression of ΔNanog-TAT can be strongly detected within the crude lysate (Fig. 15B - lane 2). A high proportion of about 50% of the recombinant protein is found in the pellet fraction, i.e. the insoluble part of the fusion protein (Fig. 15B - lane 3). Obviously the fusion protein appears to be trapped in inclusion bodies. As the SDS-PAGE does not reveal the loss of a substantial amount of ΔNanog-TAT, immunoblot analysis clearly indicates that a big amount of the fusion proteins is lost in the flow through fraction (Fig. 15B – lane 5). A big fraction of ΔNanog-TAT remains in the soluble fraction though (Fig. 15B - lane 4). Upon washing, increasing fractions of ΔNanog-TAT are lost. Nevertheless, a major part of the contaminations accompanying ΔNanog-TAT can be eliminated as seen in SDS-PAGE analysis. As in the early fractions the α-Nanog antibody recognizes additional bands besides the one detecting the recombinant fusion protein, no additional bands are detected in later fractions (Fig. 15B - lanes 16 to 29). In contrast to the full-length protein, ΔNanog-TAT is visible throughout all fractions of the imidazole gradient on the immunoblot, verifying observations made in SDS-PAGE analysis. This phenomenon is likely due to the tailing effect described above.

3.1.5 Purifying ΔNanog-TAT under optimized conditions

Based on the data gained from the SDS-PAGE and immunoblot analysis an optimized purification protocol for ΔNanog-TAT could be established. ΔNanog-TAT was eluted with a high concentration of imidazole. As the recombinant protein was detectable throughout all fractions of the imidazole gradient in the SDS-PAGE, a final washing step with a buffer including EDTA instead of imidazole was performed. As EDTA exhibits a higher affinity to the nickel ions of the Ni-NTA matrix than imidazole, this procedure ensured complete displacement of ΔNanog-TAT from the column. As analyzed by SDS-PAGE these fractions did not contain any recombinant fusion protein (data not shown).

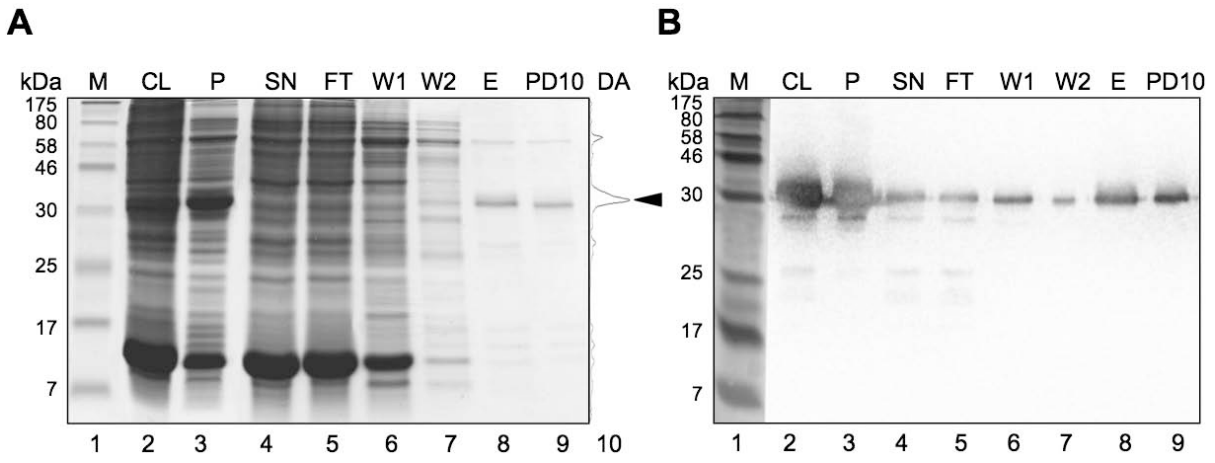

Figure 16: Optimized purification protocol for ΔNanog-TAT analyzed by SDS-PAGE and immunoblot
(**A**) A chronological loading of samples taken during the process of purification of ΔNanog-TAT under optimized conditions is shown in the SDS-PAGE. Washing with 100mM of imidazole yields a pure ΔNanog-TAT fusion protein that can be enriched in the eluate fraction (black arrowhead). (**B**) Immunoblot analysis applying α-Nanog antibody identifies ΔNanog-TAT and verifies the results obtained in SDS-PAGE analysis. SDS-PAGE and immunoblot were performed with a gel exhibiting 15% (bis)acrylamide. M: marker; CL: cleared lysate; P: pellet; SN: supernatant; FT: flow through; W: washing; E: eluate; PD10: PD10 desalting column; DA: densitometric analysis

The optimized purification protocol for ΔNanog-TAT yields a highly pure eluate fraction as analyzed in the SDS-PAGE. A faint band indicating a contamination at a molecular mass of around 60 can be observed within the eluate fraction. Additionally low molecular contaminations at a molecular mass of 17 and smaller are visible (Fig. 16A – lane 8). None of these contaminations are detected in the corresponding immunoblot (Fig. 16B – lane 8). Densitometric analysis indicates that 54% of the whole mount protein represents ΔNanog-TAT (Fig. 16A – lane 10). Although SDS-PAGE does not suggest a substantial loss of recombinant protein (Fig. 16A – lanes 5 to 7), immunoblot reveals control fusion protein within the flow through fraction as well as the washing fractions (Fig. 16B – lanes 5 to 7). However, a considerable amount of ΔNanog-TAT can be detected in the eluate fraction. Additional bands at a molecular mass of 25 are seen on the immunoblot within the crude lysate, supernatant and flow through (Fig. 16B – lane 2, 4, 5).

The ΔNanog-TAT fusion protein could not be dialyzed at 4°C as the control protein tended to precipitate (data not shown) during this buffer exchange procedure.

Therefore buffer exchange for ΔNanog-TAT was conducted using a PD10 desalting column. The control protein could be detected after PD10 treatment in both, SDS-PAGE and immunoblot (Fig. 16A, B – lane 9). ΔNanog-TAT was stable under cell culture conditions, i.e. cell culture medium consisting of Advanced D-MEM supplemented with 5% FCS at 37°C. As for Nanog-TAT it was necessary to pre-incubate the control protein at 37°C for 2 hours before final usage in cell

culture experiments. This measure ensured that all of the fusion protein prone to precipitation under cell culture conditions would be eliminated.

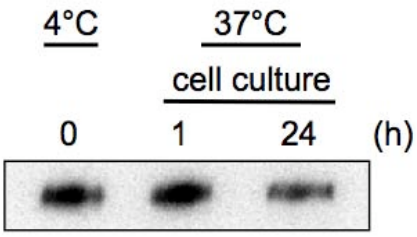

Figure 17: Stability of ΔNanog-TAT under cell culture conditions is 24h
ΔNanog-TAT was applied onto fibroblast cells. After indicated time points samples for immunoblot analysis were taken and analyzed applying α-Nanog antibody. After 24h the intensity of the Nanog band is diminished to 41% determined by densitometric analysis. Immunoblot was performed with a gel exhibiting 15% (bis)acrylamide.

Stability of ΔNanog-TAT was assessed via immunoblotting (Fig. 17). After incubation of fibroblasts with ΔNanog-TAT for 1 hour and 24 hours, samples were taken and compared to medium stored at 4°C. After 1 hour at 37°C almost no protein is lost compared to medium stored at 4°C. 59% of the control protein is lost after incubation for 24 hours at 37°C on fibroblast cells (Fig. 17 - right lane). Therefore a change of medium was conducted every 24 hours in all experiments performed with the ΔNanog-TAT fusion protein. Dot blot analysis revealed that the final concentration of ΔNanog-TAT under cell culture conditions was approximately 50nM. The concentration of ΔNanog-TAT could not be further increased using fewer volumes of elution buffer, since there appears to be a certain threshold of maximal soluble recombinant control protein as observed for Nanog-TAT.

In conclusion, ΔNanog-TAT could be reproducibly expressed in and purified from *E.coli* and could be brought to physiological conditions at a final concentration of 50nM. These established conditions represent a robust basis to perform experiments with ΔNanog-TAT in cell culture.

3.2 Functional validation of Nanog-TAT and ΔNanog-TAT

3.2.1 Recombinant Nanog-TAT specifically binds to consensus sequence

Since Nanog, being a transcription factor, can exert its main functionality only when capable of binding to distinct DNA sequences the recombinant Nanog-TAT as well as the control protein ΔNanog-TAT were subjected to an electrophoretic mobility shift assay (EMSA). To test for protein-DNA binding both proteins were incubated with a Nanog consensus sequence (Pan and

Pei, 2005). Specificity of the binding reaction was analyzed by addition of excess competitor, i.e. unlabeled DNA.

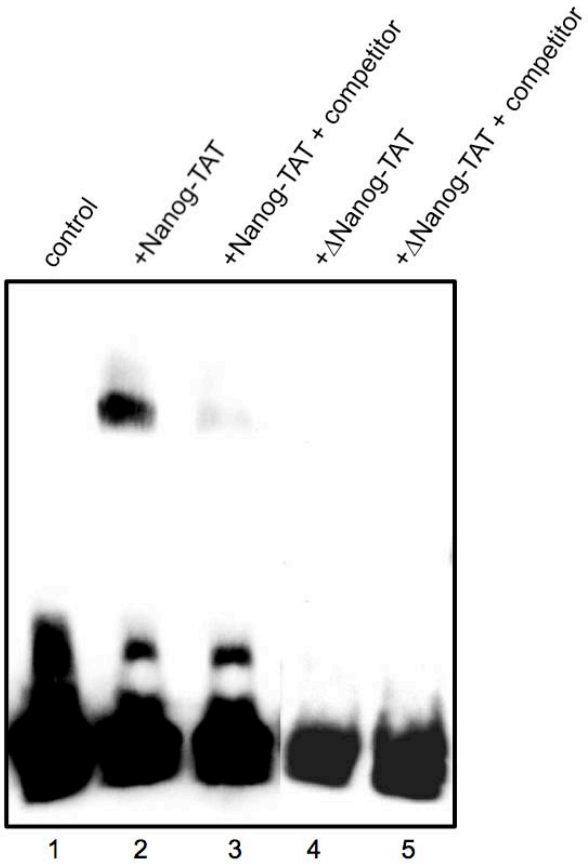

Figure 18: EMSA reveals binding of Nanog-TAT to consensus sequence
Nanog-TAT was subjected to an EMSA employing a specific Nanog consensus sequence. A shift of the protein-DNA complex is observed. The shift can be prevented by the addition of excess unlabeled DNA (competitor). No shift is observed in case of the control protein ΔNanog-TAT. The binding reaction containing 100ng of recombinant protein respectively was subjected to a native PAGE exhibiting 5% (bis)acrylamide. After the gel run was completed the protein-DNA complexes were transferred onto a corresponding membrane and the shift was detected using streptavidin-HRP conjugates.

A clear shift could be observed in lane 2 of the blot, indicating recognition and consequently binding of Nanog-TAT to the corresponding consensus sequence (Fig. 18). The specificity of the protein-DNA binding was verified by the addition of excess unlabeled DNA seen in lane 3. No shift was observed when Nanog-TAT was omitted from the binding reaction as seen in lane 1, which served as a control. Free DNA probe is accumulated at the bottom of the blot in all three lanes. In contrast, the control protein ΔNanog-TAT was not capable of binding to the Nanog consensus sequence (Fig.18 - lane 4). No shift was visible if the control protein or an excess of unlabeled DNA was present in the binding reaction as seen in lane 5 (Fig. 18). Free DNA probe could be detected at the very bottom of the blot.

3.2.2 Nanog-TAT as well as ΔNanog-TAT is able to translocate into mammalian cells

After demonstrating that recombinant Nanog-TAT is able to specifically bind to DNA *in vitro*, the ability to translocate into cultured cells was explored. The cell membrane poses a natural barrier for molecules trying to enter the cell. Through the addition of the protein transduction domain TAT to both fusion proteins the ability to cross this frontier, i.e. to translocate into the cell, should be conferred. To investigate the ability of Nanog-TAT as well as ΔNanog-TAT to accomplish TAT-mediated trans-membrane transport into mammalian cells, the two fusion proteins were applied onto CV1 fibroblast cells. After 5 hours cells were washed with heparin, fixed with 4% PFA and analyzed by ICC employing α-Nanog antibody, which represents a standard protocol for the evaluation of cellular uptake (Kaplan et al., 2005). Washing with heparin ensures the stripping of recombinant fusion protein from the cellular surface.

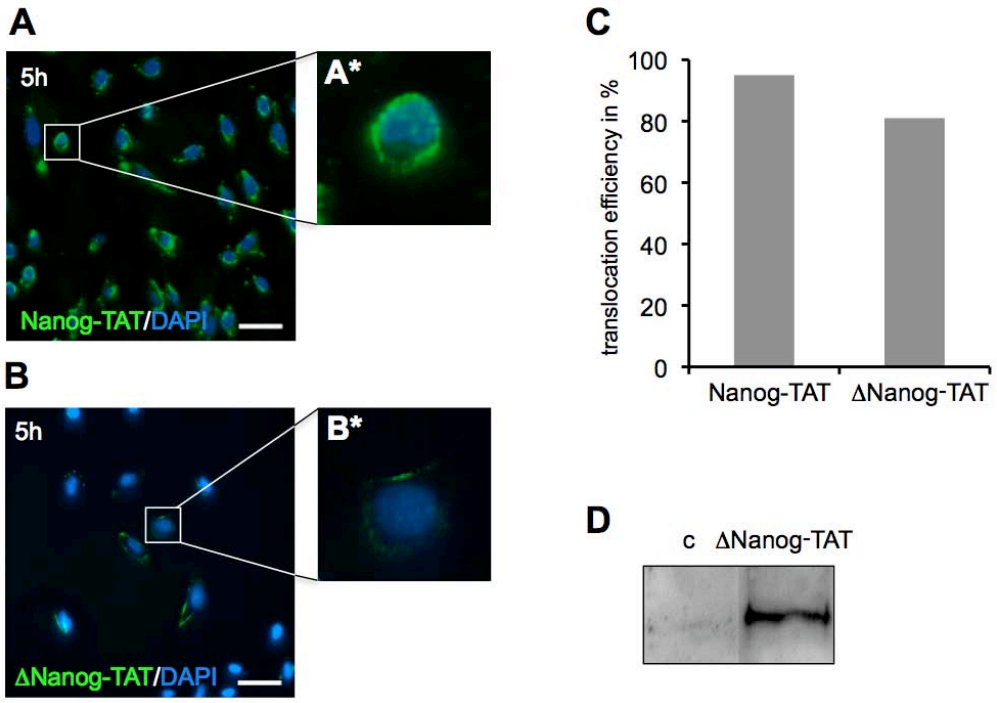

Figure 19: Assessing cellular translocation of Nanog fusion proteins into mammalian cells
(**A** and **B**) 100nM of Nanog-TAT as well as 50nM of ΔNanog-TAT were subjected onto fibroblast cells (CV1) for 5h. Cells were then washed using heparin and fixed. Immunocytochemistry employing an α-Nanog antibody revealed translocation of both fusion proteins into CV1 cells. A high-resolution picture of a single cell cultivated with Nanog-TAT (**A***) and ΔNanog-TAT (**B***) for 5h is shown. Nuclei were counterstained with DAPI. Scale bar 25µm. (**C**) A quantification of CV1 cells staining positive for Nanog is depicted. Nanog-TAT can be detected in >95% of all cells analyzed, whereas cells cultivated with ΔNanog-TAT exhibited 80% positive cells. (**D**) Like for Nanog-TAT (Peitz, 2007), within nuclear extracts of CV1 cells cultivated with ΔNanog-TAT, the recombinant control protein was detectable via immunoblot, whereas nuclear extracts of control cells did not show any signal. Immunoblot was performed with a gel exhibiting 10% (bis)acrylamide; c: control.

After 5 hours of cultivation with 100nM of Nanog-TAT over 95% of the cells stained vastly for cytoplasmatic vesicles enriched for Nanog (Fig. 19A, C) and the recombinant protein strongly accumulated in a perinuclear pattern, which can be seen in detail at a higher magnification of a single transduced cell (Fig. 19A*). In contrast, after 5 hours of cultivation with 50nM of ΔNanog-TAT only 80% (Fig. 19B, C) of CV1 cells stained positive for Nanog, basically in the cytoplasm though. Only a minority of the fibroblast cells already displayed a staining in a perinuclear pattern. The process of TAT-mediated trans-membrane trafficking for ΔNanog-TAT seems to be decelerated, when compared to cells tranduced with Nanog-TAT. Eventually the lower concentration of 50nM of ΔNanog-TAT compared to 100nM of Nanog-TAT might be causal for the observation above, although Nanog-TAT exhibits similar or even more articulate effects when applied at 50nM or 100nM in a foci formation assay on NIH 3T3 cells (Winnemöller, 2007). For a more detailed view of a single cell cultivated with ΔNanog-TAT for 5 hours, see Fig. 19B*. Additionally, ΔNanog-TAT is detectable by immunoblot applying α-Nanog antibody within nuclear extracts of CV1 cells cultivated for 2 days with 50nM of recombinant control protein (Fig.19 D). Just as ΔNanog-TAT, Nanog-TAT is detectable within nuclear extracts of CV1 fibroblast cells (Peitz, 2007), suggesting transport of both recombinant fusion proteins into the nucleus of mammalian cells.

Taken together, these results lead to the assumption that both fusion proteins were able to cross the cellular membrane. The washing step performed with heparin excludes the possibility that extracellular recombinant protein was detected in ICC analysis.

3.2.3 Direct delivery of Nanog-TAT specifically circumvents LIF dependence of murine ES cells

Initial studies in our workgroup showed that Nanog-TAT is able to liberate murine ES cells from LIF dependence, a feature known from murine ES cells overexpressing Nanog (Chambers et al., 2003). Nanog-TAT is able to sustain 'undifferentiated', AP-positive ES cells in the absence of LIF, the addition of the peptide TAT-HA2 was required though. TAT-HA2 is known to promote the process of protein transduction, but unexpectedly the addition of TAT-HA2 also led to precipitation of Nanog-TAT. In the absence of TAT-HA2, Nanog-TAT is able to maintain mixed ES cell colonies over 3 days (Fig. 20A; black arrowhead). A pluripotent population arises as judged by activity of the Oct3/4 promoter region driving GFP expression upon cultivation of Oct3/4 GiP ES cells in the absence of LIF and in the presence of 100nM of Nanog-TAT (Peitz, 2007). In order to assess the morphological effect of Nanog-TAT on murine ES cells, cells were fixed and ES cell colonies were classified into three categories. The first category, termed 'undifferentiated', encompassed compact colonies with sharp edges strongly staining for AP. The second category

comprised colonies, which already lost the sharp edges and stained partially for AP. This category was named 'mixed'. The third category was named 'differentiated' and contains colonies, which already lost the compact, three-dimensional structure and did not stain for AP.

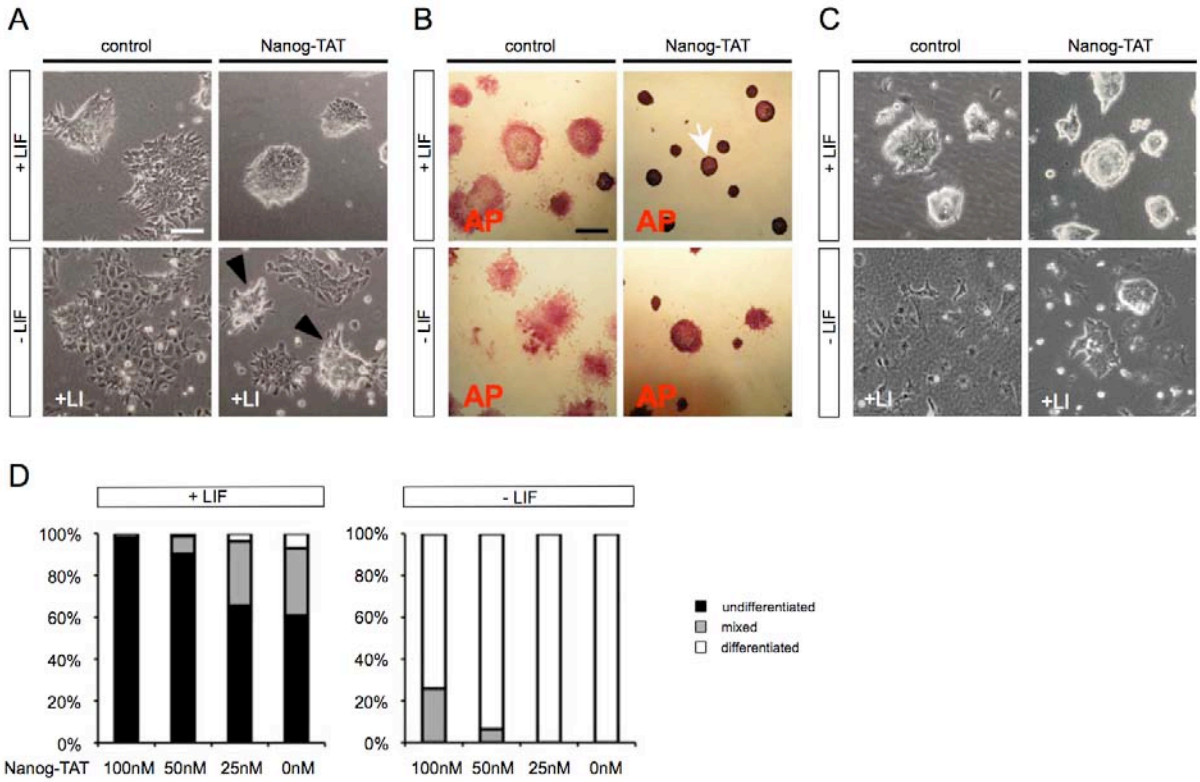

Figure 20: Nanog-TAT sustains pluripotency in ES cells in the absence of LIF
(**A**) 100nM of Nanog-TAT was subjected onto C57BL/6 ES cells for 3 days either in the absence or presence of cytokine LIF. Experiments performed in the absence of LIF additionally contained LIF inhibitor (Vernallis et al., 1997) to completely exclude LIF signaling. Namely, LIF activity is expected to occur upon spontaneous differentiation in a paracrine manner. Over a 3-day period cells cultivated without LIF and in the presence of Nanog-TAT start to differentiate but still show mixed colonies (black arrowhead). ES cells cultivated with control medium differentiate. Scale bar: 50µm (**B**). After 3 days, ES cells were fixed and stained for alkaline phosphatase. In the presence of LIF and 100nM of Nanog-TAT only undifferentiated ES colonies are present, whereas ES cells cultivated in the absence of LIF and the presence of 100nM of Nanog-TAT contain mixed colonies. Scale bar: 100µm. (**C**) After 3 passages, Oct3/4 GiP ES cells cultivated in the absence of LIF and in the presence of 100nM of Nanog-TAT still exhibit mixed colonies. (**D**) A quantification of the morphological effect of Nanog-TAT on C57BL/6 ES cells cultivated for 5 days in different concentrations of Nanog-TAT in the presence or absence of LIF is shown. For classification see text. LIF: leukemia inhibitory factor, LI: LIF inhibitor, AP: alkaline phosphatase (in collaboration with M. Peitz, unpublished data)

In the presence of LIF the amount of undifferentiated ES cell colonies increases from 60% to over 95%. In the absence of LIF, differentiation of ES cells is inhibited. In the presence of Nanog-TAT, 25% of mixed colonies are still observed, whereas the complete absence of Nanog-TAT leads to full differentiation (Fig. 20D). In order to investigate whether the effect observed on C57BL/6 ES cells is also apparent on Oct3/4 GiP ES cells, cells were cultivated either in the presence or absence of the cytokine LIF together with 100nM of Nanog-TAT. After 3 passages in the absence of LIF, ES like colonies are still present (Fig. 20C).

To unambiguously demonstrate that the effect observed upon Nanog-TAT treatment is specific, the use of a control protein was advisable. The use of a different protein like the transducible site-specific recombinase Cre (Peitz et al., 2002) for instance, cannot serve as a proper control due to potentially different contaminating proteins co-purified with the Cre recombinase compared to Nanog-TAT. A point mutation of Nanog, leading to a non-functional variant of the stemness factor is still unknown, so the ommitance of the sequence mediating DNA binding could lead to a proper control protein.

To summarize, a detailed analysis whether or not these effects are specifically due to intracellular Nanog activity was lacking. So as to investigate the specificity, murine ES cells were cultivated in the presence of the newly generated control protein.

3.2.4 ΔNanog-TAT is not able to sustain pluripotency in murine ES cells

In order to investigate if the effects observed were specific for the full-length Nanog fusion protein, the control protein ΔNanog-TAT was applied onto Oct3/4 GiP ES cells. Oct3/4 GiP cells express a puromycin resistence gene under the control of a transgenic Oct3/4 promoter. In order to obtain a stringent pluripotent ES cell population, cells were cultivated with puromycin prior to experiments. Subsequently ES cells were cultivated with ΔNanog-TAT in the presence or absence of LIF. Experiments performed in the absence of LIF additionally contained LIF inhibitor (Vernallis et al., 1997) to completely exclude spontaneously occurring paracrine LIF signaling. Brightfield pictures of each culture condition were taken from day 1 to day 3.

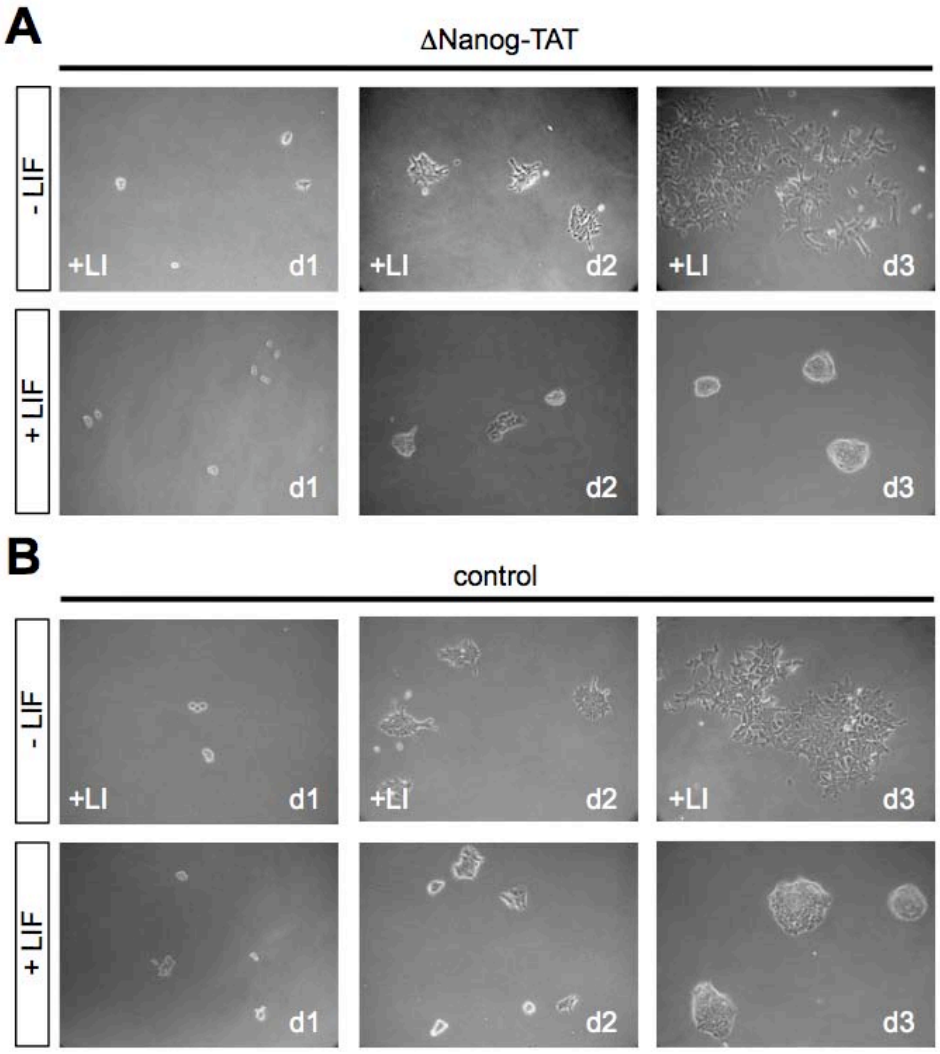

Figure 21: ΔNanog-TAT is not able to sustain pluripotency in ES cells in the absence of LIF
(**A**) 50nM of ΔNanog-TAT was subjected onto Oct3/4 GiP ES cells for 1 to 3 days either in the absence or presence of cytokine LIF. Experiments performed in the absence of LIF additionally contained LIF inhibitor (Vernallis et al., 1997) to completely exclude LIF signaling, as LIF activity is expected to occur upon spontaneous differentiation in a paracrine manner. Over a 3-day period cells cultivated without LIF start to differentiate just like cells cultivated with control ES cell medium (**B**). In the presence of LIF no visible difference between cells treated with ΔNanog-TAT or control ES cell medium is apparent. Magnification 5x. d: day, LIF: leukemia inhibitory factor, LI: LIF inhibitor

Murine ES cells cultivated with ΔNanog-TAT in the absence of the cytokine LIF start to differentiate over the time course of 3 days (Fig. 21A, upper row). ES cell colonies lose the three-dimensional structure as well as the distinct edges otherwise shining brightly. In contrast, ES cells cultivated for 3 days with ΔNanog-TAT and LIF form compact, three-dimensional colonies with bright edges (Fig. 21A, lower row). ES cells cultivated in control medium in the absence of LIF differentiate, i.e. they lose the three-dimensional, pluripotent phenotype resulting in cells growing as a monolayer first, before they finally differentiate. These cells also do not exhibit bright edges (Fig. 21B, upper row). Murine ES cells cultivated with LIF, instead show

densely packed, three-dimensional colonies exhibiting brightly shining edges. The colonies appear to be slightly bigger then the ES cells cultivated with ΔNanog-TAT and LIF.

3.2.5 ES cells cultivated with ΔNanog-TAT show similar expression of alkaline phosphatase as control ES cells

In order to analyze for the capability of sustaining pluripotency, the amount of 'undifferentiated' ES cell colonies of each condition was determined by staining for AP after 3 days of cultivation. Elevated expression of this enzyme is associated with undifferentiated pluripotent stem cells. Colonies were classified into the 3 different categories described in chapter 3.2.3.

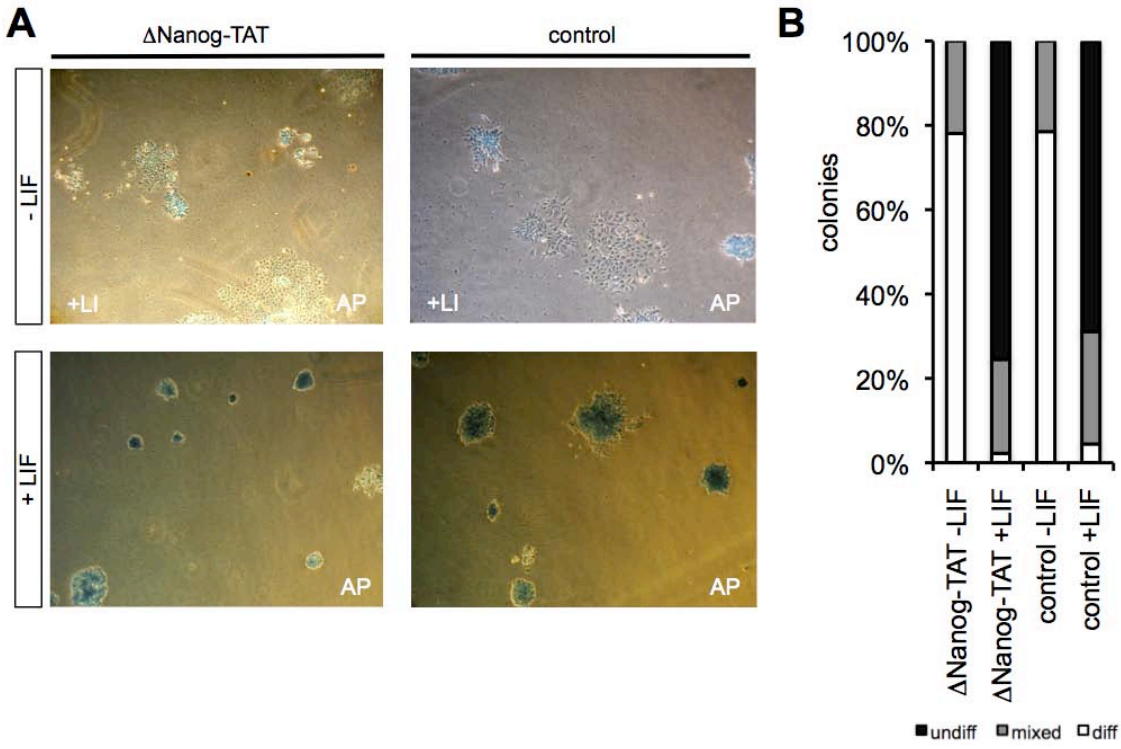

Figure 22: ΔNanog-TAT treated ES cells show similar AP expression pattern compared to cells treated with control medium
(**A**) Murine Oct3/4 GiP ES cells were cultivated with either ΔNanog-TAT or control medium for 3 days in the absence or presence of the cytokine LIF. Cells were then fixed and stained for Alkaline Phosphatase (AP), a marker associated with pluripotency. Cells cultivated in the absence of LIF differentiated almost completely, whereas cells cultivated in the presence of LIF remained undifferentiated. (**B**) A quantification of the AP staining is depicted. 3 types of colonies are distinguished. For classification see text. Magnification in A: 5x

After 3 days, ES cells cultivated with ΔNanog-TAT in the absence of LIF did not contain any 'undifferentiated' colonies. 22% of the colonies displayed a 'mixed' phenotype; the remaining 78% of the colonies were 'differentiated' (Fig. 22A, upper left and Fig. 22B). Cells treated with ΔNanog-TAT and LIF contained 76% of 'undifferentiated' colonies. 22% of the colonies are 'mixed' and 2% of all colonies are 'differentiated' (Fig. 22A, lower left and Fig. 22B). ES cells

cultivated in control medium without LIF exhibited no ‘undifferentiated’ colonies, 22% of ‘mixed’ colonies and 78% of all colonies were ‘differentiated’ (Fig. 22A, upper right and Fig. 22B). In contrast, cells cultivated in control medium supplemented with LIF showed a similar phenotype as the cells cultivated with ΔNanog-TAT and LIF. 70% of the colonies were ‘undifferentiated’, whereas 26% exhibited a ‘mixed’ phenotype. Only 4% of the cells were ‘differentiated’.

In conclusion, these results indicate that the control protein ΔNanog-TAT does not sustain pluripotency of murine ES cells in the absence of LIF nor does it exhibit any kind of synergistical effect when applied in the presence of LIF. The observations made for the full-length protein Nanog-TAT therefore are specific and can be led back to the introduction of Nanog activity via protein transduction.

3.2.6 Functional analysis of Nanog in murine somatic cells

Nanog protein transduction in murine somatic cells has been shown to cause loss of contact inhibition in NIH 3T3 cells as well as an enhanced proliferation rate in MEFs (Winnemöller, 2007). However, the molecular events underlying this phenotypic changes remained unclear. In order to analyze whether or not cell cycle factors are involved, Oct3/4 GiP MEFs cultivated with Nanog-TAT were analyzed applying RT-PCR as well as immunoblot.

3.2.7 Analysis of Nanog function in murine somatic cells on cell cycle factors

The molecular events causing the above mentioned phenotypes in MEFs were investigated by cell cycle analysis. For this purpose MEFs were synchronized at S phase of the cell cycle. MEFs were then incubated with control medium, ΔNanog-TAT and Nanog-TAT. After 5, 8 and 21 hours cells were harvested and subjected to RT-PCR analysis.

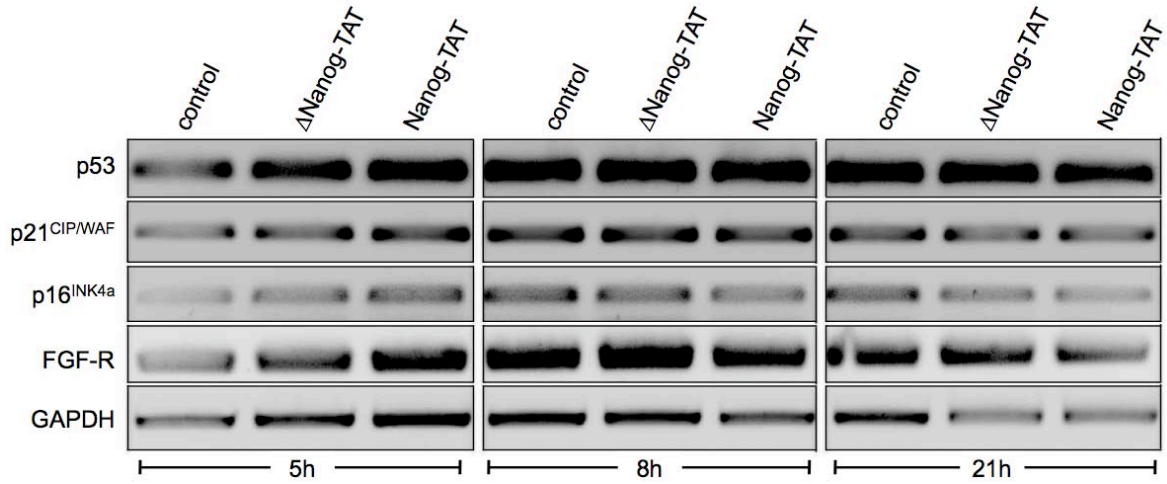

Figure 23: RT-PCR analysis of Nanog-TAT-treated MEFs
MEFs were synchronized and afterwards cultivated with control medium, ΔNanog-TAT and Nanog-TAT respectively. After 5h, 8h and 21h the fibroblasts were harvested and the expression levels of different key molecules involved in proliferation as well as cell cycle regulation were assessed via RT-PCR. After 5h 8h and 21h no striking change in transcription levels is apparent for p53, $p21^{CIP/WAF}$, $p16^{INK4a}$ and FGF-receptor 1. GAPDH serves as loading control. FGF-R: FGF receptor 1; GAPDH: Glyceraldehyde 3-phosphate dehydrogenase

p53, commonly referred to as the 'guardian of the genome', fulfills a variety of functions, i.e. p53 is involved in the initiation of DNA repair, induction of growth arrest for means of DNA repair as well as the initiation of apoptosis in case DNA damage is irreparable. $p16^{INK4a}$ is a marker that can be used for the identification of a senescent phenotype in cells, just like $p21^{CIP/WAF}$. Besides this, $p21^{CIP/WAF}$ also acts downstream of p53 in regulating transition through the cell cycle in G1 phase. FGF receptor 1 expression can indicate for a proliferative status in fibroblast cells. None of the above-mentioned factors was found to be transcriptionally modulated judged by RT-PCR analysis (Fig. 23) after 5, 8 and 21 hours.

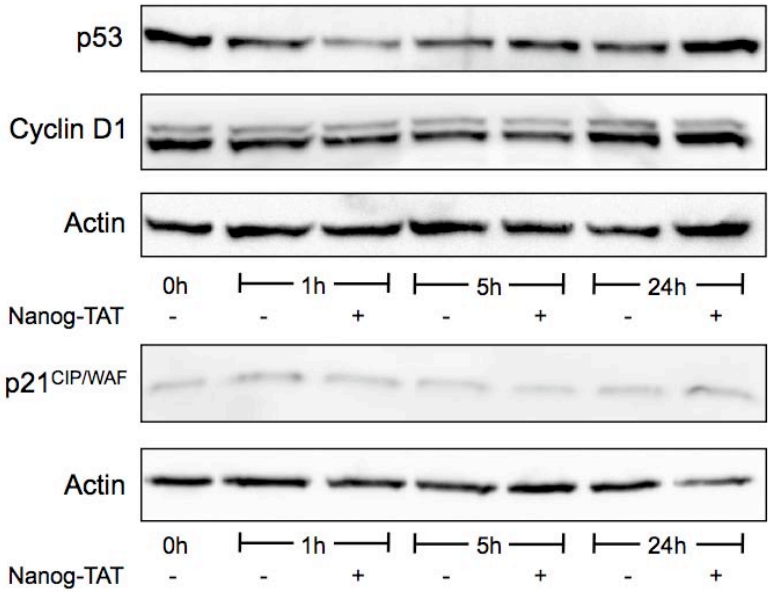

Figure 24: Cell cycle analysis of Nanog-TAT-treated MEFs via immunoblot
The expression levels of different key molecules involved in the cell cycle control were assessed. MEFs were synchronized and treated with Nanog-TAT-supplemented medium. After 1h, 5h and 24h the fibroblasts were harvested and subjected to immunoblot analysis with the corresponding antibodies. Fibroblasts treated with Nanog-TAT show no striking differences in expression of p53, Cyclin D1 or $p21^{CIP/WAF}$ compared to MEFs treated with control medium or to cells at 0h. Actin serves as a loading control. SDS-PAGE and immunoblot were performed with a gel exhibiting 10 or 15% (bis)acrylamide respectively.

In order to evaluate a putative change in protein expression levels of factors involved in cell cycle regulation, fibroblast cells were treated with Nanog-TAT supplemented medium as well as control medium. Protein lysates were prepared after 0, 1, 5 and 24 hours, subjected to immunoblot applying corresponding antibodies. The role of p53 and $p21^{CIP/WAF}$ was already described above, Cyclin D1 was chosen as an additional cell cycle regulator as down-regulation thereof can result in cell cycle arrest in G1 phase. At a protein level none of the factors analyzed via immunoblot shows significant changes after 1h, 5h and 24h (Fig. 24). Cyclin D1 exhibits an additional band in immunoblot analysis. This phenomenon observed is due to the rodent origin of cells, as stated in the datasheet provided by the manufacturer of the antibody.

3.2.8 Nanog-TAT delivery results in diminished levels of $p27^{KIP1}$ expression in murine somatic cells

A potent cell cycle regulator exhibiting partially redundant functions like $p21^{CIP/WAF}$ is $p27^{KIP1}$. Both molecules belong to the group of cyclin-dependent kinase inhibitors (CKI) and are able to influence cyclin dependent kinases' functional potential. Complexes of cyclin dependent kinases and their corresponding cyclins are known to phosphorylate certain substrates. One substrate to be phosphorylated by these complexes is the Retinoblastoma protein (pRb). In order to assess

whether Nanog influences p27^{KIP1} mRNA expression levels in mouse embryonic fibroblasts, cells were treated with Nanog-TAT. RNA expression levels were assessed after 5, 8 and 21 hours. For quantification the results are normalized to GAPDH expression.

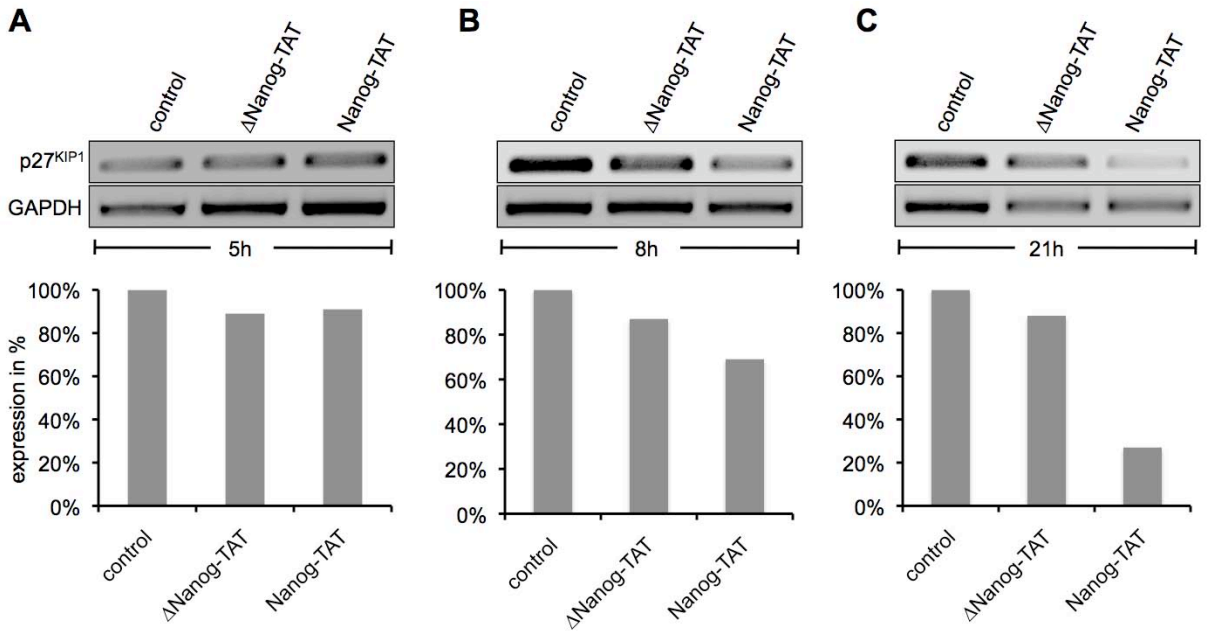

Figure 25: Nanog-TAT delivery results in decreased RNA expression levels of p27^{KIP1}
(**A**) MEFs were synchronized and afterwards cultivated in the presence of control medium, ΔNanog-TAT and Nanog-TAT. After indicated time points RNA expression levels were analyzed via RT-PCR. GAPDH served as a loading control. A slight down-regulation of p27^{KIP1} is already observed after 5h. (**B**) Treatment with Nanog-TAT leads to a distinct down-regulation of p27^{KIP1}after 8h and 21h. Expression of p27^{KIP1} was quantified densitometrically. Results are normalized to GAPDH. Expression levels of p27^{KIP1} are down-regulated to 69% after 8h of Nanog-TAT treatment compared to untreated fibroblasts. (**C**) After 21h the expression decreases to 27% in cells cultivated with Nanog-TAT. GAPDH: Glyceraldehyde 3-phosphate dehydrogenase

After 5 hours of Nanog-TAT treatment the expression of p27^{KIP1} was reduced to 91% compared to fibroblasts cultivated in control medium. The incubation with ΔNanog-TAT led to a slight reduction of p27^{KIP1} as well. The expression was down-regulated to 89% (Fig. 25A). 8 hours of application of Nanog-TAT resulted in a diminished expression of p27^{KIP1} to 69% compared to fibroblasts incubated with control medium, whereas cells treated with ΔNanog-TAT only showed a decrease of p27^{KIP1} expression to 87% (Fig.25B). After 21 hours of cultivation of fibroblasts with Nanog-TAT the expression of p27^{KIP1}was vastly down-regulated to 27% compared to cells incubated with control medium. The expression of p27^{KIP1} in fibroblasts treated with ΔNanog-TAT was decreased to 88% compared to MEFs cultivated in control medium (Fig. 25C).

In order to verify the results obtained by RT-PCR, changes of p27^{KIP1} protein expression levels were analyzed by immunoblot. Fibroblast cells were cultivated for distinct time points in the

presence of control medium or Nanog-TAT. Cells were then harvested and subsequently subjected to SDS-PAGE followed by immunoblot using an antibody directed against p27^{KIP1} (Fig. 26).

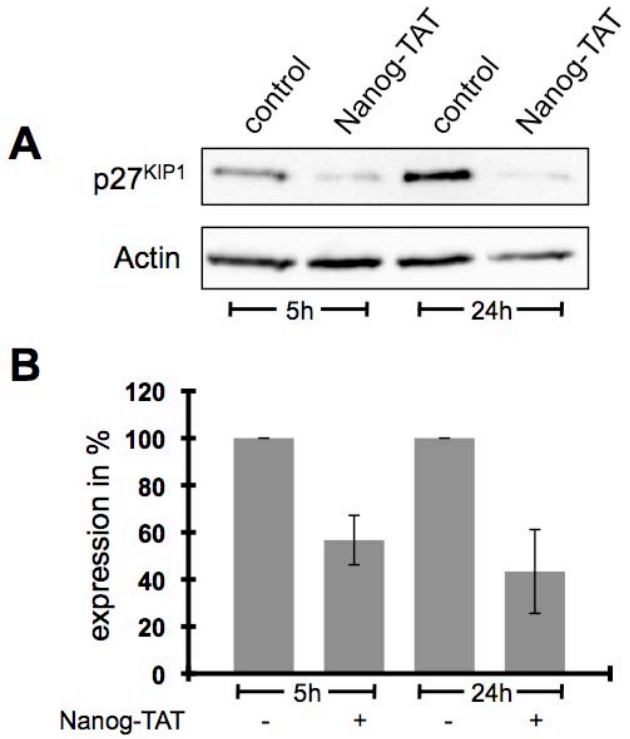

Figure 26: Expression of p27^{KIP1} decreases upon Nanog-TAT treatment
(**A**) MEFs were synchronized and incubated with control medium and Nanog-TAT. After indicated time points, MEFs were harvested and subjected to immunoblot analysis. A representative immunoblot is shown. Actin serves as a loading control. (**B**) Densitometric analysis of p27^{KIP1} expression levels is presented. Quantification is normalized to Actin. Upon treatment with Nanog-TAT, p27^{KIP1} expression is down-regulated after 5h as well as after 24h. n=3. SDS-PAGE and immunoblot were performed with a gel exhibiting 15% (bis)acrylamide.

Cultivation of MEFs with Nanog-TAT resulted in a clear reduction of p27^{KIP1} expression after 5 hours and 24 hours (Fig. 26A). Results from 3 independent experiments were used for densitometric quantification. After 5 hours of Nanog-TAT treatment, protein expression of p27^{KIP1} diminished to 56%. 24 hours of incubation with Nanog-TAT further decreased protein expression levels of p27^{KIP1} to 43% (Fig. 26B).

To test for the specificity of this effect, cells incubated with ΔNanog-TAT were analyzed as well. The expression of p27^{KIP1} is reliably down-regulated upon cultivation of fibroblast cells with Nanog-TAT after 5, 8 and 21 hours (Fig.27 A). After 5 hours of Nanog-TAT treatment the expression of p27^{KIP1} was decreased to 45%, after 8 hours p27^{KIP1} expression was reduced to 71% and after 21 hours of Nanog-TAT cultivation p27^{KIP1} expression was diminished to 64% (Fig. 27B). No down-regulation of p27^{KIP1} was observed upon ΔNanog-TAT treatment independent of the time point analyzed (Fig. 27A). The densitometric analysis even indicates a

slightly higher protein expression level of p27^{KIP1} in MEFs treated with control protein compared to fibroblasts cultivated with control medium (Fig. 27B).

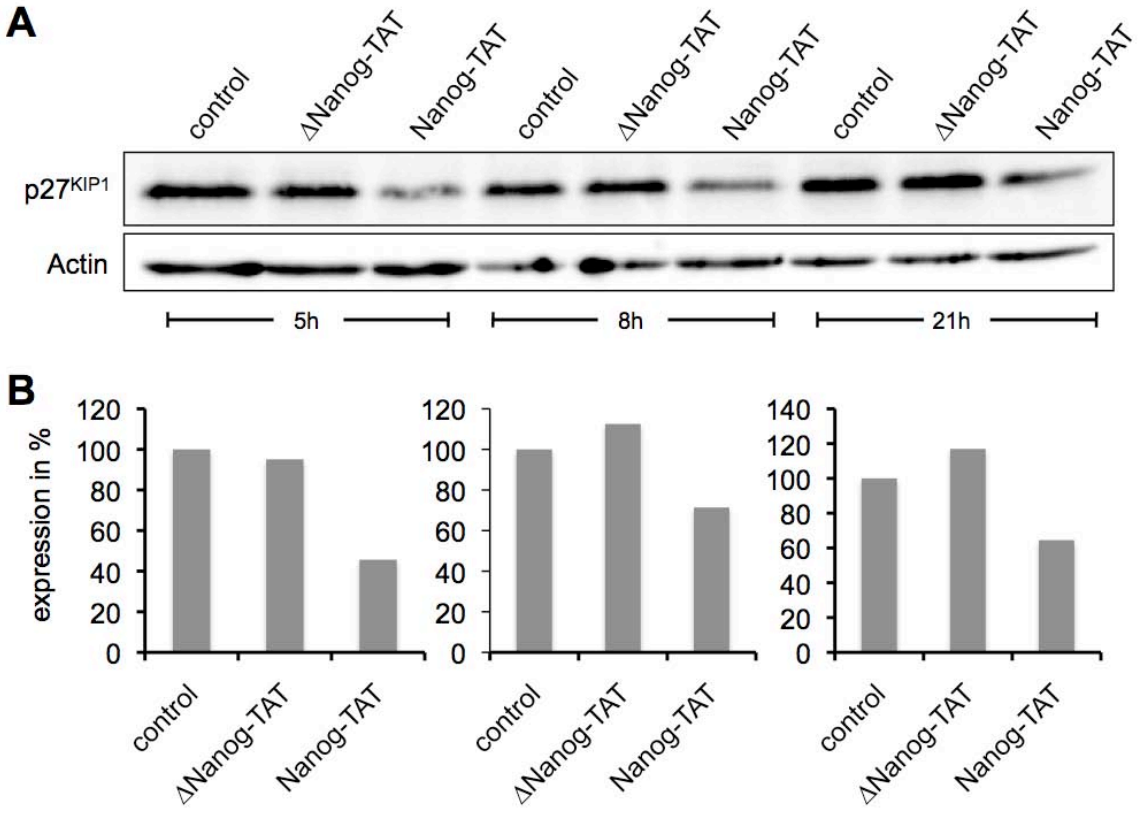

Figure 27: Cultivation of MEFs with ΔNanog-TAT does not induce a down-regulation of p27^{KIP1}
(**A**) MEFs were synchronized and incubated with control medium, control protein as well as Nanog-TAT for indicated periods of time. Upon cultivation of MEFs with Nanog-TAT, p27^{KIP1} expression is down-regulated after 5h, 8h and 21h. Cultivation of MEFs with ΔNanog-TAT does not change protein expression levels of p27^{KIP1} compared to cells treated with control medium (**B**). The immunoblot was quantified densitometrically and quantification of p27^{KIP1}expression is depicted. After 5h of Nanog-TAT treatment the expression of p27^{KIP1} is decreased to 45%, after 8h p27^{KIP1} expression is reduced to 71% and after 21h of Nanog-TAT cultivation p27^{KIP1} expression is diminished to 64%. SDS-PAGE and immunoblot were performed with a gel exhibiting 15% (bis)acrylamide.

3.2.9 Nanog promotes the expression as well as the phosphorylation of Retinoblastoma protein

One known down-stream target of p27^{KIP1} is the Retinoblastoma protein (pRb). p27^{KIP1}, as a CKI, inhibits cyclin-CDK complexes otherwise responsible for the phosphorylation of pRb. So a down-regulation of p27^{KIP1} should consequently lead to an accelerated phosphorylation of pRb. In order to assess the expression level and phosphorylation status of pRb upon Nanog-TAT delivery, murine fibroblasts were incubated with control medium as well as Nanog-TAT. Cell lysates were harvested at distinct time points and the expression as well as the phosphorylation

status of pRb was assessed performing immunoblot applying a pan-Rb antibody. This antibody recognizes unphosphorylated pRb as well as phosphorylated variants of the protein.

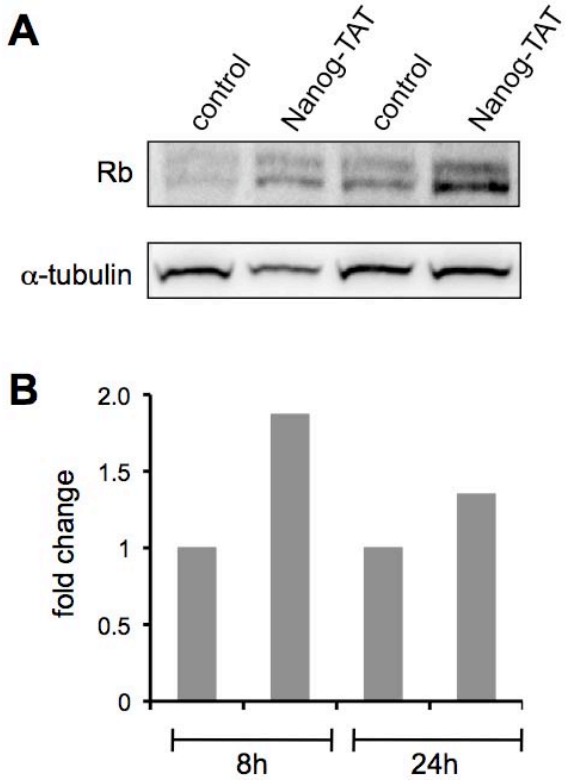

Figure 28: Nanog-TAT enhances expression levels as well as phosphorylation of Retinoblastoma protein
(**A**) After 8h of cultivation with Nanog-TAT, MEFs exhibit an increase in pRb expression as well as enhanced phosphorylation of pRb compared to MEFs cultivated with control medium. A similar observation was made after 24h of Nanog-TAT treatment. A representative immunoblot is shown. (**B**) Densitometric quantification of pRb signals observed in immunoblot analysis is presented. Results are normalized to α-tubulin. SDS-PAGE and immunoblot were performed with a gel exhibiting 7.5% (bis)acrylamide.

Upon treatment with Nanog-TAT, MEFs exhibit a higher protein level of pRb, both the unphosphorylated as well as the phosphorylated variant, compared to cells cultivated with control medium after 8 hours (Fig. 28A). Densitometric analysis reveals an increase in fold change of total pRb expression by the factor of 1.87 (Fig. 28B). After 24 hours cells treated with recombinant Nanog fusion protein still exhibit a higher protein expression level of unphosphorylated and phosphorylated pRb (Fig. 28A). Quantification of the immunoblot indicates an elevated expression level by the factor 1.35 (Fig. 28B).

3.2.10 Analysis of Nanog function in human somatic cells

Although the homology between murine Nanog and human Nanog on basis of aa is only about 55% (Hart et al., 2004), Nanog-TAT exhibited functionality on human ES cells by inhibiting differentiation thereof (Peitz, 2007). Hence, the question whether or not delivery of Nanog-TAT would also exhibit an effect on human somatic cells was addressed.

3.2.11 Nanog protein transduction enhances proliferation of human somatic cells

MP-AF cells, (primary human dermal fibroblasts) were cultivated with Nanog-TAT over several passages to analyze the effect of Nanog in human somatic cells. After each passage, cell numbers were determined in order to assess the proliferation rate. To determine a potential juvenescent effect of Nanog-TAT, fibroblasts cultivated with the transducible stemness factor were analyzed for the expression of senescence-associated (SA) β-Galactosidase.

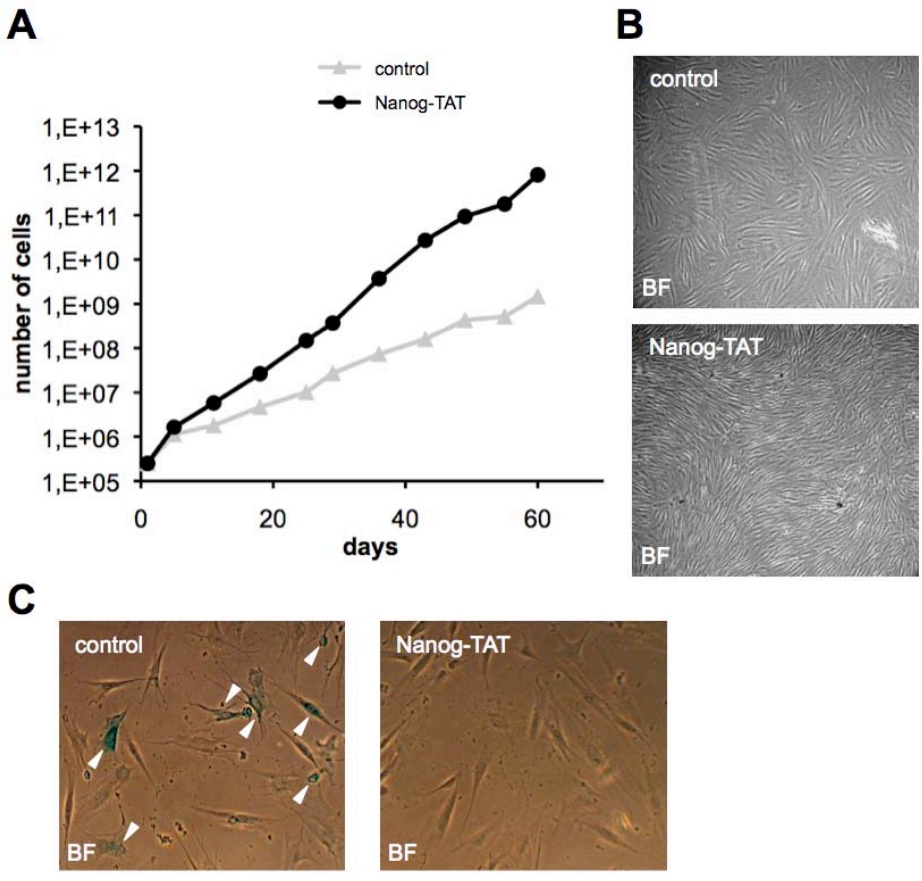

Figure 29: Nanog-TAT promotes proliferation of human dermal fibroblasts
(**A**) Human dermal fibroblasts (MP-AF) were cultivated in the presence or absence of Nanog-TAT. After each passage cells were counted. A representative proliferation analysis via growth curve is depicted. Cumulative cell numbers are shown. (**B**) Pictures of fibroblast cells cultivated with control medium or Nanog-TAT are shown. (**C**) Cells cultivated with control medium exhibit SA β-Glactosidase activity whereas fibroblasts cultivated with Nanog-TAT do not stain for SA β-Galactosidase. Magnification for B: 5x; Magnification for C: 20x; BF: bright field; SA: senescence-associated.

Nanog protein transduction into human dermal fibroblasts resulted in an increased proliferation rate, which mirrors the effect observed in MEFs. From a starting cell number of 250.000 cells, Nanog-TAT treated fibroblasts exhibit a final cumulative cell number of $8x10^{11}$ after 10 passages. In contrast 250.000 MP-AF fibroblast cells cultivated with control medium only give rise to $1.5x10^{9}$ after 10 passages (Fig. 29A). Representative pictures after 14 days of both experimental conditions are shown in Fig. 29B. Nanog-TAT-treated cells grow densely packed. Additionally, fibroblast cells cultivated with Nanog-TAT undergo a change in morphology. They adopt an even more spindle-like shape and the ratio of cytoplasm to nucleus declines. The observation of enhanced proliferation might indicate that Nanog eventually suppresses senescence. In order to assess senescence in Nanog-TAT-treated cells a senescence-associated β-Galactosidase assay was performed. This assay is reported to specifically stain senescent cells (Dimri et al., 1995) at a pH of 6.0. Human dermal fibroblasts cultivated with Nanog-TAT did not stain positive for SA-β-Galactosidase. In contrast, fibroblasts cultivated in control medium did exhibit SA-β-Galactosidase activity. For both approaches cells were cultivated non-confluently (Fig. 29C). In order to analyze for further proliferative markers a TRAP assay was performed but no telomerase activity could be detected within both populations. The same result was obtained by RT-PCR analyzing the RNA expression levels of telomerase reverse transcriptase. In contrast, human ES cells that served as a positive control exhibited telomerase activity in both experimental setups (data not shown).

3.2.12 Molecular analysis of Nanog-TAT function in human somatic cells

To gain insight into transcriptional changes of human dermal fibroblasts cultivated with Nanog-TAT, micro-array analysis was performed and compared to cells treated with control medium. To this end dermal fibroblast cells were cultivated with or without Nanog-TAT for several passages, i.e. the time period sufficient to induce morphological changes as described above. RNA was subsequently isolated and subjected to microarray analysis. The chip was loaded in triplicates. The results obtained from the Illumina whole genome expression chip were analyzed and fold-change in expression between fibroblast cells cultivated with Nanog-TAT compared to cells treated with control medium was determined. These experiments were performed in collaboration with Dr. Michael Alexander.

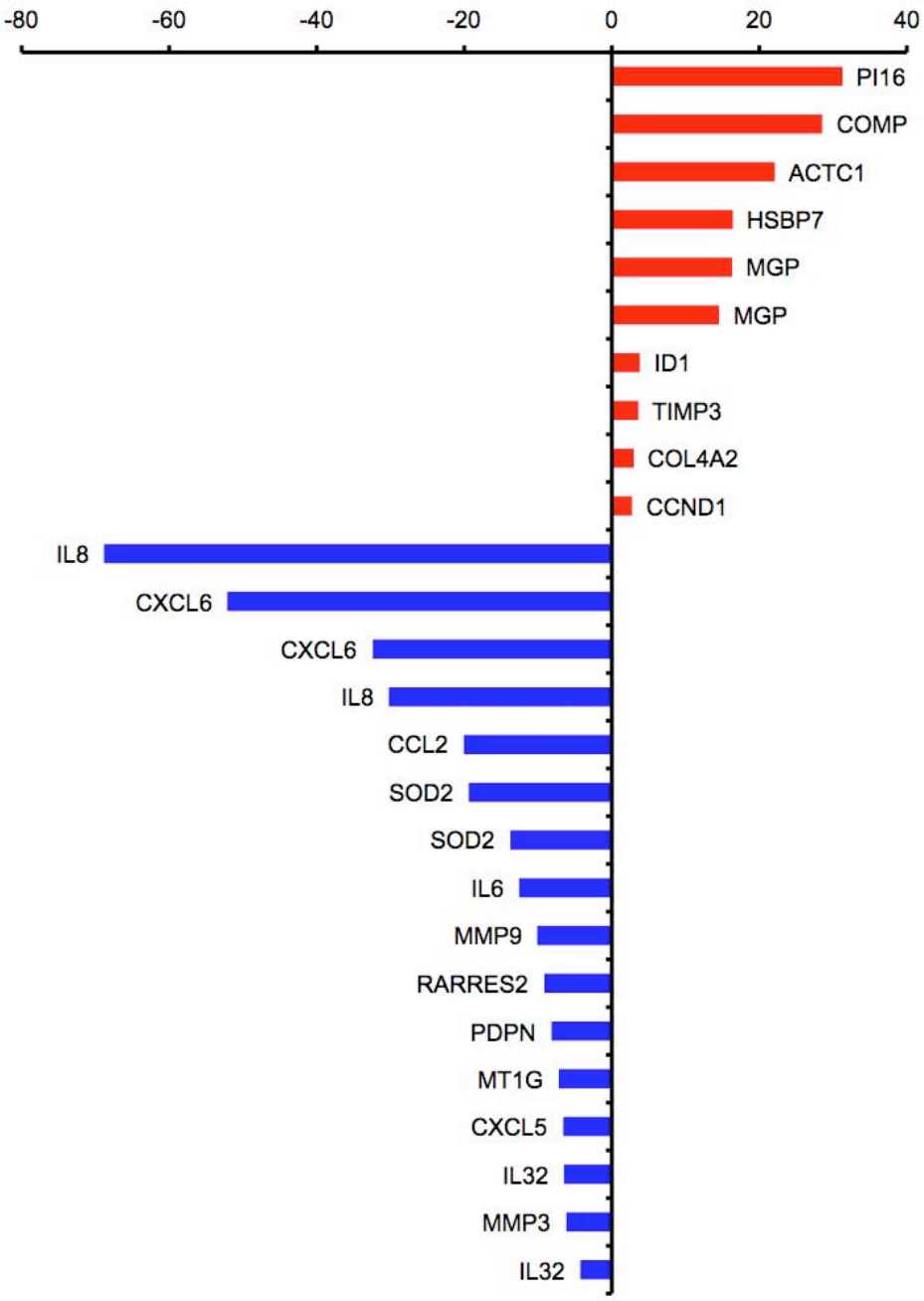

Figure 30: Selection of genes modulated in MP-AF fibroblasts upon Nanog-TAT cultivation
Human somatic fibroblast cells were treated with or without Nanog-TAT. RNA was then isolated and microarray analysis was performed. A selection of gene expression modulated upon Nanog-TAT cultivation is depicted. Red bars indicate up-regulation, blue bars show down-regulation.

Among the genes up-regulated in fibroblast cells cultivated with Nanog were PI16, the peptidase inhibitor 16 (fold change 31.2), COMP, the cartilage oligomeric matrix protein (fold change 28.5), ACTC1, an abbreviated gene symbol for actin alpha cardiac muscle (fold change 22.1), HSPB7, the heat shock 27kDa protein family, member 7 (fold change 16.4) and MGP, the matrix gla protein (fold change 14.5), as well as ID1, the inhibitor of differentiation (Fig. 30). Moreover, CCDN1 expression, which represents the abbreviated gene symbol for Cyclin D1 was up-regulated. The fold change for ID1 was 3.8 and was enhanced for Cyclin D1 by the factor 2.7

compared to untreated cells. Besides that, collagen alpha-1 (IV) chain (COL4A1) and metalloproteinase inhibitor 3 (TIMP3) were up-regulated additionally by the factor 7.0 and 3.6 respectively (Fig. 30).

Genes that became down-regulated upon Nanog-TAT treatment of dermal fibroblasts are listed in Figure 30 as well. IL8, interleukin-8 was down-regulated (fold change 68.8 and 30.2) in cells cultivated with Nanog-TAT as well as CXCL6, the chemokine (C-X-C motif) ligand 6 (fold change 52.1 and 32.4) and CCL2, which represents the chemokine (C-C motif) ligand 2 (fold change 20.0). Moreover IL6, interleukin-6, was down-regulated (fold change 12.5) upon Nanog-TAT treatment in dermal fibroblasts as well as the mitochondrial superoxide dismutase 2 (SOD2) and MMP9, the matrix metallopeptidase 9. Moreover, retinoic acid receptor responder protein 2 (RARRES2) and the chemokine (C-X-C motif) ligand 5 (CXCL5) as well as IL35, interleukin-35 were down-regulated upon Nanog-TAT treatment. Furthermore, Podoplanin (PDPN), Metallothionein-1G (MT1G) and Stromelysin-1 (MMP3) were down-regulated.

3.3 The influence of Nanog on the process of reprogramming

As cellular reprogramming cannot only be achieved through the classical factors Oct3/4, Klf4, Sox2 and c-myc (OKSM) identified by Takahashi and Yamanaka (Takahashi and Yamanaka, 2006), but with a combination of Oct3/4, Sox2, Nanog and Lin-28 as well, the share of Nanog on the process of reprogramming is of great interest; especially as a role is assigned to Nanog in governing the gateway to a ground state of pluripotency (Chambers et al., 2007) - a function most likely pivotal in the process of reprogramming. There are few publications, which reach out to analyze the function of Nanog in the act of cellular reprogramming; a clear understanding is still missing though. Therefore the influence of Nanog on the process of cellular reprogramming was addressed using Nanog-TAT fusion protein.

To assess whether the influence of Nanog-TAT on the proliferation of somatic cells could have a promoting effect on the reprogramming efficiency, MEFs retrovirally transduced with OKSM, were incubated with Nanog-TAT either before retroviral transduction or for 5 days *post infection*. No significant increase in reprogramming efficiency was observed judged by the number of evolving iPS cell colonies (data not shown). Moreover, an enduring application of Nanog-TAT to MEFs virally transduced with OKSM did not provoke an enhancing effect on reprogramming efficiency. This finding was strengthened by observations made in MEFs virally transduced with OKSM plus an additional retroviral vector carrying the genetic information for murine Nanog (Marc Thier, personal communication), which basically resulted in an enhanced transformation rate of the cells to be reprogrammed. With the Nanog-TAT fusion protein at hand it was feasible to apply Nanog in a time-dependent manner without limitations posed by viral

transduction. In order to analyze the influence of Nanog at different stages of the reprogramming process MEFs virally transduced with OKSM were incubated with Nanog-TAT starting from different time points.

3.3.1 Nanog-TAT advances reprogramming when applied 10 days *post infection*

Oct3/4-GIP MEFs were transduced with OKSM. Additionally Nanog-TAT fusion protein was applied onto the cells after 6, 8 or 10 days. One day prior to Nanog-TAT treatment, cells were splitted to ensure proper protein transduction. Control cells, i.e. cells virally transduced with OKSM and cultivated in advanced medium, were treated equally. After 15 days cells were fixed and analyzed for GFP fluorescence, indicating re-activation of the Oct3/4 regulatory sequences (Fig. 31A). Certain criteria were applied to classify the emerging iPS cells. First of all, only cells exhibiting high GFP fluorescence were taken into account. As a second criterion, the morphology of the iPS cell colonies was used to discriminate between colonies exhibiting clear borders in phase contrast and fluorescence light, i.e. iPS cell colonies, and the remaining cells not fulfilling this criterion (Fig. 31B). These experiments were performed in collaboration with Marc Thier.

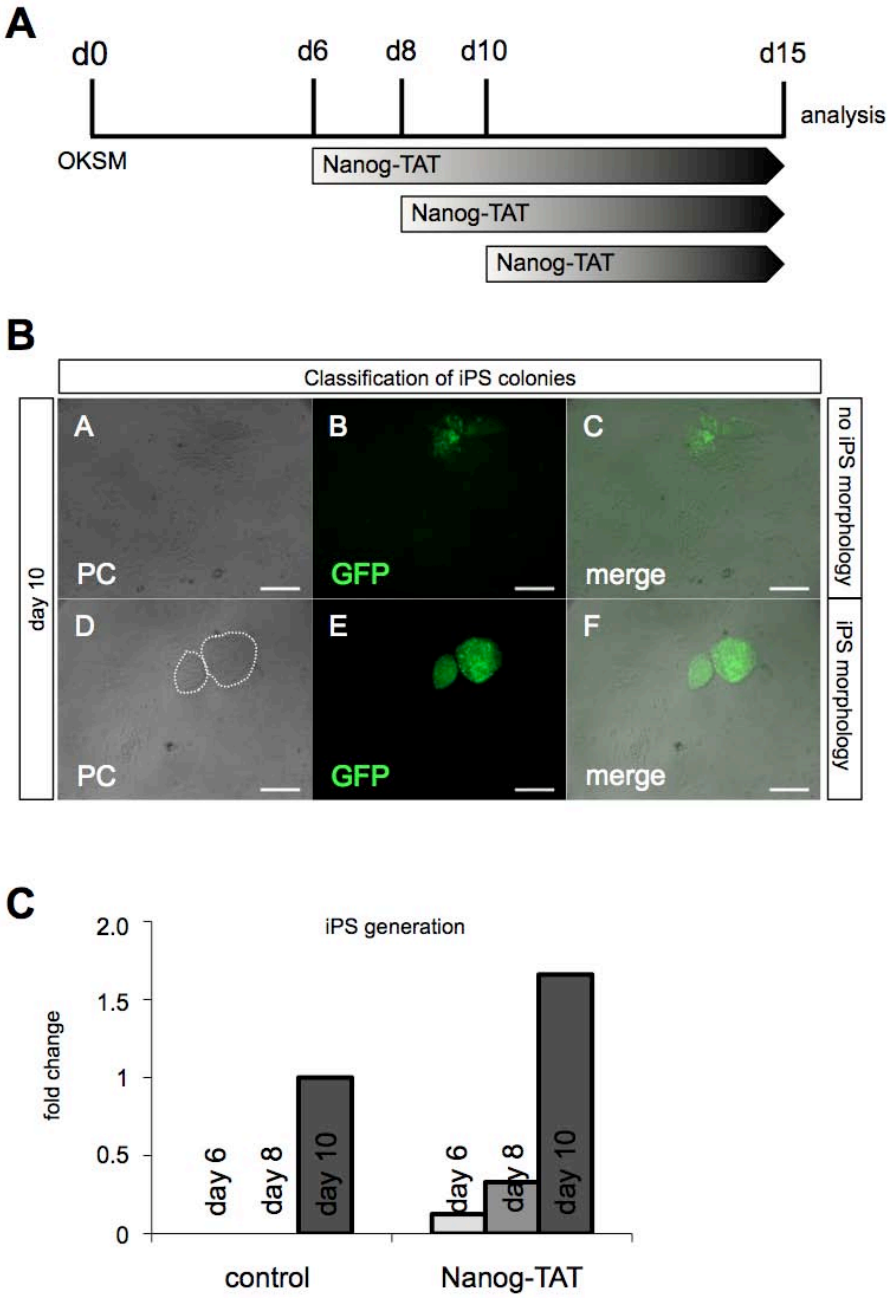

Figure 31: Application of Nanog-TAT at day 10 enhances reprogramming
(**A**) The experimental setup used is depicted. MEFs were virally transduced with OKSM and 100nM of Nanog-TAT was applied after 6, 8 and 10 days *post infection* until the end of the experiment. At day 15 cells were fixed and analyzed. (**B**) Typical examples of morphology used to classify iPS cells are shown. For details on the classification see text. The pictures originate from an experiment involving Nanog-TAT applied from day 10 onwards. (**C**) The fold change in efficiency of generating iPS cells was assessed. A fold change in efficiency of generating iPS cells by the factor of 1.7 was achieved upon Nanog-TAT application from day 10 onwards compared to the corresponding control condition from day 10. The quantification is based on 3 independent experiments. PC: phase contrast; GFP: green fluorescent protein. Scale bar: 100µm

Under all temporal conditions the amount of GFP-positive iPS cells was higher when Nanog-TAT was present in the cell culture medium. In the experimental setup where Nanog-TAT was applied from day 6 onwards, only very few iPS cell colonies could be observed. In contrast no iPS cell colonies fulfilling both criteria are visible in the control experiment at day 6. When

Nanog-TAT is applied from day 8 to day 15, the rate of iPS cells is still low, although more colonies form compared to the experimental setting where Nanog is applied at day 6. Again, the control experiment from day 8 does not harbor any iPS colonies exhibiting high GFP expression as well as colony-like morphology (see Table 5). A fold change in efficiency of generating iPS cells by the factor of 1.7 was achieved when Nanog-TAT was applied from day 10 onwards compared to the control condition from day 10.

Table 5: Amount of colonies fulfilling the different criteria mentioned above observed in a representative OKSM +/-Nanog-TAT reprogramming paradigm

	control day 6	Nanog-TAT day 6	control day 8	Nanog-TAT day 8	control day 10	Nanog-TAT day 10
total GFP positive colonies	2	11	16	30	34	38
strong GFP expression /no iPS morphology	2	8	4	6	3	3
strong GFP expression / iPS morphology	0	1	0	2	3	5

3.3.2 Nanog-TAT enhances reprogramming efficiency by the factor of 3 when applied at later stages of reprogramming

As from the previous preliminary experiment, conducted under suboptimal reprogramming conditions, the optimal time point for the application of Nanog-TAT during the process of cellular reprogramming could be identified, the Nanog-TAT fusion protein was now applied onto OKSM virally transduced MEFs starting from day 10 post infection in order to analyze for a quantifiable enhancement of cellular reprogramming under optimal conditions. The fusion protein was applied onto the fibroblasts for 10 days. At day 20 the experiment was stopped (Fig. 32A) and emerging colonies were analyzed for Oct3/4 reporter activity as well as additional pluripotency markers such as AP and SSEA-1. The amount of colonies was determined and compared to the approach cultivated with control medium. These experiments were performed in collaboration with Marc Thier.

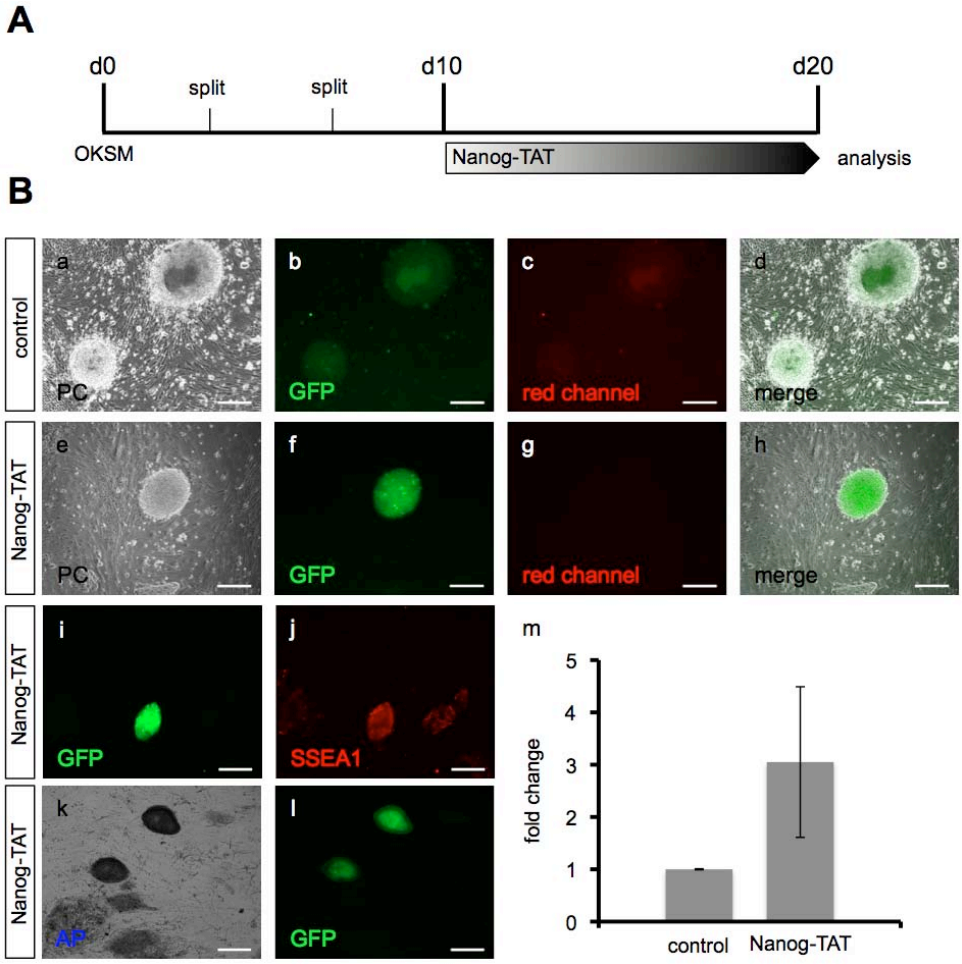

Figure 32: Nanog-TAT increases reprogramming efficiency by the factor of 3
(**A**) The experimental setup used is depicted. (**B**) [a to d] shows iPS colonies derived from a control experiment with OKSM retrovirally transduced MEFs. Colonies show ES-like morphology but exhibit low GFP expression. In contrast, retrovirally OKSM transduced MEFs cultivated with Nanog-TAT from day 10 onwards give rise to iPS colonies exhibiting ES-like morphology and high GFP expression levels as seen in [e to h]. Pictures taken from red channel indicate background fluorescence. Those GFP-positive cells [i & l] also stain positive for SSEA-1 as seen in [j] as well as for AP seen in [k]. Fold change in efficiency of generating iPS colonies is depicted [m]. 3 independent experiments were used for quantification. PC: phase contrast; GFP: green fluorescent protein; SSEA-1: stage-specific embryonic antigen-1; AP: alkaline phosphatase. Scale bar 100µm

Virally transduced MEFs cultivated with Nanog-TAT from day 10 on for a time period of 10 days gave rise to iPS colonies with ES-like morphology and additionally expressed GFP at high levels (Fig 32B; e – h). In contrast, OKSM reprogramming of MEFs in the absence of Nanog-TAT results in iPS cells exhibiting ES-like morphology and weak GFP expression (Fig. 32B; a – d). IPS colonies derived without (data not shown) and with Nanog-TAT express the pluripotency markers SSEA-1 (Fig. 32B; j) and AP (Fig. 32B; k), a marker associated with pluripotency. The addition of exogenous Nanog at late stages of the reprogramming process enhances reprogramming efficiency by the factor of 3 compared to the control (Fig. 32B; m) determined by quantification of 3 independent experiments.

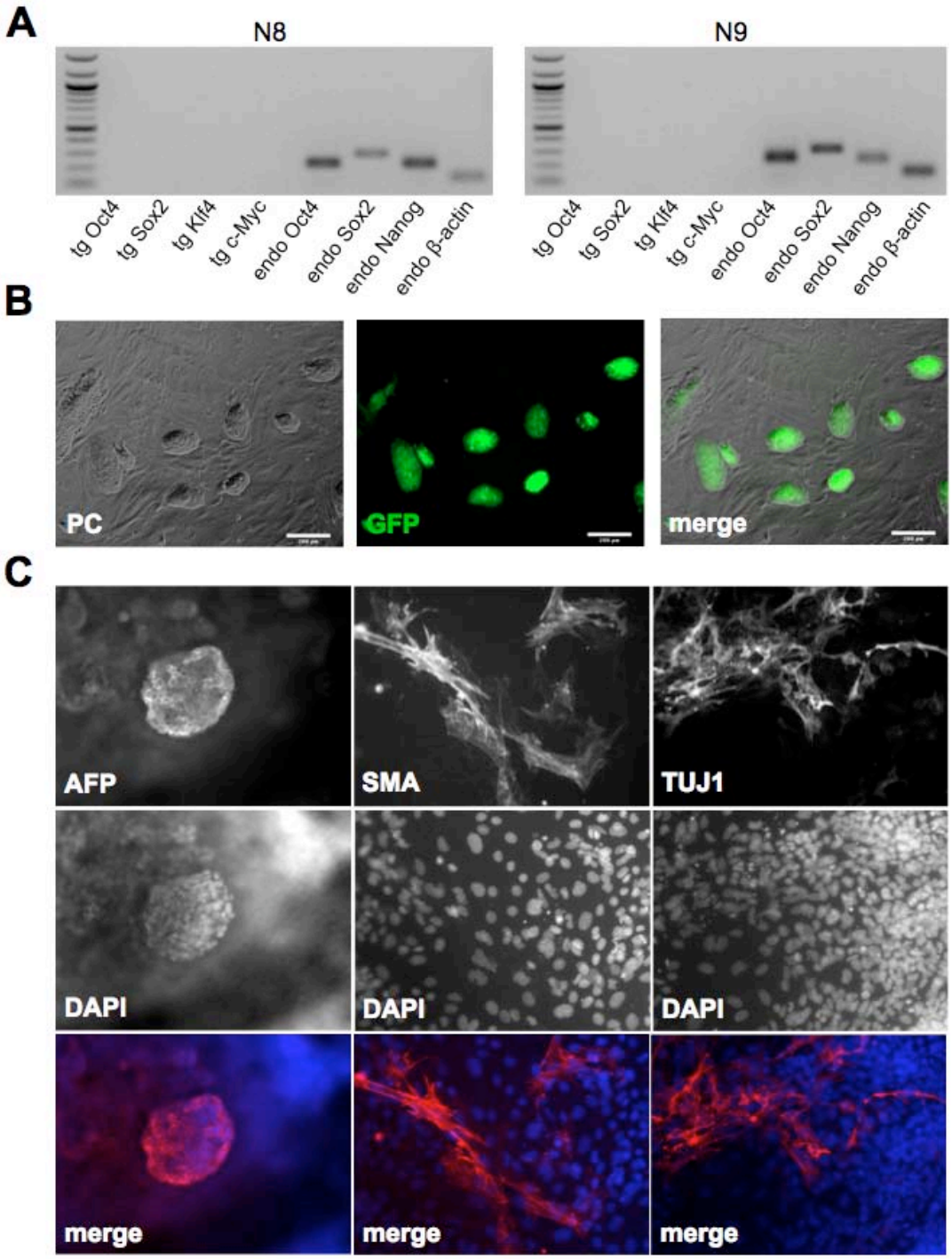

Figure 33: Validation of Nanog-TAT derived iPS
(**A**) iPS cells generated in the presence of Nanog-TAT were analyzed for silencing of transgenes as well as for re-activation of endogenous pluripotency markers using RT-PCR. N8: Nanog-iPS clone 8; N9: Nanog-iPS clone 9; tg: transgene; endo: endogenous. (**B**) Stable clone generated in the presence of Nanog-TAT exhibits high GFP expression after prolonged cultivation. One representative clone of passage 18 is shown. Scale bar: 200µm (**C**) Clones established employing Nanog-TAT are able to give rise to all three germlayers upon EB-based differentiation. Stainings for smooth muscle actin (SMA), alpha-fetoprotein (AFP) and β-III-tubulin (TUJ1) in plated EBs are shown. Magnification: 20x.

In order to analyze the differentiation potential of iPS clones generated in the presence of Nanog-TAT, silencing of the four reprogramming factors OKSM was assessed. All iPS clones analyzed showed silencing of reprogramming transgenes and at the same time endogenous pluripotency markers Oct3/4, Sox2 and Nanog as judged by RT-PCR were re-activated (Figure 33A). iPS clones were stable over a prolonged period of time and still strongly expressed GFP originating from the Oct3/4 GiP reporter construct. Figure 33B shows representative pictures of an iPS clone derived in the presence of Nanog-TAT at passage 18. Upon an embryoid body-based differentiation paradigm, Nanog-TAT treated iPS clones gave rise to all three germ layers as the differentiated clones stained positive for smooth muscle actin (SMA), alpha-fetoprotein (AFP) and beta-III-tubulin (TUJ1) (Figure 33C).

4 Discussion

4.1 Expression and purification of the Nanog-TAT fusion protein and its corresponding control protein ΔNanog-TAT

A part of this work covers the establishment of a purification protocol for Nanog-TAT and its corresponding control protein ΔNanog-TAT as well as the assessment of the biochemical properties of both recombinant proteins.

Poor solubility of recombinant Nanog-TAT fusion protein and formation of inclusion bodies are the major impediments for the application of Nanog protein transduction. The denaturing purification of Nanog-TAT, aiming at overcoming the poor solubility, was successful concerning the purity and the stability of the recombinant fusion protein under physiological conditions. However, the only conditions allowing successful refolding of Nanog-TAT contained Triton-X100. After dialysis against PBS the recombinant protein could be applied in cell culture. Fibroblast cells cultivated with Nanog-TAT purified under denaturing conditions underwent apoptosis though. Most likely the Triton-X100 molecules attached to the recombinant Nanog-TAT protein permeabilized the membrane of the target cells, which would explain the cell death observed. Detergent removal can usually be obtained by three different methods: dialysis, gel filtration and binding to hydrophobic gels. Triton-X100 exhibits a very low critical micelle concentration (cmc), also indicating a strong binding of the detergent to proteins. For these reasons the first two methods mentioned therefore will not be feasible and in the case of dialysis the results obtained in this work strengthen these thoughts. A potential way to remove traces of Triton-X100 molecules would be the use of hydrophobic gels. After laborious preparation of the corresponding material, the detergent could eventually be removed by mixing the gel material with the recombinant protein. As a way to circumvent this challenging procedure, one could also try to use detergents with a higher cmc, such as octyl-β-glucoside. Of course cell viability assays with this substance should be performed beforehand to ensure that even the slightest amount of this detergent would not harm the target cells.

Through the application of an imidazole gradient an optimized purification procedure for the full-length protein could be established. In a first attempt Nanog-TAT was purified natively using high concentrations of imidazole resulting in a pure recombinant protein. This purified protein was not stable under cell culture conditions though, leading to the assumption that contaminations originating from *E.coli* are needed to stabilize Nanog-TAT. The identification of these contaminations via tryptic digestion followed by MALDI-TOF could be of great interest as these stabilizing peptides could be used for other hardly soluble recombinant proteins as well.

Additionally one could make use of stabilizing peptides, which have been shown to confer enhanced solubility to fusion partners. Examples for these stabilizing peptides are the Protein A

IgG ZZ repeat domain (Zhao et al., 2005) or the Protein G B1 domain (Bao et al., 2006) as well as the synthetic solubility enhancing tag (Zhang et al., 2004).

Lowering the imidazole concentration during the purification process of Nanog-TAT resulted in a minor increase in contaminating bacterial proteins, i.e. the potentially stabilizing proteins, within the eluate fraction but at the same time allowed for keeping Nanog-TAT in a soluble state even under physiological conditions at a concentration of 100nM at 37°C. Similar as well as lower concentrations of transducible proteins were shown to be sufficient to induce biological effects (Asoh et al., 2002; Krosl et al., 2003; Nagahara et al., 1998).

In addition to the purification protocol for the full-length protein, optimized purification conditions for ΔNanog-TAT were established. In principle the design of the control protein was based on the full-length Nanog-TAT protein, i.e. a NLS at the N-terminal part was included as well as a TAT domain and a Histidin tag at the C-terminal domain of the control protein. In contrast to Nanog-TAT, the purity of the control protein was higher in the eluate fraction; still the fusion protein was stable under cell culture conditions for at least 24h. This observation may indicate that the omission of the homeodomain conferred enhanced solubility to ΔNanog-TAT without the need of exogenous, potentially stabilizing proteins derived from *E.coli*. This phenomenon could be explained on the one hand by the fact that within the homeodomain of murine Nanog two AGG codons, very rarely occurring in *E.coli* (Chen and Inouye, 1994) are present. On the other hand two codons encoding for cysteines are found within the homeodomain as well, that likely play a role in disulfide bond formation, a process being difficult to accomplish in the *E.coli* environment though, unless a mutation in the thioredoxin reductase is occurring (Derman et al., 1993). The lack of the above-mentioned codons could have led to an i) enhanced expression as well as an ii) enhanced solubility of the control protein even in the absence of stabilizing bacterial proteins. Although the concentration of ΔNanog-TAT did not exceed 50nM, this and even lower concentrations of transducible proteins were shown to be sufficient to trigger biological effects (Asoh et al., 2002; Krosl et al., 2003; Nagahara et al., 1998).

Based on the expression and purification optimization worked out in this study 1 liter of bacterial expression culture of Nanog-TAT finally results in 5mL of cell culture medium. Especially in the case of reprogramming experiments, it would be desirable to have a more efficient expression system at hand. In order to obtain more soluble Nanog-TAT protein, several options are considerable. Obviously, expression cultures using fermenters would lead to a higher yield of biomass due to the circumstance that a higher optical density within the expression culture could be achieved. This would only circumvent the causative problem though. An approach to solve the causal reason for the poor amount of soluble Nanog-TAT could be i) the use of a genetic sequence optimized for codon usage in *E.coli* or the ii) use of a biochemically modified protein.

In a first attempt, a variant of Nanog-TAT codon-optimized for the expression in *E.coli* was investigated. Employing an imidazole gradient, the optimal purification conditions were assessed. The codon-optimized variant of Nanog could be expressed in and purified from *E.coli*. In contrast to Nanog-TAT, a major part of the recombinant protein was found within the soluble fraction and although a part is lost in the flow-through and washing fractions, still a considerable amount of codon-optimized Nanog can be detected within the eluate fraction by SDS-PAGE and immunoblot. The fact that more Nanog is present within the soluble fraction may be well explained by the optimized codon-usage being beneficial for *E.coli* regarding the proper folding of the recombinant protein. It has to be further analyzed whether this enhanced fusion protein remains stable under cell culture conditions as this represents the most crucial point during the purification process. Via immuno dot blot assay the concentration of the codon-optimized construct could be compared to Nanog-TAT in order to investigate whether or not more codon-optimized, soluble recombinant protein is present. Consequently the biological functionality of the newly generated fusion protein should be analyzed.

It was shown that VP16, a transactivation domain derived from herpes simplex virus, (Sadowski et al., 1988; Triezenberg et al., 1988) fused to the N-terminal part of Nanog was able to confer higher transactivational activity to Rex-1, a pluripotency-associated protein, in NIH 3T3 cells compared to wild-type Nanog (Shi et al., 2006). Hence, in a second preliminary attempt to biochemically modify the recombinant Nanog protein, VP16 was fused to the C-terminal domain of the full-length Nanog. This construct could be expressed in and purified from *E.coli*. Purification conditions were analyzed via imidazole gradient by SDS-PAGE and immunoblot. Although Nanog fused to VP16 constitutes only 20% of the whole mount protein, the VP16 domain could eventually confer stabilizing properties to the fusion protein as this phenomenon was observed with other recombinant proteins analyzed in our workgroup. Additionally the transactivation of the newly generated recombinant protein could be higher compared to the wild type Nanog variant. As for the codon-optimized Nanog variant the concentration as well as the functionality of Nanog fused to the VP16 domain should be elucidated.

4.2 Biological activity of Nanog-TAT and ΔNanog-TAT

As both fusion proteins were stable under physiological conditions, the biochemical properties thereof were assessed. In order to analyze for the DNA binding ability of Nanog-TAT an EMSA was performed. A clear shift was observed that could not be detected when ΔNanog-TAT was subjected to an EMSA verifying the specificity of the binding. The Nanog homeodomain therefore seems to be responsible for DNA binding, a property analyzed in detail by Jauch and colleagues (Jauch et al., 2008). To further strengthen the specificity, an α-Nanog antibody could be subjected to the binding reaction along with Nanog-TAT, which should result in a so-called

supershift, since the protein-DNA complex would additionally be recognized by the specific anti-Nanog antibody. Some workgroups have assigned Nanog the ability to dimerize (Mullin et al., 2008; Torres and Watt, 2008; Wang et al., 2008b), a phenomenon that could not be observed by EMSA in this work, as no further shifted bands were detectable. Since post-translational modifications of the fusion proteins expressed and purified in and from *E.coli* are not occurring, the absence thereof could also have an influence on the dimerization capability of Nanog-TAT as this was shown to play a role for other proteins (Connors et al., 2007).

Next, both fusion proteins were analyzed for their ability to translocate into mammalian cells. CV1 fibroblast cells were chosen for translocation studies since these cells represent a reliable and robust cellular system. Moreover, since for a major part of this work Nanog-TAT and ΔNanog-TAT were applied on somatic fibroblast cell lines, CV1 cells, possessing similar morphological properties compared to the aforementioned cell types, mirror the target cell's phenotype. Since Nanog-TAT within the eluate and dialysis fraction still contained some contaminating proteins, a labeling of the fusion protein with fluorescent dye (Tunnemann et al., 2006) was not appropriate, as it is not possible to selectively label Nanog-TAT. The other contaminating proteins would have been labeled as well and distorted the experimental outcome. This procedure would have allowed for the analysis on living, i.e. non-fixed cells though. Fixation of cells is known to potentially provoke an artificial internalization of the protein of interest (Richard et al., 2003) and hence can only partially elucidate the process of translocation.

CV1 cells were incubated with both fusion proteins for 5h and cells were washed thereafter with Heparin, to ensure no recombinant protein stuck on the cellular surface, is detected by the primary antibody (Kaplan et al., 2005). Finally, cells were fixed and subsequent ICC analysis was performed. Both fusion proteins were able to translocate into the CV1 fibroblast cells, the process of cellular uptake seemed to be decelerated for ΔNanog-TAT though. After 5h, Nanog-TAT was detectable within vesicles inside the cytoplasm already forming a perinuclear pattern. In contrast, ΔNanog-TAT could be detected in the cytoplasm as well, but was only starting to accumulate around the nucleus. The trapping of the two fusion proteins inside cytoplasmic vesicles as well as the perinuclear pattern thereof is a feature also observed by confocal microscopy of living cells cultivated with a transducible Cre recombinase labeled with Alexa Fluor 633 (Tunnemann et al., 2006). Using confocal microscopy does not allow widespread detection of transducible Cre recombinase inside the nucleus though, but in contrast a sensitive reporter assay indicated Cre-mediated recombination nevertheless. This observation is unsurprising since 99% of the cargo proteins remain inside of the macropinosomes and do not get released into the cytosol (Kaplan et al., 2005). Therefore a co-localization of Nanog-TAT with the nuclei of CV1 cells has to be regarded with suspicion. The deceleration of the cellular uptake

of ΔNanog-TAT could be due to the fact that within the homeodomain of murine Nanog an aa sequence is present, which exhibits 62.5% homology to the 16 aa long penetratin domain, derived from the third helix of Antennapedia, which was shown to translocate into neural cells. In particular, the tryptophan W_6 of the penetratin domain is conserved inside the Nanog homeodomain and is known to play a major role in the translocation process (Derossi et al., 1994). Since this sequence is missing in the control protein, the process of translocation could likely be decelerated as no cumulative effect of the artificial TAT PTD combined with the homeodomain of Nanog, potentially harboring an endogenous NLS, can take place. Taken together the results of the ICC analysis of Nanog-TAT and ΔNanog-TAT exhibit a picture similar to the observation made in living cells, indicating cellular uptake of both fusion proteins.

Initial studies in our workgroup showed that Nanog-TAT is able to liberate murine Oct3/4 GiP ES cells from LIF dependence, a feature known from murine ES cells overexpressing Nanog (Chambers et al., 2003). Nanog-TAT was able to sustain 'undifferentiated', AP-positive ES cells in the absence of LIF, the addition of the peptide TAT-HA2 was required though. Thereafter transduced ES cells cultivated for several passages in the absence of LIF but in the presence of Nanog-TAT were still able to give rise to all three germ layers in an EB differentiation paradigm as well as they formed teratomas upon injection into immune-compromised mice. Within these teratomas tissues of all three germ layers were present. Moreover, Nanog-TAT transduced ES cells gave rise to chimeric animals upon blastocyst injection, although to a weak extent (Peitz, 2007).

To test for specificity of the effect of Nanog-TAT in Oct3/4 GiP ES cells, the same ES cells were cultivated in medium containing 50nM of the control protein ΔNanog-TAT for 3 days either in the presence or absence of LIF. Over this period of time, ES cells in the absence of LIF differentiated independent of the application of ΔNanog-TAT. In contrast, a major part of the ES cells cultivated with LIF retained an 'undifferentiated' phenotype, again independent of ΔNanog-TAT. After 3 days cells were stained for AP in order to determine the amount of ES cells exhibiting a pluripotent phenotype. In the presence of the cytokine LIF the amount of 'undifferentiated' cells within the control mirrored the quantity of 'undifferentiated' ES cells in the wells incubated with ΔNanog-TAT. Spontaneous differentiation occurred in both of these approaches since 22% and 26% of mixed colonies could be detected, respectively. A negligible amount of completely differentiated colonies was observed in both approaches as well. The size of the ES cell colonies did differ though. ES cells cultivated with the control protein gave rise to smaller colonies compared to the control. This phenomenon was also apparent for Nanog-TAT and could be due to the stress ES cells eventually undergo when protein transduction is conducted. ES cells cultivated with or without ΔNanog-TAT in the absence of LIF and the presence of LIF inhibitor interestingly exhibited exactly the same number of differentiated

colonies and mixed colonies, i.e. 78% of differentiated colonies and 22% of mixed colonies. No 'undifferentiated' colonies could be observed in both approaches. Taken together, these results suggest that ΔNanog-TAT can indeed serve as a proper control protein in further experimental setups, since it shows equal behavior to the control approach when applied on murine ES cells. Thus, the specificity of the effect of Nanog-TAT on murine ES cells could be hereby verified.

4.3 Molecular function of Nanog-TAT in somatic cells

Since the overexpression of Nanog in fibroblast cells led to apoptosis of target cells, most likely due to the toxic effect of the strong Nanog expression (Winnemöller, 2007), the technique of protein transduction offered a suitable tool to investigate the function of Nanog in a time-dependent manner. Moreover, the morphology of fibroblast cells favors them over ES cells regarding protein transduction, since fibroblast cells exhibit a larger surface combined with a monolayer growth enabling optimal exposure to extrinsic stimuli. Additionally fibroblast cells represent a robust and reliable cellular system for the investigation of transformation, proliferation as well as reprogramming.

Previous studies in our workgroup showed that NIH 3T3 cells, typically exhibiting strict contact inhibition, gave rise to three-dimensional foci upon cultivation with Nanog-TAT in a reversible manner. Soft agar assays confirmed the results obtained from transduced NIH 3T3 cells. Additionally, MEFs treated with Nanog-TAT exhibited enhanced proliferation rates, thereby seeming to bypass cellular senescence. At the same time the chromosome set of the Nanog-TAT treated fibroblast population remained stable in contrast to MEFs cultivated with control medium (Winnemöller, 2007).

To investigate the molecular mechanisms behind the phenotype observed in MEFs, cells synchronized for cell cycle were incubated with Nanog-TAT for distinct time points and subsequently the RNA expression profile for several key molecules involved in senescence as well as cell cycle regulation was assessed via RT-PCR. No significant change in RNA expression levels as well as protein expression could be detected for $p16^{INK4a}$, $p21^{CIP/WAF}$, p53, FGF receptor 1 and Cyclin D1. After 21 hours a reduction of 73% in the transcription of $p27^{KIP1}$ was detected though, and this observation could be further verified by immunoblot analysis. In contrast fibroblasts cultivated with control medium or ΔNanog-TAT did not show a down-regulation of $p27^{KIP1}$, neither in RT-PCR nor immunoblot analysis. $p27^{KIP1}$, together with other cyclin-dependent kinase inhibitors (CKI), is responsible for regulating cell cycle progression. $p27^{KIP1}$ was initially described as an inhibitor of Cyclin E-CDK2 and Cyclin D-CDK4 complex activity (Polyak et al., 1994; Toyoshima and Hunter, 1994). Thereby $p27^{KIP1}$ is regulating the transition from G1 to S phase within the cell cycle as it causes the inhibition of pRb

phosphorylation (Ji and Zhu, 2005; Sa et al., 2005). A hyperphosphorylated form of pRb is needed in order to pass the restriction point within the cell cycle, i.e. to proliferate (Hitomi et al., 2006). Upon translocation of $p27^{KIP1}$ from the nucleus into the cytosol, a process mediated by Cyclin D2 (Susaki et al., 2007), $p27^{KIP1}$ is degraded by Kip1 ubiquitylation-promoting complex (KPC)-dependent proteolysis (Hara et al., 2005; Kamura et al., 2004; Kotoshiba et al., 2005). In order to further investigate the molecular path of $p27^{KIP1}$ in MEFs upon Nanog-TAT treatment, it would be for instance interesting to take a look at the phosphorylation of $p27^{KIP1}$ on serine 10 since this is one initial step in the process of translocation of $p27^{KIP1}$ to the cytosol where degradation of the CKI takes place. Moreover one could determine the activity of Cyclin-CDK complexes via kinase assay to analyze direct down-stream targets of $p27^{KIP1}$. This experimental approach would close the gap between down-regulation of $p27^{KIP1}$ and the effects observed on pRb expression and phosphorylation.

Namely, upon the treatment with Nanog-TAT for distinct periods of time, synchronized MEFs exhibited an enhanced expression as well as an increase in phosphorylation of pRb. According to the stage of the cell cycle pRb either is unphosphorylated or becomes hyperphosphorylated. In its unphosphorylated state pRb is active (Buchkovich et al., 1989; Knudsen and Wang, 1996; Knudsen and Wang, 1997; Ludlow et al., 1989), i.e. it prevents the cell from progression through the cell cycle. As soon as pRb gets hyperphosphorylated the protein becomes inactive (Harbour et al., 1999; Rubin et al., 2005) and allows cell cycle transition resulting in the activation of E2F transcription factors, which are needed during later stages of the cell cycle (Chellappan et al., 1991; Kaelin et al., 1992).

In G0 phase pRb exists completely unphosphorylated before it becomes hypophosphorylated on very few serine and threonine residues in G1 phase. CDK4/6-cyclin D complexes execute this initial phosphorylation of pRb (Kitagawa et al., 1996). pRb gets hyperphosphorylated on large numbers of serine and threonine residues as soon as the cell has passed beyond the restriction point in late G1 phase, a task fulfilled by CDK2-cyclin E complexes (Lundberg and Weinberg, 1998). Throughout the rest of the cell cycle pRb remains hyperphosphorylated due to activities of CDK-cyclin E, A and B complexes. When mitosis is finished the phosphate groups are removed from pRb via an enzyme called protein phosphatase type 1 (PP1) (Berndt et al., 1997). The cell is now ready for a new division. For a simplified scheme see Figure 33.

As pRb is a direct target of Cyclin-CDK complex activity, resulting in phosphorylation thereof, it could be demonstrated that Nanog-TAT is indeed influencing the expression of $p27^{KIP1}$ including one of its down-stream targets. Through the enhanced expression and phosphorylation of pRb, MEFs transduced with Nanog-TAT were able to progress over restriction points within the cell cycle faster than control cells, as these did not exhibit enhanced proliferation and phosphorylation of pRb, thus were not able to accelerate cell cycle progression. The

phenotypical observations initially made by growth curve analysis on MEFs (Winnemöller, 2007) could hereby be linked to molecular changes within the cell cycle.

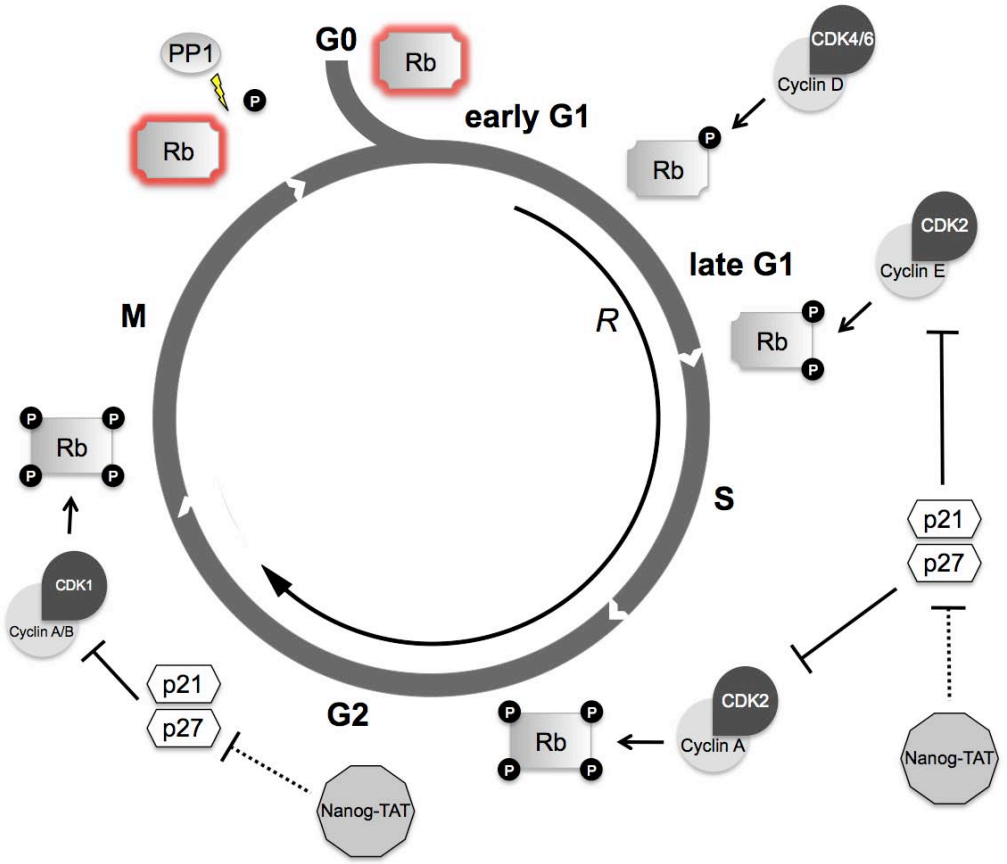

Figure 33: Simplified overview on cell cycle regulation by Cyclins, CDKs and CKIs
During early G1 phase Retinoblastoma protein (Rb) is unphosphorylated, i.e. active. CDK4/6- Cyclin D complexes initiate hypophosphorylation of Rb during G1 phase allowing the cell to pass beyond the restriction point in late G1 phase. Hyperphosphorylation of Rb is mediated and sustained by other CDK-Cyclin complexes. Phosphorylated pRb is inactive and cells can progress through the cell cycle. During Mitosis pRb is dephosphorylated by PP1 and shifted back into its active state. CKIs like $p21^{CIP/WAF}$ and $p27^{KIP1}$ can inhibit cell cycle progression though. Nanog, on the other hand, appears to be able to inhibit the expression of $p27^{KIP1}$ thereby allowing cells to pass through a restriction point in cell cycle allowing enhanced proliferation. G0: zero gap phase; G1: first gap phase; S: synthesis phase; G2: second gap phase; M: mitosis; R: restriction point; PP1: protein phosphatase 1 (adapted from Daniel, 2002).

In order to investigate any potential direct interaction between $p27^{KIP1}$ and Nanog co-immunoprecipitation experiments could be conducted as of today no direct link between the stemness factor and the CKI is known.

Since murine Nanog only shares a homology of 55% on aa basis (Hart et al., 2004) with human Nanog, it was interesting that Nanog-TAT exhibited an influence on human ES cells by partially inhibiting their differentiation (Peitz, 2007). In order to investigate the influence of Nanog-TAT on human somatic cells, dermal fibroblasts were cultivated with Nanog-TAT for several passages. These fibroblast cells showed a change in morphology compared to cells treated with

control medium. Cells cultivated with Nanog-TAT exhibited a more spindle-like shape and the ratio of cytoplasm to nucleus declined compared to control populations. Although SA β-Galactosidase is widely used to detect senescent cells *in vitro*, younger cells also express this marker gene although to a lower extent (Kurz et al., 2000). Interestingly, human dermal fibroblasts cultivated with Nanog-TAT exhibited only few cells expressing SA β-Galactosidase compared to a higher amount of SA β-Galactosidase-positive control cells. This observation may serve as a first indication for a juvenescent effect of Nanog-TAT. Growth curve analysis over a period of 10 passages indicated an enhanced proliferation rate for fibroblasts cultivated with Nanog-TAT. In contrast to murine fibroblasts, human fibroblast cells exhibit a longer, still limited, proliferating life span *in vitro*. A period of intense proliferation is followed by a progressive loss thereof until fibroblast cells cease to proliferate but still remain viable. This phenomenon was termed 'replicative senescence' (Hayflick and Moorhead, 1961). The lifespan of fibroblasts was shown to be independent of the age of the cell donor (Cristofalo et al., 1998) suggesting independence of the process of aging *in vivo* from replicative senescence *in vitro*. Senescence in human fibroblasts was shown to be influenced by several molecules, namely p53, $p21^{CIP/WAF}$, $p16^{INK4a}$ as well as pRb (Alcorta et al., 1996; Kulju and Lehman, 1995; Rogan et al., 1995; Tahara et al., 1995; Whitaker et al., 1995). A disruption of the $p21^{CIP/WAF}$ gene enables fibroblast cells to bypass senescence (Brown et al., 1997), an effect observed as well upon treatment with dexamethason, which also results in a change of $p21^{CIP/WAF}$ expression (Li et al., 1998).

So as to investigate the molecular events leading to the morphological changes as well as the enhanced proliferation observed in human dermal fibroblasts in this thesis, RNA was isolated thereof after cultivation with Nanog-TAT for at least 2 weeks. These unsynchronized cells did already exhibit changes in morphology as described above. Expression levels were analyzed via microarray analysis. Untreated cells served as a control. Interestingly, other factors altered their expression in human dermal fibroblasts cultivated with Nanog-TAT than in MEFs treated with the transducible stemness factor, as no change in the expression level of $p27^{KIP1}$ could be observed. Additionally, no change in RNA expression levels of $p16^{INK4a}$, $p21^{CIP/WAF}$, p53 or pRb could be detected. Moreover, a recent publication suggested that Nanog exhibits a function in the G1 to S phase transition of human ES cells. The authors could link this observation to the direct interaction of Nanog with CDK6 and the promoter region of CDC25A as well. Nanog overexpressing human ES cells exhibited an increased level of CDK6 and CDC25 as analyzed by immunoblot (Zhang et al., 2009). However, analyzing the whole genome expression of human dermal fibroblasts in this work indicated no change in expression of these two cell cycle regulators.

Instead, genes encoding for inflammatory cytokines and chemokines, e.g. interleukin-6, interleukin-8, interleukin-35, chemokine (C-X-C motif) ligand 6 as well as chemokine (C-C motif) ligand 2, were down-regulated in human dermal fibroblasts upon cultivation with Nanog-TAT. Additionally, the matrix metallopeptidase 9, Metallothionein-1G and Stromelysin-1 were expressed to a lower extent compared to control cells. Amongst the genes whose expression was up-regulated upon Nanog-TAT cultivation, the oligomeric matrix protein (COMP), the inhibitor of differentiation 1 (ID1) protein as well as Cyclin D1, the metalloproteinase inhibitor 3 (TIMP3) and collagen alpha-1 (IV) chain protein (COL4A1) were found. An increased expression of Stromelysin was observed by Millis *et al.* in human fibroblast cells upon cellular aging (Millis et al., 1992). The expression of matrix proteases as well as inflammatory chemokines and cytokines was found to be a common feature in senescent dermal fibroblasts (Millis et al., 1992; Shelton et al., 1999). Moreover, collagen and keratin expression was down-regulated in aging dermal fibroblasts (Shelton et al., 1999). West and colleagues could show that senescent fibroblasts expressed a relatively weak level of the metalloproteinase inhibitor (TIMP) (West et al., 1989). In accordance with this observation, TIMP-1 expression was also found to be low in senescent fibroblasts as shown by others. Interestingly, expression thereof could not be induced by serum (Millis et al., 1992). Hence, it appears as cultivation of human dermal fibroblasts with Nanog-TAT leads to a partially inverted transcription profile normally observed in senescent human fibroblasts, further indicating a juvenescent effect of Nanog-TAT. The strong expression of cartilage oligomeric matrix protein (COMP) in Nanog-TAT treated fibroblasts could not be linked to published data, since the expression thereof was found to be high in aging fibroblasts (Ly et al., 2000). As the age of the cell donor does not influence the fibroblast lifespan (Cristofalo et al., 1998), one should take into consideration that the dermal fibroblast cells treated with Nanog-TAT exhibited a passage number of 18, i.e. these cells depict a population of cells where senescence may still be in its early onset. Therefore the influence of Nanog-TAT on COMP expression cannot fully be compared to completely senescent fibroblast cells analyzed by Ly and colleagues. The expression of actin alpha protein and collagen alpha-1 (IV) protein was highly up-regulated in cells cultivated with Nanog-TAT and could be due to the morphological changes these cells undergo, although actin type alpha is mainly restricted to cardiac muscle. Collagen alpha-1 (IV) is mostly responsible for the membrane basement structure of mammalian cells. ID1 is generally considered a protein to be involved in cell growth and senescence and was shown to delay senescence in keratinocytes (Nickoloff et al., 2000), an observation matching findings in this work. An up-regulation of Cyclin D1 - being part of the cell cycle regulatory machinery - upon Nanog-TAT treatment, could indicate an extension of the replicative lifespan, as it was shown for keratinocytes overexpressing Cyclin D1 (Opitz et al., 2001). Peptidase inhibitor 16 (PI16) is found to be expressed in prostate cancer and may eventually suggest a transforming event within the cell culture dish upon Nanog-TAT treatment. Taken together, the

RNA expression analysis of cells cultivated with Nanog-TAT shows a pattern resembling that of juvenile fibroblasts in contrast to the control cells.

It would be of great interest to further propagate dermal fibroblasts in the presence of Nanog-TAT until these cells become fully senescent. Then again RNA expression analysis as well as additional immunoblot analysis should be conducted to analyze whether a change in the expression of p53, $p21^{CIP/WAF}$, $p16^{INK4a}$ as well as pRb can be detected to finally link the phenotypic observations to molecular events known to be involved in cellular aging. Moreover, karyotypic analysis of long-term propagated fibroblasts should be performed to check whether the stabilizing effect on the chromosome set observed in MEFs (Winnemöller, 2007) is apparent in human somatic cells as well.

In conclusion, Nanog activity in aging human somatic cells results in a partially juvenescent cellular phenotype, i.e. a high nucleocytoplasmic ratio (small cell size) as well as low expression of for instance stromelysin, inflammatory genes, extracellular matrix-degrading enzymes and SA β-Galactosidase expression.

4.4 The role of Nanog in the process of reprogramming

Given its crucial role in the circuitry of pluripotency (Boyer et al., 2005; Loh et al., 2006) one may wonder about Nanog not being one of the originally identified 4 reprogramming factors. Interestingly, in a 9 factor reprogramming approach, including Oct3/4, Klf4, c-myc and Nanog but not Sox2, Takahashi and Yamanaka could observe iPS cell emergence (Takahashi and Yamanaka, 2006). Eventually the other 5 factors besides Oct3/4, Klf4, c-myc and Nanog lowered the reprogramming efficiency, which might have resulted in missing the effective combination of Oct3/4, Nanog, Klf4 and c-myc. So as Nanog appears to be an important, however not pivotal factor in the act of reprogramming and no detailed understanding of the influence of Nanog on the process of reprogramming was apparent at the time, the idea was to investigate the function of the stemness factor during cellular reprogramming. As Nanog-TAT offers the possibility to modulate Nanog function in a time-dependent manner, the effect during different phases of the process of reprogramming could be analyzed. Moreover, Nanog-TAT was successfully applied onto MEFs during cell cycle analysis in this work, underlining its sound protein transduction capability as well as its functional abilities; especially since target cells are the same. In a first instance, it was interesting to analyze whether the influence of Nanog on the cell cycle of MEFs, i.e. the target cells of reprogramming, could enhance the efficiency of cellular reprogramming. However, MEFs cultivated with Nanog-TAT either prior to viral transduction with OKSM or for 5 days post infection with OKSM did not show an increase in reprogramming efficiency. Additionally, a permanent application of Nanog-TAT starting from day 1 up to day 15 did not

lead to a higher reprogramming efficiency. The first experiments showed that the influence of Nanog-TAT on MEFs, i.e. the down-regulation of $p27^{KIP1}$, which results in an enhanced proliferation, could not provoke a higher reprogramming efficiency. Apart from that, hypothetically it would not have been an enhanced reprogramming process but rather an emergence of more iPS colonies due to better retroviral infection caused by higher proliferation rates of MEFs. The observation of no beneficial effect may be due to the fact that the cellular noise caused by the viral transduction of OKSM simply overlays the effect caused by Nanog-TAT observed in MEFs. The introduction of c-myc alone results in drastic cellular changes, like an enhanced proliferation. Namely, the overexpression of c-myc enables melanoma cells to suppress senescence (Zhuang et al., 2008) whereas the depletion of c-myc inhibits the proliferation of tumor cells (Wang et al., 2008a). Moreover, the introduction of c-myc together with simian virus 40 large T antigen is able to immortalize human fibroblasts (Kim et al., 2001), emphasizing the striking potential of c-myc. On the other hand, c-myc individually was found to also promote the most ES-like expression pattern in fibroblasts compared to the other three reprogramming factors Oct3/4, Klf4 and Sox2 (Sridharan et al., 2009). Probably the protein transduction technique in the case of Nanog-TAT, as it is today, is limited in this matter, as it can hardly compete against the major cellular alterations evoked by the integration of four retroviruses initially resulting in a cellular chaos that can lead to several cell fates besides reprogramming like apoptosis, transformation or reprogramming-induced senescence (RIS), which stands in contrast to stress- or oxygen-induced senescence (Banito and Gil, 2010). A different, i.e. higher concentration of Nanog-TAT could eventually be important to overcome the above-mentioned limitations. This hypothesis is further reinforced, since the depletion of several key molecules of the cell cycle in contrast was shown to greatly promote reprogramming efficiency (Hong et al., 2009; Kawamura et al., 2009; Li et al., 2009; Marion et al., 2009; Utikal et al., 2009). Little is known about the karyotypic status of those cells though.

The second experiment seems to indicate that the permanent presence of Nanog during the complete process of reprogramming is not conducive to iPS cell generation. This assumption is further strengthened by the observation that the viral transduction of MEFs with OKSM plus an additional retroviral vector encoding for Nanog led to higher transformation within the culture dish (Marc Thier, personal communication). Maherali and colleagues did generate human iPS cells using the classical four reprogramming factors OKSM as well as OKSM plus an additional viral construct encoding for Nanog. They do not state any difference between these two approaches (Maherali et al., 2008). In line with this finding, another publication by Lowry at al., where on the one hand OCT3/4, SOX2, C-MYC and KLF4 as well as on the other hand the beforehand mentioned factors together with a retrovirus carrying the genetic information for NANOG were used to generate human iPS cells, could not show any difference between these two experimental setups (Lowry et al., 2008). A combination of six reprogramming factors, i.e.

OCT3/4, SOX2, C-MYC, KLF4, LIN28 and NANOG led to a ten-fold increase in iPS cell generation (Liao et al., 2008) though. Moreover the appearance of those iPS cell colonies was accelerated. Since LIN28 was used in this experimental setup in addition to NANOG and OKSM it cannot be ruled out that the effect observed is due to LIN28 only, known to influence cell proliferation.

Recently, two publications defined molecular cornerstones during the process of reprogramming (Brambrink et al., 2008; Stadtfeld et al., 2008a). It was shown that with the decrease of the representative fibroblast-specific marker Thy1, the sequential increase of pluripotency markers was accompanied. First, AP expression could be detected starting from day 3 post infection with OKSM. This event was followed by the expression of SSEA-1 around day 6 and finally led to the expression of Nanog and Oct3/4 starting at day 10 of the reprogramming process. Additionally telomerase activity as well as the reactivation of the X chromosome was demonstrated. The observation that the pluripotency factors Oct3/4 and Nanog became activated around day 10 post infection, led to the hypothesis that Nanog most likely has an influence on the act of reprogramming during later stages of the process. Cultivation of MEFs - retrovirally transduced with OKSM - with Nanog-TAT at three defined time points, indicated that the exogenous Nanog expression was of great benefit for the reprogramming efficiency when applied for 5 consecutive days starting at day 10. Application of Nanog-TAT from day 6 and day 8 *post infection* did not show a substantial beneficial effect on the generation of iPS cells. It was now interesting to exactly determine the enhancement of reprogramming efficiency. To this end, Nanog-TAT was applied for 10 days on OKSM transduced MEFs starting from day 10 post infection. In the end, colonies that had re-activated the Oct3/4 promoter and showed iPS cell morphology were counted. Compared to control cells infected only with OKSM, Nanog-TAT treated cells exhibited an increase in iPS cell generation by the factor of 3, an observation not completely surprising due to several data already published. In 2006, Silva and colleagues could show that an elevated level of Nanog would facilitate reprogramming in a cell fusion paradigm (Silva et al., 2006). In a follow-up publication the authors could further elucidate the role of Nanog in the process of reprogramming, an event which Silva and colleagues termed the 'establishment of the ground state of pluripotency'. They showed that Nanog mediates both, the acquisition of embryonic as well as induced pluripotency. Interestingly they found Nanog to be dispensable in the beginning of cellular reprogramming but essential to partially reprogrammed cells to transit to the ground state of pluripotency. Nanog mRNA was found to be up-regulated from day 7 onwards *post infection* in the reprogramming process, the same time where other pluripotency markers became up-regulated as well. Especially the observation that Nanog-deficient cells could be reprogrammed underlines its full dispensability in the initial steps of the reprogramming process (Silva et al., 2009). The process as such can be divided into several stages. The first step, mediated by Oct3/4, Sox2 and Klf4 seems to be the generation of dedifferentiated pre-iPS cells. For the acquisition of the next step

cells have to overcome certain obstacles, as they appear to be trapped in this pre-iPS cell stage (Okita et al., 2007). For the relief of this stage the expression of Nanog is assumed to play an important role. A possible function of Nanog within this process may be its ability to orchestrate transition to the ground state of pluripotency as it could facilitate the cooperative binding of the core pluripotency factors to their related ES cell targets. A high throughput screen for small molecules able to substitute viral reprogramming factors led to the emergence of RepSox, namely a replacement molecule for Sox2 (Ichida et al., 2009). In murine replacement reprogramming approaches RepSox, an inhibitor of TGF-β signaling, was able to give rise to iPS cells upon retroviral transduction with OKM only, and this is likely due to the fact that RepSox induces the expression of Nanog as it was shown by the authors. Furthermore the time window for the application of RepSox could be narrowed down to an optimal time point of application. Application of RepSox 11 days *post retroviral infection* with the reprogramming factors OKM seems to yield highest fold change in the generation of iPS cells. Unfortunately, the authors did not show the fold change of iPS cell generation for day 10 *post infection*, but in contrast the treatment with RepSox at day 9 *post retroviral infection* did not lead to an enhanced reprogramming process. Day 10 *post infection* could therefore likely be the optimal time point for the application of RepSox, i.e. the induction of Nanog. This would be in line with the observations made in this work. RepSox was able to replace not only Sox2 but c-myc as well. Additionally, retrovirally transduced Nanog could replace Sox2 in MEFs infected with OKM (Ichida et al., 2009). Of course it would now be of interest to investigate whether Nanog-TAT is able to beneficially contribute to the generation of iPS cells derived from MEFs infected with Oct3/4, Sox2 and Klf4 only. As both reprogramming factors, Oct3/4 and Sox2, are on hand in our workgroup (Bosnali and Edenhofer, 2008) in the form of transducible proteins, their use together with Nanog-TAT could lead to a reprogramming paradigm, where only one viral factor would be necessary. This factor could finally be removed using one of three recombinases available in our workgroup (Anastassiadis et al., 2009; Patsch et al., 2010; Peitz et al., 2002). In a very recent study it was shown that Tbx3 was able to improve the germ-line competency of iPS cells (Han et al., 2010). It was suggested that this finding is linked to the observation that Tbx3 appears to regulate many pluripotency-associated target genes as judged by chromatin immunoprecipitation sequence analysis. Moreover, Tbx3 shares several common downstream targets of Nanog for example. The authors propose that Tbx3 exhibits a role during initial phases of the reprogramming process as well as during later stages. Therefore it is likely that the beneficial effects on germ-line competency arise from the fact that Tbx3 and Nanog initiate the expression of shared downstream target genes thereby conciliating enhanced germ-line competency. Taken into consideration that recently Niwa and colleagues suggested a parallel circuitry for LIF-signaling, namely LIF not only exhibiting functionality via the Stat3 pathways, which leads to the activation of Klf4 and subsequently Sox2, but instead LIF also being able to

regulate phosphoinositide 3(PI3)-kinase as well as mitogen-activated protein kinase (MAPK), this may further strengthen the above mentioned hypothesis. As on the one hand PI3K was demonstrated to activate Tbx3 in the presence of LIF, MAPK signaling was shown to inhibit Tbx3 activity upon LIF stimulation on the other hand. Nanog, being downstream of Tbx3 then regulates the expression of Oct3/4 in concert with Sox2 (Niwa et al., 2009). It would therefore be conceivable that not Tbx3 but Nanog alone could be sufficient to impart enhanced germ-line competency to iPS cells. To elucidate this hypothesis an experimental reprogramming setup employing Nanog-TAT transduction could be meaningful. Moreover it could be determined if it is eventually feasible to generate murine iPS cells in the absence of the cytokine LIF but in the presence of Nanog-TAT. LIF signaling would not lead to the inhibition of Tbx3 via the MAPK pathway and exogenous Nanog-TAT would introduce intrinsic Nanog activity in the absence of LIF.

4.5 Outlook

A transducible variant of Nanog, as analyzed in this work could be of great use under various aspects. As Nanog-TAT was able to confer juvenescent properties to various primary somatic cell lines one potential application could be found in tissue replacement therapy. One major limitation therein is the cell expansion of primary cells *in vitro* (Sipe, 2002). The application of Nanog-TAT would offer a non-genetic approach to enhance cell proliferation whilst maintaining a stable karyotype. Another potential application could be the process of reprogramming via cell cycle modulation, since the efficiencies thereof are still low. The depletion of major cell cycle factors like p53, $p21^{CIP/WAF}$ or $p16^{INK4a}$ was shown to greatly facilitate reprogramming but the target cells were likely to apply an aberrant karyotype. Nanog-TAT, potentially able to circumvent this limitation, was not able to overcome the cellular background noise occurring after introduction of the four classical retroviral reprogramming factors. There are several cell fates, which thereby can occur. First of all, cells may become apoptotic. Secondly cells can undergo transforming events and finally cells may acquire a senescent phenotype acquired due to RIS before they make their way towards partially reprogrammed cells to finally give rise to iPS cells (reviewed in Banito and Gil, 2010). Maybe the use of an enhanced Nanog fusion protein, exhibiting i) a higher applicable concentration in cell culture as well as ii) the additional usage of alternative peptides beneficial for the process of protein transduction, cellular stability and activity, could exhibit functionality during initial stages of reprogramming and help overcoming RIS. Interestingly, Nanog-TAT could enhance reprogramming efficiency when applied at later stages of the reprogramming process. As the ommitance of c-myc during reprogramming is highly desirable, due to potential tumor formation of the target cells, it decreases the reprogramming efficiency though. Thus, Nanog-TAT, in concert with certain small molecules

shown to increase reprogramming efficiency like AZA, TSA or VPA (reviewed in Feng et al., 2009) could be used to substitute for c-myc. As transducible variants of Oct3/4 and Sox2 are at hand in our group a reprogramming paradigm applying these two factors together with Nanog-TAT would be imaginable. Only Klf4 would be introduced using viral vectors and could be excised when flanked by recognition sites for site-specific recombinases. It was shown for human ES cells that NANOG is regulated by KLF4 and PBX1 (Chan et al., 2009), since the overexpression of KLF4 resulted in an up-regulation of Nanog promoter activity. Maybe with the choice of a cell line already exhibiting Klf4 expression, Nanog-TAT could replace even Klf4. Moreover, it would be of great interest to analyze a transducible variant of human Nanog, already generated in our workgroup, for its functionality in the reprogramming process of human cells or its beneficial effects on the maintenance of pluripotency. To further analyze the influence of Nanog-TAT on the process of reprogramming one could think of several experiments. Since Nanog was shown to compensate for the cytokine LIF, reprogramming paradigms of murine fibroblasts with OKSM in the presence of Nanog-TAT and the absence of LIF could be conducted. To gain further insight into molecular changes occurring during application of Nanog-TAT during reprogramming, feeder-free reprogramming approaches using OKSM transduced MEFs and Nanog-TAT at distinct time points could be performed with a subsequent analysis of genome-wide transcriptional analysis. In order to further verify the beneficial effect of Nanog-TAT on iPS cell generation, so-called pre-iPS cells could be cultivated with Nanog-TAT to investigate whether the transducible stemness factor is able to shift these cells into fully mature iPS cells. With the appearance of so-called ‘naïve’ human ES and iPS cells (Buecker et al., 2010; Hanna et al., 2010), an experimental set-up involving transducible Nanog combined with the cytokine LIF, Forskolin, a TGF-beta inhibitor, a MEK inhibitor and a GSK3 inhibitor could be used to investigate whether it is possible to shift ‘primed’ pluripotent human cells towards their ‘naïve’ pluripotent state, thereby allowing genetic modification in a feasible manner.

5 Summary

Pluripotency of embryonic stem (ES) cells is maintained through various extrinsic and intrinsic influences. In the center of intrinsic stemness signaling, a triad of transcription factors, namely Nanog, Oct3/4 and Sox2, sustain ES cell properties. Among these, Nanog is a particular factor since it mediates acquisition of pluripotency, however, the molecular mechanism underlying stemness function remains unclear. In order to analyze the role of Nanog, a non-genetic gain-of-function paradigm was applied by employing direct protein delivery of Nanog into cells (protein transduction). The biological activity of cell-permeant recombinant Nanog protein, in the following called Nanog-TAT, was assessed using immunofluorescence techniques as well as EMSA demonstrating cellular uptake as well as binding to a specific consensus sequence. A control protein lacking the homeodomain of Nanog (ΔNanog-TAT) showed no binding to the specific consensus sequence. Nanog protein transduction specifically results in an enhanced pluripotent phenotype since the transducible stemness factor liberates murine ES cells from LIF dependence, a phenotype known from genetic overexpression of Nanog in murine ES cells. As it has been shown previously, upon incubation of NIH 3T3 cells with Nanog-TAT, those cells lose contact inhibition and primary mouse embryonic fibroblasts (MEFs) exhibited enhanced proliferation, thereby seeming to bypass senescence. Comprehensive analysis of cell cycle factors revealed that these phenotypic characteristics could be linked to an influence of Nanog-TAT on the cyclin dependent kinase inhibitor (CKI) $p27^{KIP1}$. Nanog-TAT delivery diminished the expression of $p27^{KIP1}$ in somatic cells. Western Blot analysis confirmed the mRNA expression analysis. Repression of CKI $p27^{KIP1}$ subsequently led to the hyperphosphorylation of the tumor suppressor retinoblastoma protein (pRb) thus shifting the protein into its inactive state. These results indicate that MEFs are able to pass beyond the restriction point in cell cycle control otherwise guarded by pRb. A phenotype similar to Nanog-TAT-treated MEFs could be observed upon cultivation of human dermal fibroblasts with Nanog-TAT as those cells exhibit enhanced proliferation rates and additionally do not show senescence-associated β-Galactosidase activity, a marker associated with senescence. Whole genome expression analysis revealed that MP-AF cells cultivated with Nanog-TAT show partially inverted modulation of gene expression compared to senescent human fibroblasts. At later stages during the process of cellular reprogramming, Nanog protein transduction enhanced the efficiency of induction of pluripotency analyzed by re-activation of the Oct3/4 promoter region 3-fold. The thereby established induced pluripotent stem (iPS) cells, generated by retroviral transduction with Oct3/4, Klf4, Sox2 and c-myc (OKSM) and the application of Nanog-TAT from day 10 onwards, did not differ from iPS cells established by retroviral transduction of OKSM alone as judged by the expression of alkaline phosphatase (AP), SSEA-1 and Oct3/4 and their differentiation potential *in vitro*. Thus, Nanog protein transduction is able to conditionally manipulate the stemness status of cells and provides an experimental basis for the molecular analysis of pluripotency maintenance and induction.

6 Declaration

I hereby declare that the work in this thesis is original and has been carried out by myself at the Institute for Reconstructive Neurobiology, Medical Center, University of Bonn. This thesis was prepared under the supervision of Prof. Dr. Oliver Brüstle in fulfillment of the requirements of the doctoral degree of natural sciences of the University of Bonn. I further declare that this work has not been the basis for the awarding of any degree, diploma, fellowship, associateship or similar title at any university or institution.

Bonn, 15/09/2010 _____

Bernhard Münst

7 Acknowledgment

I would like to sincerely thank Prof. Dr. Oliver Brüstle for supervising this thesis and giving me the opportunity to work at the Institute of Reconstructive Neurobiology. I am deeply grateful to Prof. Dr. Hubert Schorle who agreed to act as a second assessor of this thesis. Additionally, I would like to thank Prof. Dr. Walter Witke and PD Dr. Gerhilt van Echten-Deckert for their willingness to examine this thesis as well.

I owe a dept of gratitude to PD Dr. Frank Edenhofer for yielding this fascinating scientific topic on the pluripotency factor Nanog to me. I would like to thank him for the trust placed in me concerning the strategic alignment and the realization of this thesis. Over and above, I am much obliged to him for his willingness to discuss and correct this thesis thoroughly.

To list all the people at the Institute of Reconstructive Neurobiology who deserve to be thanked would go beyond the scope of this acknowledgement, so I have to single out all former and current members of the Stem Cell Engineering Group and the workgroup Peitz and would like to thank them for providing an inspiring working atmosphere. In particular, I would like to thank the people more or less extensively involved in the Nanog project, i.e. first of all Dr. Michael Peitz, Dr. Dirk Winnemöller and Marc Thier (bringing together the transducible Nanog and cellular reprogramming was fun, so thanks Marc), as well as Michael Hons and Amir Keric. In this context, my gratitude is of course appertaining to Nicole Russ as well, since she provided more than just excellent technical assistance, but high spirits on top, which helped a lot not becoming desperate on the way.

I am indebted to Dr. Michael Alexander and Nadine Kluck, who helped with the whole genome expression analysis of the human primary fibroblasts.

Christoph Patsch accompanied me on this long and sometimes rocky path. He is one of the few people I could and always will be able to rely on. Thanks for everything and have a great start in Basel!

Not only did Sabine Schenk proof-read this thesis but she did so much more throughout the whole time we have come to known each other. There is no way I can ever thank her enough, but I can start right now. Thank you with all my heart.

Lastly, I would like to wholeheartedly thank my parents for their encouragement and advice whenever it was needed. Not everybody is lucky enough to have beloved people around him providing unconditional support of any kind.

8 Publications

Munst, B.*, Thier, M.*, Winnemoller, D.*, Peitz, M. and Edenhofer, F. - Nanog protein transduction results in down-regulated $p27^{KIP1}$ protein and suppression of cellular senescence (submitted)

Peitz, M., Munst, B., Yamanaka, S., Brustle, O. and Edenhofer, F. - Modulating stem cell properties by cell-permeable Nanog protein (Manuscript in preparation)

Thier, M., Munst, B. and Edenhofer, F. (2010) - Exploring refined conditions for reprogramming cells by recombinant factors (accepted)

Munst, B.*, Patsch, C.* and Edenhofer, F. (2009) - Engineering cell-permeable protein. *J Vis Exp*.

Bosnali, M.*, Munst, B.*, Thier, M.* and Edenhofer, F. (2009) - Deciphering the stem cell machinery as a basis for understanding the molecular mechanism underlying reprogramming. *Cell Mol Life Sci* **66**, 3403-20.

* authors contributed equally

9 Bibliography

Alcorta, D. A., Xiong, Y., Phelps, D., Hannon, G., Beach, D. and Barrett, J. C. (1996). Involvement of the cyclin-dependent kinase inhibitor p16 (INK4a) in replicative senescence of normal human fibroblasts. *Proc Natl Acad Sci U S A* **93**, 13742-7.

Amit, M., Carpenter, M. K., Inokuma, M. S., Chiu, C. P., Harris, C. P., Waknitz, M. A., Itskovitz-Eldor, J. and Thomson, J. A. (2000). Clonally derived human embryonic stem cell lines maintain pluripotency and proliferative potential for prolonged periods of culture. *Dev Biol* **227**, 271-8.

Anastassiadis, K., Fu, J., Patsch, C., Hu, S., Weidlich, S., Duerschke, K., Buchholz, F., Edenhofer, F. and Stewart, A. F. (2009). Dre recombinase, like Cre, is a highly efficient site-specific recombinase in E. coli, mammalian cells and mice. *Dis Model Mech* **2**, 508-15.

Asoh, S., Ohsawa, I., Mori, T., Katsura, K., Hiraide, T., Katayama, Y., Kimura, M., Ozaki, D., Yamagata, K. and Ohta, S. (2002). Protection against ischemic brain injury by protein therapeutics. *Proc Natl Acad Sci U S A* **99**, 17107-12.

Avilion, A. A., Nicolis, S. K., Pevny, L. H., Perez, L., Vivian, N. and Lovell-Badge, R. (2003). Multipotent cell lineages in early mouse development depend on SOX2 function. *Genes Dev* **17**, 126-40.

Banito, A. and Gil, J. (2010). Induced pluripotent stem cells and senescence: learning the biology to improve the technology. *EMBO Rep* **11**, 353-9.

Bao, W. J., Gao, Y. G., Chang, Y. G., Zhang, T. Y., Lin, X. J., Yan, X. Z. and Hu, H. Y. (2006). Highly efficient expression and purification system of small-size protein domains in Escherichia coli for biochemical characterization. *Protein Expr Purif* **47**, 599-606.

Beattie, G. M., Lopez, A. D., Bucay, N., Hinton, A., Firpo, M. T., King, C. C. and Hayek, A. (2005). Activin A maintains pluripotency of human embryonic stem cells in the absence of feeder layers. *Stem Cells* **23**, 489-95.

Bendall, S. C., Stewart, M. H., Menendez, P., George, D., Vijayaragavan, K., Werbowetski-Ogilvie, T., Ramos-Mejia, V., Rouleau, A., Yang, J., Bosse, M. et al. (2007). IGF and FGF cooperatively establish the regulatory stem cell niche of pluripotent human cells in vitro. *Nature* **448**, 1015-21.

Berndt, N., Dohadwala, M. and Liu, C. W. (1997). Constitutively active protein phosphatase 1alpha causes Rb-dependent G1 arrest in human cancer cells. *Curr Biol* **7**, 375-86.

Boeuf, H., Hauss, C., Graeve, F. D., Baran, N. and Kedinger, C. (1997). Leukemia inhibitory factor-dependent transcriptional activation in embryonic stem cells. *J Cell Biol* **138**, 1207-17.

Bosnali, M. and Edenhofer, F. (2008). Generation of transducible versions of transcription factors Oct4 and Sox2. *Biol Chem* **389**, 851-61.

Bosnali, M., Munst, B., Thier, M. and Edenhofer, F. (2009). Deciphering the stem cell machinery as a basis for understanding the molecular mechanism underlying reprogramming. *Cell Mol Life Sci* **66**, 3403-20.

Boyer, L. A., Lee, T. I., Cole, M. F., Johnstone, S. E., Levine, S. S., Zucker, J. P., Guenther, M. G., Kumar, R. M., Murray, H. L., Jenner, R. G. et al. (2005). Core transcriptional regulatory circuitry in human embryonic stem cells. *Cell* **122**, 947-56.

Boyer, L. A., Plath, K., Zeitlinger, J., Brambrink, T., Medeiros, L. A., Lee, T. I., Levine, S. S., Wernig, M., Tajonar, A., Ray, M. K. et al. (2006). Polycomb complexes repress developmental regulators in murine embryonic stem cells. *Nature* **441**, 349-53.

Bradley, A., Evans, M., Kaufman, M. H. and Robertson, E. (1984). Formation of germ-line chimaeras from embryo-derived teratocarcinoma cell lines. *Nature* **309**, 255-6.

Brambrink, T., Foreman, R., Welstead, G. G., Lengner, C. J., Wernig, M., Suh, H. and Jaenisch, R. (2008). Sequential expression of pluripotency markers during direct reprogramming of mouse somatic cells. *Cell Stem Cell* **2**, 151-9.

Brons, I. G., Smithers, L. E., Trotter, M. W., Rugg-Gunn, P., Sun, B., Chuva de Sousa Lopes, S. M., Howlett, S. K., Clarkson, A., Ahrlund-Richter, L., Pedersen, R. A. et al. (2007). Derivation of pluripotent epiblast stem cells from mammalian embryos. *Nature* **448**, 191-5.

Brown, J. P., Wei, W. and Sedivy, J. M. (1997). Bypass of senescence after disruption of p21CIP1/WAF1 gene in normal diploid human fibroblasts. *Science* **277**, 831-4.

Brustle, O., Jones, K. N., Learish, R. D., Karram, K., Choudhary, K., Wiestler, O. D., Duncan, I. D. and McKay, R. D. (1999). Embryonic stem cell-derived glial precursors: a source of myelinating transplants. *Science* **285**, 754-6.

Buchkovich, K., Duffy, L. A. and Harlow, E. (1989). The retinoblastoma protein is phosphorylated during specific phases of the cell cycle. *Cell* **58**, 1097-105.

Buecker, C., Chen, H. H., Polo, J. M., Daheron, L., Bu, L., Barakat, T. S., Okwieka, P., Porter, A., Gribnau, J., Hochedlinger, K. et al. (2010). A murine ESC-like state facilitates transgenesis and homologous recombination in human pluripotent stem cells. *Cell Stem Cell* **6**, 535-46.

Caron, N. J., Quenneville, S. P. and Tremblay, J. P. (2004). Endosome disruption enhances the functional nuclear delivery of Tat-fusion proteins. *Biochem Biophys Res Commun* **319**, 12-20.

Chambers, I., Colby, D., Robertson, M., Nichols, J., Lee, S., Tweedie, S. and Smith, A. (2003). Functional expression cloning of Nanog, a pluripotency sustaining factor in embryonic stem cells. *Cell* **113**, 643-55.

Chambers, I., Silva, J., Colby, D., Nichols, J., Nijmeijer, B., Robertson, M., Vrana, J., Jones, K., Grotewold, L. and Smith, A. (2007). Nanog safeguards pluripotency and mediates germline development. *Nature* **450**, 1230-4.

Chan, K. K., Zhang, J., Chia, N. Y., Chan, Y. S., Sim, H. S., Tan, K. S., Oh, S. K., Ng, H. H. and Choo, A. B. (2009). KLF4 and PBX1 directly regulate NANOG expression in human embryonic stem cells. *Stem Cells* **27**, 2114-25.

Chellappan, S. P., Hiebert, S., Mudryj, M., Horowitz, J. M. and Nevins, J. R. (1991). The E2F transcription factor is a cellular target for the RB protein. *Cell* **65**, 1053-61.

Chen, G. T. and Inouye, M. (1994). Role of the AGA/AGG codons, the rarest codons in global gene expression in Escherichia coli. *Genes Dev* **8**, 2641-52.

Chen, Q. M., Liu, J. and Merrett, J. B. (2000). Apoptosis or senescence-like growth arrest: influence of cell-cycle position, p53, p21 and bax in H2O2 response of normal human fibroblasts. *Biochem J* **347**, 543-51.

Chew, J. L., Loh, Y. H., Zhang, W., Chen, X., Tam, W. L., Yeap, L. S., Li, P., Ang, Y. S., Lim, B., Robson, P. et al. (2005). Reciprocal transcriptional regulation of Pou5f1 and Sox2 via the Oct4/Sox2 complex in embryonic stem cells. *Mol Cell Biol* **25**, 6031-46.

Connors, L. H., Jiang, Y., Budnik, M., Theberge, R., Prokaeva, T., Bodi, K. L., Seldin, D. C., Costello, C. E. and Skinner, M. (2007). Heterogeneity in primary structure, post-translational modifications, and germline gene usage of nine full-length amyloidogenic kappa1 immunoglobulin light chains. *Biochemistry* **46**, 14259-71.

Console, S., Marty, C., Garcia-Echeverria, C., Schwendener, R. and Ballmer-Hofer, K. (2003). Antennapedia and HIV transactivator of transcription (TAT) "protein transduction domains" promote endocytosis of high molecular weight cargo upon binding to cell surface glycosaminoglycans. *J Biol Chem* **278**, 35109-14.

Cristofalo, V. J., Allen, R. G., Pignolo, R. J., Martin, B. G. and Beck, J. C. (1998). Relationship between donor age and the replicative lifespan of human cells in culture: a reevaluation. *Proc Natl Acad Sci U S A* **95**, 10614-9.

Daheron, L., Opitz, S. L., Zaehres, H., Lensch, M. W., Andrews, P. W., Itskovitz-Eldor, J. and Daley, G. Q. (2004). LIF/STAT3 signaling fails to maintain self-renewal of human embryonic stem cells. *Stem Cells* **22**, 770-8.

Daniel, P. (2002). Deregulation von Zellzyklus und Apoptose

als molekulare Grundlage der Therapieresistenz von Tumoren. In *Medical Center of the Charité*, vol. Habilitation (ed. Berlin: Humboldt University.

Darr, H., Mayshar, Y. and Benvenisty, N. (2006). Overexpression of NANOG in human ES cells enables feeder-free growth while inducing primitive ectoderm features. *Development* **133**, 1193-201.

Derossi, D., Joliot, A. H., Chassaing, G. and Prochiantz, A. (1994). The third helix of the Antennapedia homeodomain translocates through biological membranes. *J Biol Chem* **269**, 10444-50.

Di Leonardo, A., Linke, S. P., Clarkin, K. and Wahl, G. M. (1994). DNA damage triggers a prolonged p53-dependent G1 arrest and long-term induction of Cip1 in normal human fibroblasts. *Genes Dev* **8**, 2540-51.

Dietrich, J. E. and Hiiragi, T. (2007). Stochastic patterning in the mouse pre-implantation embryo. *Development* **134**, 4219-31.

Dietz, G. P. and Bahr, M. (2004). Delivery of bioactive molecules into the cell: the Trojan horse approach. *Mol Cell Neurosci* **27**, 85-131.

Dimri, G. P., Lee, X., Basile, G., Acosta, M., Scott, G., Roskelley, C., Medrano, E. E., Linskens, M., Rubelj, I., Pereira-Smith, O. et al. (1995). A biomarker that identifies senescent human cells in culture and in aging skin in vivo. *Proc Natl Acad Sci U S A* **92**, 9363-7.

Ebert, A. D., Yu, J., Rose, F. F., Jr., Mattis, V. B., Lorson, C. L., Thomson, J. A. and Svendsen, C. N. (2009). Induced pluripotent stem cells from a spinal muscular atrophy patient. *Nature* **457**, 277-80.

Elliott, G. and O'Hare, P. (1997). Intercellular trafficking and protein delivery by a herpesvirus structural protein. *Cell* **88**, 223-33.

Elliott, G. and O'Hare, P. (1999). Intercellular trafficking of VP22-GFP fusion proteins. *Gene Ther* **6**, 149-51.

Eminli, S., Foudi, A., Stadtfeld, M., Maherali, N., Ahfeldt, T., Mostoslavsky, G., Hock, H. and Hochedlinger, K. (2009). Differentiation stage determines potential of hematopoietic cells for reprogramming into induced pluripotent stem cells. *Nat Genet* **41**, 968-76.

Evans, M. J. and Kaufman, M. H. (1981). Establishment in culture of pluripotential cells from mouse embryos. *Nature* **292**, 154-6.

Ezhevsky, S. A., Nagahara, H., Vocero-Akbani, A. M., Gius, D. R., Wei, M. C. and Dowdy, S. F. (1997). Hypo-phosphorylation of the retinoblastoma protein (pRb) by cyclin D:Cdk4/6 complexes results in active pRb. *Proc Natl Acad Sci U S A* **94**, 10699-704.

Feng, B., Ng, J. H., Heng, J. C. and Ng, H. H. (2009). Molecules that promote or enhance reprogramming of somatic cells to induced pluripotent stem cells. *Cell Stem Cell* **4**, 301-12.

Ferri, A. L., Cavallaro, M., Braida, D., Di Cristofano, A., Canta, A., Vezzani, A., Ottolenghi, S., Pandolfi, P. P., Sala, M., DeBiasi, S. et al. (2004). Sox2 deficiency causes neurodegeneration and impaired neurogenesis in the adult mouse brain. *Development* **131**, 3805-19.

Frankel, A. D. and Pabo, C. O. (1988). Cellular uptake of the tat protein from human immunodeficiency virus. *Cell* **55**, 1189-93.

Graham, V., Khudyakov, J., Ellis, P. and Pevny, L. (2003). SOX2 functions to maintain neural progenitor identity. *Neuron* **39**, 749-65.

Greber, B., Lehrach, H. and Adjaye, J. (2007). Fibroblast growth factor 2 modulates transforming growth factor beta signaling in mouse embryonic fibroblasts and human ESCs (hESCs) to support hESC self-renewal. *Stem Cells* **25**, 455-64.

Green, M. and Loewenstein, P. M. (1988). Autonomous functional domains of chemically synthesized human immunodeficiency virus tat trans-activator protein. *Cell* **55**, 1179-88.

Gurdon, J. B. (1962). Adult frogs derived from the nuclei of single somatic cells. *Dev Biol* **4**, 256-73.

Hall, H., Williams, E. J., Moore, S. E., Walsh, F. S., Prochiantz, A. and Doherty, P. (1996). Inhibition of FGF-stimulated phosphatidylinositol hydrolysis and neurite outgrowth by a cell-membrane permeable phosphopeptide. *Curr Biol* **6**, 580-7.

Han, J., Yuan, P., Yang, H., Zhang, J., Soh, B. S., Li, P., Lim, S. L., Cao, S., Tay, J., Orlov, Y. L. et al. (2010). Tbx3 improves the germ-line competency of induced pluripotent stem cells. *Nature* **463**, 1096-100.

Hanna, J., Cheng, A. W., Saha, K., Kim, J., Lengner, C. J., Soldner, F., Cassady, J. P., Muffat, J., Carey, B. W. and Jaenisch, R. (2010). Human embryonic stem cells with biological and epigenetic characteristics similar to those of mouse ESCs. *Proc Natl Acad Sci U S A* **107**, 9222-7.

Hara, T., Kamura, T., Kotoshiba, S., Takahashi, H., Fujiwara, K., Onoyama, I., Shirakawa, M., Mizushima, N. and Nakayama, K. I. (2005). Role of the UBL-UBA protein KPC2 in degradation of p27 at G1 phase of the cell cycle. *Mol Cell Biol* **25**, 9292-303.

Harbour, J. W., Luo, R. X., Dei Santi, A., Postigo, A. A. and Dean, D. C. (1999). Cdk phosphorylation triggers sequential intramolecular interactions that progressively block Rb functions as cells move through G1. *Cell* **98**, 859-69.

Hart, A. H., Hartley, L., Ibrahim, M. and Robb, L. (2004). Identification, cloning and expression analysis of the pluripotency promoting Nanog genes in mouse and human. *Dev Dyn* **230**, 187-98.

Haupt, S., Edenhofer, F., Peitz, M., Leinhaas, A. and Brustle, O. (2007). Stage-specific conditional mutagenesis in mouse embryonic stem cell-derived neural cells and postmitotic neurons by direct delivery of biologically active Cre recombinase. *Stem Cells* **25**, 181-8.

Hay, D. C., Sutherland, L., Clark, J. and Burdon, T. (2004). Oct-4 knockdown induces similar patterns of endoderm and trophoblast differentiation markers in human and mouse embryonic stem cells. *Stem Cells* **22**, 225-35.

Hayashi, K., Lopes, S. M., Tang, F. and Surani, M. A. (2008). Dynamic equilibrium and heterogeneity of mouse pluripotent stem cells with distinct functional and epigenetic states. *Cell Stem Cell* **3**, 391-401.

Hayflick, L. (1965). The Limited in Vitro Lifetime of Human Diploid Cell Strains. *Exp Cell Res* **37**, 614-36.

Hayflick, L. and Moorhead, P. S. (1961). The serial cultivation of human diploid cell strains. *Exp Cell Res* **25**, 585-621.

Herbig, U., Jobling, W. A., Chen, B. P., Chen, D. J. and Sedivy, J. M. (2004). Telomere shortening triggers senescence of human cells through a pathway involving ATM, p53, and p21(CIP1), but not p16(INK4a). *Mol Cell* **14**, 501-13.

Hitomi, M., Yang, K., Guo, Y., Fretthold, J., Harwalkar, J. and Stacey, D. W. (2006). p27Kip1 and cyclin dependent kinase 2 regulate passage through the restriction point. *Cell Cycle* **5**, 2281-9.

Hong, H., Takahashi, K., Ichisaka, T., Aoi, T., Kanagawa, O., Nakagawa, M., Okita, K. and Yamanaka, S. (2009). Suppression of induced pluripotent stem cell generation by the p53-p21 pathway. *Nature* **460**, 1132-5.

Hough, S. R., Clements, I., Welch, P. J. and Wiederholt, K. A. (2006). Differentiation of mouse embryonic stem cells after RNA interference-mediated silencing of OCT4 and Nanog. *Stem Cells* **24**, 1467-75.

Huangfu, D., Osafune, K., Maehr, R., Guo, W., Eijkelenboom, A., Chen, S., Muhlestein, W. and Melton, D. A. (2008). Induction of pluripotent stem cells from primary human fibroblasts with only Oct4 and Sox2. *Nat Biotechnol* **26**, 1269-75.

Humphrey, R. K., Beattie, G. M., Lopez, A. D., Bucay, N., King, C. C., Firpo, M. T., Rose-John, S. and Hayek, A. (2004). Maintenance of pluripotency in human embryonic stem cells is STAT3 independent. *Stem Cells* **22**, 522-30.

Hyslop, L., Stojkovic, M., Armstrong, L., Walter, T., Stojkovic, P., Przyborski, S., Herbert, M., Murdoch, A., Strachan, T. and Lako, M. (2005). Downregulation of NANOG induces differentiation of human embryonic stem cells to extraembryonic lineages. *Stem Cells* **23**, 1035-43.

Ichida, J. K., Blanchard, J., Lam, K., Son, E. Y., Chung, J. E., Egli, D., Loh, K. M., Carter, A. C., Di Giorgio, F. P., Koszka, K. et al. (2009). A small-molecule inhibitor of tgf-Beta signaling replaces sox2 in reprogramming by inducing nanog. *Cell Stem Cell* **5**, 491-503.

Inoue, H., Nojima, H. and Okayama, H. (1990). High efficiency transformation of Escherichia coli with plasmids. *Gene* **96**, 23-8.

Itahana, K., Zou, Y., Itahana, Y., Martinez, J. L., Beausejour, C., Jacobs, J. J., Van Lohuizen, M., Band, V., Campisi, J. and Dimri, G. P. (2003). Control of the replicative life span of human fibroblasts by p16 and the polycomb protein Bmi-1. *Mol Cell Biol* **23**, 389-401.

Ivanova, N., Dobrin, R., Lu, R., Kotenko, I., Levorse, J., DeCoste, C., Schafer, X., Lun, Y. and Lemischka, I. R. (2006). Dissecting self-renewal in stem cells with RNA interference. *Nature* **442**, 533-8.

James, D., Levine, A. J., Besser, D. and Hemmati-Brivanlou, A. (2005). TGFbeta/activin/nodal signaling is necessary for the maintenance of pluripotency in human embryonic stem cells. *Development* **132**, 1273-82.

Jauch, R., Ng, C. K., Saikatendu, K. S., Stevens, R. C. and Kolatkar, P. R. (2008). Crystal structure and DNA binding of the homeodomain of the stem cell transcription factor Nanog. *J Mol Biol* **376**, 758-70.

Jensen, F. C., Girardi, A. J., Gilden, R. V. and Koprowski, H. (1964). Infection of Human and Simian Tissue Cultures with Rous Sarcoma Virus. *Proc Natl Acad Sci U S A* **52**, 53-9.

Ji, P. and Zhu, L. (2005). Using kinetic studies to uncover new Rb functions in inhibiting cell cycle progression. *Cell Cycle* **4**, 373-5.

Jo, D., Nashabi, A., Doxsee, C., Lin, Q., Unutmaz, D., Chen, J. and Ruley, H. E. (2001). Epigenetic regulation of gene structure and function with a cell-permeable Cre recombinase. *Nat Biotechnol* **19**, 929-33.

Johnson, M. H. and Maro, B. (1985). A dissection of the mechanisms generating and stabilizing polarity in mouse 8- and 16-cell blastomeres: the role of cytoskeletal elements. *J Embryol Exp Morphol* **90**, 311-34.

Kaelin, W. G., Jr., Krek, W., Sellers, W. R., DeCaprio, J. A., Ajchenbaum, F., Fuchs, C. S., Chittenden, T., Li, Y., Farnham, P. J., Blanar, M. A. et al. (1992). Expression cloning of a cDNA encoding a retinoblastoma-binding protein with E2F-like properties. *Cell* **70**, 351-64.

Kaji, K., Norrby, K., Paca, A., Mileikovsky, M., Mohseni, P. and Woltjen, K. (2009). Virus-free induction of pluripotency and subsequent excision of reprogramming factors. *Nature* **458**, 771-5.

Kamachi, Y., Uchikawa, M., Tanouchi, A., Sekido, R. and Kondoh, H. (2001). Pax6 and SOX2 form a co-DNA-binding partner complex that regulates initiation of lens development. *Genes Dev* **15**, 1272-86.

Kamura, T., Hara, T., Matsumoto, M., Ishida, N., Okumura, F., Hatakeyama, S., Yoshida, M., Nakayama, K. and Nakayama, K. I. (2004). Cytoplasmic ubiquitin ligase KPC regulates proteolysis of p27(Kip1) at G1 phase. *Nat Cell Biol* **6**, 1229-35.

Kaplan, I. M., Wadia, J. S. and Dowdy, S. F. (2005). Cationic TAT peptide transduction domain enters cells by macropinocytosis. *J Control Release* **102**, 247-53.

Kato, Y., Tani, T., Sotomaru, Y., Kurokawa, K., Kato, J., Doguchi, H., Yasue, H. and Tsunoda, Y. (1998). Eight calves cloned from somatic cells of a single adult. *Science* **282**, 2095-8.

Kaufman, D. S., Hanson, E. T., Lewis, R. L., Auerbach, R. and Thomson, J. A. (2001). Hematopoietic colony-forming cells derived from human embryonic stem cells. *Proc Natl Acad Sci U S A* **98**, 10716-21.

Kawamura, T., Suzuki, J., Wang, Y. V., Menendez, S., Morera, L. B., Raya, A., Wahl, G. M. and Belmonte, J. C. (2009). Linking the p53 tumour suppressor pathway to somatic cell reprogramming. *Nature* **460**, 1140-4.

Kehat, I., Amit, M., Gepstein, A., Huber, I., Itskovitz-Eldor, J. and Gepstein, L. (2003). Development of cardiomyocytes from human ES cells. *Methods Enzymol* **365**, 461-73.

Kehler, J., Tolkunova, E., Koschorz, B., Pesce, M., Gentile, L., Boiani, M., Lomeli, H., Nagy, A., McLaughlin, K. J., Scholer, H. R. et al. (2004). Oct4 is required for primordial germ cell survival. *EMBO Rep* **5**, 1078-83.

Keirstead, H. S., Nistor, G., Bernal, G., Totoiu, M., Cloutier, F., Sharp, K. and Steward, O. (2005). Human embryonic stem cell-derived oligodendrocyte progenitor cell transplants remyelinate and restore locomotion after spinal cord injury. *J Neurosci* **25**, 4694-705.

Kim, D., Kim, C. H., Moon, J. I., Chung, Y. G., Chang, M. Y., Han, B. S., Ko, S., Yang, E., Cha, K. Y., Lanza, R. et al. (2009a). Generation of human induced pluripotent stem cells by direct delivery of reprogramming proteins. *Cell Stem Cell* **4**, 472-6.

Kim, H. S., Shin, J. Y., Yun, J. Y., Ahn, D. K. and Le, J. Y. (2001). Immortalization of human embryonic fibroblasts by overexpression of c-myc and simian virus 40 large T antigen. *Exp Mol Med* **33**, 293-8.

Kim, J. B., Greber, B., Arauzo-Bravo, M. J., Meyer, J., Park, K. I., Zaehres, H. and Scholer, H. R. (2009b). Direct reprogramming of human neural stem cells by OCT4. *Nature* **461**, 649-3.

Kim, J. B., Zaehres, H., Wu, G., Gentile, L., Ko, K., Sebastiano, V., Arauzo-Bravo, M. J., Ruau, D., Han, D. W., Zenke, M. et al. (2008). Pluripotent stem cells induced from adult neural stem cells by reprogramming with two factors. *Nature* **454**, 646-50.

Kitagawa, M., Higashi, H., Jung, H. K., Suzuki-Takahashi, I., Ikeda, M., Tamai, K., Kato, J., Segawa, K., Yoshida, E., Nishimura, S. et al. (1996). The consensus motif for phosphorylation by cyclin D1-Cdk4 is different from that for phosphorylation by cyclin A/E-Cdk2. *EMBO J* **15**, 7060-9.

Klug, M. G., Soonpaa, M. H., Koh, G. Y. and Field, L. J. (1996). Genetically selected cardiomyocytes from differentiating embronic stem cells form stable intracardiac grafts. *J Clin Invest* **98**, 216-24.

Knudsen, E. S. and Wang, J. Y. (1996). Differential regulation of retinoblastoma protein function by specific Cdk phosphorylation sites. *J Biol Chem* **271**, 8313-20.

Knudsen, E. S. and Wang, J. Y. (1997). Dual mechanisms for the inhibition of E2F binding to RB by cyclin-dependent kinase-mediated RB phosphorylation. *Mol Cell Biol* **17**, 5771-83.

Kopp, J. L., Ormsbee, B. D., Desler, M. and Rizzino, A. (2008). Small increases in the level of Sox2 trigger the differentiation of mouse embryonic stem cells. *Stem Cells* **26**, 903-11.

Kotoshiba, S., Kamura, T., Hara, T., Ishida, N. and Nakayama, K. I. (2005). Molecular dissection of the interaction between p27 and Kip1 ubiquitylation-promoting complex, the ubiquitin ligase that regulates proteolysis of p27 in G1 phase. *J Biol Chem* **280**, 17694-700.

Krishnamurthy, J., Torrice, C., Ramsey, M. R., Kovalev, G. I., Al-Regaiey, K., Su, L. and Sharpless, N. E. (2004). Ink4a/Arf expression is a biomarker of aging. *J Clin Invest* **114**, 1299-307.

Krosl, J., Austin, P., Beslu, N., Kroon, E., Humphries, R. K. and Sauvageau, G. (2003). In vitro expansion of hematopoietic stem cells by recombinant TAT-HOXB4 protein. *Nat Med* **9**, 1428-32.

Kulju, K. S. and Lehman, J. M. (1995). Increased p53 protein associated with aging in human diploid fibroblasts. *Exp Cell Res* **217**, 336-45.

Kuroda, T., Tada, M., Kubota, H., Kimura, H., Hatano, S. Y., Suemori, H., Nakatsuji, N. and Tada, T. (2005). Octamer and Sox elements are required for transcriptional cis regulation of Nanog gene expression. *Mol Cell Biol* **25**, 2475-85.

Kurz, D. J., Decary, S., Hong, Y. and Erusalimsky, J. D. (2000). Senescence-associated (beta)-galactosidase reflects an increase in lysosomal mass during replicative ageing of human endothelial cells. *J Cell Sci* **113 (Pt 20)**, 3613-22.

Lavon, N., Yanuka, O. and Benvenisty, N. (2004). Differentiation and isolation of hepatic-like cells from human embryonic stem cells. *Differentiation* **72**, 230-8.

Li, H., Collado, M., Villasante, A., Strati, K., Ortega, S., Canamero, M., Blasco, M. A. and Serrano, M. (2009). The Ink4/Arf locus is a barrier for iPS cell reprogramming. *Nature* **460**, 1136-9.

Li, S., Mawal-Dewan, M., Cristofalo, V. J. and Sell, C. (1998). Enhanced proliferation of human fibroblasts, in the presence of dexamethasone, is accompanied by changes in p21Waf1/Cip1/Sdi1 and the insulin-like growth factor type 1 receptor. *J Cell Physiol* **177**, 396-401.

Liang, J., Wan, M., Zhang, Y., Gu, P., Xin, H., Jung, S. Y., Qin, J., Wong, J., Cooney, A. J., Liu, D. et al. (2008). Nanog and Oct4 associate with unique transcriptional repression complexes in embryonic stem cells. *Nat Cell Biol* **10**, 731-9.

Liao, J., Wu, Z., Wang, Y., Cheng, L., Cui, C., Gao, Y., Chen, T., Rao, L., Chen, S., Jia, N. et al. (2008). Enhanced efficiency of generating induced pluripotent stem (iPS) cells from human somatic cells by a combination of six transcription factors. *Cell Res* **18**, 600-3.

Loh, Y. H., Wu, Q., Chew, J. L., Vega, V. B., Zhang, W., Chen, X., Bourque, G., George, J., Leong, B., Liu, J. et al. (2006). The Oct4 and Nanog transcription network regulates pluripotency in mouse embryonic stem cells. *Nat Genet* **38**, 431-40.

Lowry, W. E., Richter, L., Yachechko, R., Pyle, A. D., Tchieu, J., Sridharan, R., Clark, A. T. and Plath, K. (2008). Generation of human induced pluripotent stem cells from dermal fibroblasts. *Proc Natl Acad Sci U S A* **105**, 2883-8.

Ludlow, J. W., DeCaprio, J. A., Huang, C. M., Lee, W. H., Paucha, E. and Livingston, D. M. (1989). SV40 large T antigen binds preferentially to an underphosphorylated member of the retinoblastoma susceptibility gene product family. *Cell* **56**, 57-65.

Lundberg, A. S. and Weinberg, R. A. (1998). Functional inactivation of the retinoblastoma protein requires sequential modification by at least two distinct cyclin-cdk complexes. *Mol Cell Biol* **18**, 753-61.

Ly, D. H., Lockhart, D. J., Lerner, R. A. and Schultz, P. G. (2000). Mitotic misregulation and human aging. *Science* **287**, 2486-92.

Lyssiotis, C. A., Foreman, R. K., Staerk, J., Garcia, M., Mathur, D., Markoulaki, S., Hanna, J., Lairson, L. L., Charette, B. D., Bouchez, L. C. et al. (2009). Reprogramming of murine fibroblasts to induced pluripotent stem cells with chemical complementation of Klf4. *Proc Natl Acad Sci U S A* **106**, 8912-7.

Maherali, N., Ahfeldt, T., Rigamonti, A., Utikal, J., Cowan, C. and Hochedlinger, K. (2008). A high-efficiency system for the generation and study of human induced pluripotent stem cells. *Cell Stem Cell* **3**, 340-5.

Marion, R. M., Strati, K., Li, H., Murga, M., Blanco, R., Ortega, S., Fernandez-Capetillo, O., Serrano, M. and Blasco, M. A. (2009). A p53-mediated DNA damage response limits reprogramming to ensure iPS cell genomic integrity. *Nature* **460**, 1149-53.

Martens, U. M., Chavez, E. A., Poon, S. S., Schmoor, C. and Lansdorp, P. M. (2000). Accumulation of short telomeres in human fibroblasts prior to replicative senescence. *Exp Cell Res* **256**, 291-9.

Martin, G. R. (1981). Isolation of a pluripotent cell line from early mouse embryos cultured in medium conditioned by teratocarcinoma stem cells. *Proc Natl Acad Sci U S A* **78**, 7634-8.

Masui, S., Nakatake, Y., Toyooka, Y., Shimosato, D., Yagi, R., Takahashi, K., Okochi, H., Okuda, A., Matoba, R., Sharov, A. A. et al. (2007). Pluripotency governed by Sox2 via regulation of Oct3/4 expression in mouse embryonic stem cells. *Nat Cell Biol* **9**, 625-35.

Matsuda, T., Nakamura, T., Nakao, K., Arai, T., Katsuki, M., Heike, T. and Yokota, T. (1999). STAT3 activation is sufficient to maintain an undifferentiated state of mouse embryonic stem cells. *EMBO J* **18**, 4261-9.

Matsushita, M., Noguchi, H., Lu, Y. F., Tomizawa, K., Michiue, H., Li, S. T., Hirose, K., Bonner-Weir, S. and Matsui, H. (2004). Photo-acceleration of protein release from endosome in the protein transduction system. *FEBS Lett* **572**, 221-6.

Michaloglou, C., Vredeveld, L. C., Soengas, M. S., Denoyelle, C., Kuilman, T., van der Horst, C. M., Majoor, D. M., Shay, J. W., Mooi, W. J. and Peeper, D. S. (2005). BRAFE600-associated senescence-like cell cycle arrest of human naevi. *Nature* **436**, 720-4.

Millis, A. J., Hoyle, M., McCue, H. M. and Martini, H. (1992). Differential expression of metalloproteinase and tissue inhibitor of metalloproteinase genes in aged human fibroblasts. *Exp Cell Res* **201**, 373-9.

Mitsui, K., Tokuzawa, Y., Itoh, H., Segawa, K., Murakami, M., Takahashi, K., Maruyama, M., Maeda, M. and Yamanaka, S. (2003). The homeoprotein Nanog is required for maintenance of pluripotency in mouse epiblast and ES cells. *Cell* **113**, 631-42.

Morrison, S. J. and Kimble, J. (2006). Asymmetric and symmetric stem-cell divisions in development and cancer. *Nature* **441**, 1068-74.

Mullin, N. P., Yates, A., Rowe, A. J., Nijmeijer, B., Colby, D., Barlow, P. N., Walkinshaw, M. D. and Chambers, I. (2008). The pluripotency rheostat Nanog functions as a dimer. *Biochem J* **411**, 227-31.

Munst, B., Patsch, C. and Edenhofer, F. (2009). Engineering cell-permeable protein. *J Vis Exp*.

Nagahara, H., Vocero-Akbani, A. M., Snyder, E. L., Ho, A., Latham, D. G., Lissy, N. A., Becker-Hapak, M., Ezhevsky, S. A. and Dowdy, S. F. (1998). Transduction of full-length TAT fusion proteins into mammalian cells: TAT-p27Kip1 induces cell migration. *Nat Med* **4**, 1449-52.

Nagy, A., Gocza, E., Diaz, E. M., Prideaux, V. R., Ivanyi, E., Markkula, M. and Rossant, J. (1990). Embryonic stem cells alone are able to support fetal development in the mouse. *Development* **110**, 815-21.

Nakagawa, M., Koyanagi, M., Tanabe, K., Takahashi, K., Ichisaka, T., Aoi, T., Okita, K., Mochiduki, Y., Takizawa, N. and Yamanaka, S. (2008). Generation of induced pluripotent stem cells without Myc from mouse and human fibroblasts. *Nat Biotechnol* **26**, 101-6.

Nichols, J., Zevnik, B., Anastassiadis, K., Niwa, H., Klewe-Nebenius, D., Chambers, I., Scholer, H. and Smith, A. (1998). Formation of pluripotent stem cells in the mammalian embryo depends on the POU transcription factor Oct4. *Cell* **95**, 379-91.

Nickoloff, B. J., Chaturvedi, V., Bacon, P., Qin, J. Z., Denning, M. F. and Diaz, M. O. (2000). Id-1 delays senescence but does not immortalize keratinocytes. *J Biol Chem* **275**, 27501-4.

Nishimoto, M., Fukushima, A., Okuda, A. and Muramatsu, M. (1999). The gene for the embryonic stem cell coactivator UTF1 carries a regulatory element which selectively interacts with a complex composed of Oct-3/4 and Sox-2. *Mol Cell Biol* **19**, 5453-65.

Niwa, H., Burdon, T., Chambers, I. and Smith, A. (1998). Self-renewal of pluripotent embryonic stem cells is mediated via activation of STAT3. *Genes Dev* **12**, 2048-60.

Niwa, H., Miyazaki, J. and Smith, A. G. (2000). Quantitative expression of Oct-3/4 defines differentiation, dedifferentiation or self-renewal of ES cells. *Nat Genet* **24**, 372-6.

Niwa, H., Ogawa, K., Shimosato, D. and Adachi, K. (2009). A parallel circuit of LIF signalling pathways maintains pluripotency of mouse ES cells. *Nature* **460**, 118-22.

Niwa, H., Toyooka, Y., Shimosato, D., Strumpf, D., Takahashi, K., Yagi, R. and Rossant, J. (2005). Interaction between Oct3/4 and Cdx2 determines trophectoderm differentiation. *Cell* **123**, 917-29.

Nolden, L., Edenhofer, F., Haupt, S., Koch, P., Wunderlich, F. T., Siemen, H. and Brustle, O. (2006). Site-specific recombination in human embryonic stem cells induced by cell-permeant Cre recombinase. *Nat Methods* **3**, 461-7.

Ogryzko, V. V., Hirai, T. H., Russanova, V. R., Barbie, D. A. and Howard, B. H. (1996). Human fibroblast commitment to a senescence-like state in response to histone deacetylase inhibitors is cell cycle dependent. *Mol Cell Biol* **16**, 5210-8.

Okabe, S., Forsberg-Nilsson, K., Spiro, A. C., Segal, M. and McKay, R. D. (1996). Development of neuronal precursor cells and functional postmitotic neurons from embryonic stem cells in vitro. *Mech Dev* **59**, 89-102.

Okamoto, K., Okazawa, H., Okuda, A., Sakai, M., Muramatsu, M. and Hamada, H. (1990). A novel octamer binding transcription factor is differentially expressed in mouse embryonic cells. *Cell* **60**, 461-72.

Okita, K., Ichisaka, T. and Yamanaka, S. (2007). Generation of germline-competent induced pluripotent stem cells. *Nature* **448**, 313-7.

Okumura-Nakanishi, S., Saito, M., Niwa, H. and Ishikawa, F. (2005). Oct-3/4 and Sox2 regulate Oct-3/4 gene in embryonic stem cells. *J Biol Chem* **280**, 5307-17.

Olsen, C. L., Gardie, B., Yaswen, P. and Stampfer, M. R. (2002). Raf-1-induced growth arrest in human mammary epithelial cells is p16-independent and is overcome in immortal cells during conversion. *Oncogene* **21**, 6328-39.

Opitz, O. G., Suliman, Y., Hahn, W. C., Harada, H., Blum, H. E. and Rustgi, A. K. (2001). Cyclin D1 overexpression and p53 inactivation immortalize primary oral keratinocytes by a telomerase-independent mechanism. *J Clin Invest* **108**, 725-32.

Palmieri, S. L., Peter, W., Hess, H. and Scholer, H. R. (1994). Oct-4 transcription factor is differentially expressed in the mouse embryo during establishment of the first two extraembryonic cell lineages involved in implantation. *Dev Biol* **166**, 259-67.

Pan, G. and Pei, D. (2005). The stem cell pluripotency factor NANOG activates transcription with two unusually potent subdomains at its C terminus. *J Biol Chem* **280**, 1401-7.

Pan, G. and Thomson, J. A. (2007). Nanog and transcriptional networks in embryonic stem cell pluripotency. *Cell Res* **17**, 42-9.

Pan, G. J. and Pei, D. Q. (2003). Identification of two distinct transactivation domains in the pluripotency sustaining factor nanog. *Cell Res* **13**, 499-502.

Papaioannou, V. and Rossant, J. (1977). The biology of embryogenesis. Cambridge: MIT Press.

Patsch, C. and Edenhofer, F. (2007). Conditional mutagenesis by cell-permeable proteins: potential, limitations and prospects. *Handb Exp Pharmacol*, 203-32.

Patsch, C., Peitz, M., Otte, D. M., Kesseler, D., Jungverdorben, J., Wunderlich, F. T., Brustle, O., Zimmer, A. and Edenhofer, F. (2010). Engineering Cell-Permeant FLP Recombinase for Tightly Controlled Inducible and Reversible Overexpression in Embryonic Stem Cells. *Stem Cells*.

Peitz, M. (2007). Untersuchungen zur Cre-Proteintransduktion in murine embryonale Stammzellen und Etablierung einer membranpermeablen Variante des Homeobox-Proteins Nanog zur Modulation von Stammzelleigenschaften. In *Institute of Reconstructive Neurobiology*, vol. PhD (ed. Bonn: University of Bonn.

Peitz, M., Jager, R., Patsch, C., Jager, A., Egert, A., Schorle, H. and Edenhofer, F. (2007). Enhanced purification of cell-permeant Cre and germline transmission after transduction into mouse embryonic stem cells. *Genesis* **45**, 508-17.

Peitz, M., Pfannkuche, K., Rajewsky, K. and Edenhofer, F. (2002). Ability of the hydrophobic FGF and basic TAT peptides to promote cellular uptake of recombinant Cre recombinase: a tool for efficient genetic engineering of mammalian genomes. *Proc Natl Acad Sci U S A* **99**, 4489-94.

Pereira, L., Yi, F. and Merrill, B. J. (2006). Repression of Nanog gene transcription by Tcf3 limits embryonic stem cell self-renewal. *Mol Cell Biol* **26**, 7479-91.

Pesce, M. and Scholer, H. R. (2000). Oct-4: control of totipotency and germline determination. *Mol Reprod Dev* **55**, 452-7.

Pevny, L. H. and Lovell-Badge, R. (1997). Sox genes find their feet. *Curr Opin Genet Dev* **7**, 338-44.

Piestun, D., Kochupurakkal, B. S., Jacob-Hirsch, J., Zeligson, S., Koudritsky, M., Domany, E., Amariglio, N., Rechavi, G. and Givol, D. (2006). Nanog transforms NIH3T3 cells and targets cell-type restricted genes. *Biochem Biophys Res Commun* **343**, 279-85.

Polyak, K., Lee, M. H., Erdjument-Bromage, H., Koff, A., Roberts, J. M., Tempst, P. and Massague, J. (1994). Cloning of p27Kip1, a cyclin-dependent kinase inhibitor and a potential mediator of extracellular antimitogenic signals. *Cell* **78**, 59-66.

Ptaszek, L. M. and Cowan, C. A. (2009). Regulatory Networks in Stem Cells. Heidelberg: Humana Press.

Qi, X., Li, T. G., Hao, J., Hu, J., Wang, J., Simmons, H., Miura, S., Mishina, Y. and Zhao, G. Q. (2004). BMP4 supports self-renewal of embryonic stem cells by inhibiting mitogen-activated protein kinase pathways. *Proc Natl Acad Sci U S A* **101**, 6027-32.

Reubinoff, B. E., Itsykson, P., Turetsky, T., Pera, M. F., Reinhartz, E., Itzik, A. and Ben-Hur, T. (2001). Neural progenitors from human embryonic stem cells. *Nat Biotechnol* **19**, 1134-40.

Richard, J. P., Melikov, K., Vives, E., Ramos, C., Verbeure, B., Gait, M. J., Chernomordik, L. V. and Lebleu, B. (2003). Cell-penetrating peptides. A reevaluation of the mechanism of cellular uptake. *J Biol Chem* **278**, 585-90.

Rodda, D. J., Chew, J. L., Lim, L. H., Loh, Y. H., Wang, B., Ng, H. H. and Robson, P. (2005). Transcriptional regulation of nanog by OCT4 and SOX2. *J Biol Chem* **280**, 24731-7.

Rogan, E. M., Bryan, T. M., Hukku, B., Maclean, K., Chang, A. C., Moy, E. L., Englezou, A., Warneford, S. G., Dalla-Pozza, L. and Reddel, R. R. (1995). Alterations in p53 and p16INK4 expression and telomere length during spontaneous immortalization of Li-Fraumeni syndrome fibroblasts. *Mol Cell Biol* **15**, 4745-53.

Rosner, M. H., Vigano, M. A., Ozato, K., Timmons, P. M., Poirier, F., Rigby, P. W. and Staudt, L. M. (1990). A POU-domain transcription factor in early stem cells and germ cells of the mammalian embryo. *Nature* **345**, 686-92.

Rossant, J. and Tam, P. P. (2009). Blastocyst lineage formation, early embryonic asymmetries and axis patterning in the mouse. *Development* **136**, 701-13.

Rubin, S. M., Gall, A. L., Zheng, N. and Pavletich, N. P. (2005). Structure of the Rb C-terminal domain bound to E2F1-DP1: a mechanism for phosphorylation-induced E2F release. *Cell* **123**, 1093-106.

Sa, G., Guo, Y. and Stacey, D. W. (2005). The regulation of S phase initiation by p27Kip1 in NIH3T3 cells. *Cell Cycle* **4**, 618-27.

Sadowski, I., Ma, J., Triezenberg, S. and Ptashne, M. (1988). GAL4-VP16 is an unusually potent transcriptional activator. *Nature* **335**, 563-4.

Scholer, H. R., Ruppert, S., Suzuki, N., Chowdhury, K. and Gruss, P. (1990). New type of POU domain in germ line-specific protein Oct-4. *Nature* **344**, 435-9.

Serrano, M., Lin, A. W., McCurrach, M. E., Beach, D. and Lowe, S. W. (1997). Oncogenic ras provokes premature cell senescence associated with accumulation of p53 and p16INK4a. *Cell* **88**, 593-602.

Shelton, D. N., Chang, E., Whittier, P. S., Choi, D. and Funk, W. D. (1999). Microarray analysis of replicative senescence. *Curr Biol* **9**, 939-45.

Shi, W., Wang, H., Pan, G., Geng, Y., Guo, Y. and Pei, D. (2006). Regulation of the pluripotency marker Rex-1 by Nanog and Sox2. *J Biol Chem* **281**, 23319-25.

Shi, Y., Desponts, C., Do, J. T., Hahm, H. S., Scholer, H. R. and Ding, S. (2008). Induction of pluripotent stem cells from mouse embryonic fibroblasts by Oct4 and Klf4 with small-molecule compounds. *Cell Stem Cell* **3**, 568-74.

Silva, J., Chambers, I., Pollard, S. and Smith, A. (2006). Nanog promotes transfer of pluripotency after cell fusion. *Nature* **441**, 997-1001.

Silva, J., Nichols, J., Theunissen, T. W., Guo, G., van Oosten, A. L., Barrandon, O., Wray, J., Yamanaka, S., Chambers, I. and Smith, A. (2009). Nanog is the gateway to the pluripotent ground state. *Cell* **138**, 722-37.

Singh, A. M., Hamazaki, T., Hankowski, K. E. and Terada, N. (2007). A heterogeneous expression pattern for Nanog in embryonic stem cells. *Stem Cells* **25**, 2534-42.

Sipe, J. D. (2002). Tissue engineering and reparative medicine. *Ann N Y Acad Sci* **961**, 1-9.

Smith, A. G., Heath, J. K., Donaldson, D. D., Wong, G. G., Moreau, J., Stahl, M. and Rogers, D. (1988). Inhibition of pluripotential embryonic stem cell differentiation by purified polypeptides. *Nature* **336**, 688-90.

Soldner, F., Hockemeyer, D., Beard, C., Gao, Q., Bell, G. W., Cook, E. G., Hargus, G., Blak, A., Cooper, O., Mitalipova, M. et al. (2009). Parkinson's disease patient-derived induced pluripotent stem cells free of viral reprogramming factors. *Cell* **136**, 964-77.

Soria, B. (2001). In-vitro differentiation of pancreatic beta-cells. *Differentiation* **68**, 205-19.

Sridharan, R., Tchieu, J., Mason, M. J., Yachechko, R., Kuoy, E., Horvath, S., Zhou, Q. and Plath, K. (2009). Role of the murine reprogramming factors in the induction of pluripotency. *Cell* **136**, 364-77.

Stadtfeld, M., Maherali, N., Breault, D. T. and Hochedlinger, K. (2008a). Defining molecular cornerstones during fibroblast to iPS cell reprogramming in mouse. *Cell Stem Cell* **2**, 230-40.

Stadtfeld, M., Nagaya, M., Utikal, J., Weir, G. and Hochedlinger, K. (2008b). Induced pluripotent stem cells generated without viral integration. *Science* **322**, 945-9.

Suda, Y., Suzuki, M., Ikawa, Y. and Aizawa, S. (1987). Mouse embryonic stem cells exhibit indefinite proliferative potential. *J Cell Physiol* **133**, 197-201.

Susaki, E., Nakayama, K. and Nakayama, K. I. (2007). Cyclin D2 translocates p27 out of the nucleus and promotes its degradation at the G0-G1 transition. *Mol Cell Biol* **27**, 4626-40.

Suzuki, A., Raya, A., Kawakami, Y., Morita, M., Matsui, T., Nakashima, K., Gage, F. H., Rodriguez-Esteban, C. and Izpisua Belmonte, J. C. (2006). Nanog binds to Smad1 and blocks bone morphogenetic protein-induced differentiation of embryonic stem cells. *Proc Natl Acad Sci U S A* **103**, 10294-9.

Tada, M., Takahama, Y., Abe, K., Nakatsuji, N. and Tada, T. (2001). Nuclear reprogramming of somatic cells by in vitro hybridization with ES cells. *Curr Biol* **11**, 1553-8.

Tahara, H., Sato, E., Noda, A. and Ide, T. (1995). Increase in expression level of p21sdi1/cip1/waf1 with increasing division age in both normal and SV40-transformed human fibroblasts. *Oncogene* **10**, 835-40.

Takahashi, K., Tanabe, K., Ohnuki, M., Narita, M., Ichisaka, T., Tomoda, K. and Yamanaka, S. (2007). Induction of pluripotent stem cells from adult human fibroblasts by defined factors. *Cell* **131**, 861-72.

Takahashi, K. and Yamanaka, S. (2006). Induction of pluripotent stem cells from mouse embryonic and adult fibroblast cultures by defined factors. *Cell* **126**, 663-76.

Tepper, C. G., Seldin, M. F. and Mudryj, M. (2000). Fas-mediated apoptosis of proliferating, transiently growth-arrested, and senescent normal human fibroblasts. *Exp Cell Res* **260**, 9-19.

Tesar, P. J., Chenoweth, J. G., Brook, F. A., Davies, T. J., Evans, E. P., Mack, D. L., Gardner, R. L. and McKay, R. D. (2007). New cell lines from mouse epiblast share defining features with human embryonic stem cells. *Nature* **448**, 196-9.

Thomson, J. A., Itskovitz-Eldor, J., Shapiro, S. S., Waknitz, M. A., Swiergiel, J. J., Marshall, V. S. and Jones, J. M. (1998). Embryonic stem cell lines derived from human blastocysts. *Science* **282**, 1145-7.

Tokuzawa, Y., Kaiho, E., Maruyama, M., Takahashi, K., Mitsui, K., Maeda, M., Niwa, H. and Yamanaka, S. (2003). Fbx15 is a novel target of Oct3/4 but is dispensable for embryonic stem cell self-renewal and mouse development. *Mol Cell Biol* **23**, 2699-708.

Tomioka, M., Nishimoto, M., Miyagi, S., Katayanagi, T., Fukui, N., Niwa, H., Muramatsu, M. and Okuda, A. (2002). Identification of Sox-2 regulatory region which is under the control of Oct-3/4-Sox-2 complex. *Nucleic Acids Res* **30**, 3202-13.

Torres, J. and Watt, F. M. (2008). Nanog maintains pluripotency of mouse embryonic stem cells by inhibiting NFkappaB and cooperating with Stat3. *Nat Cell Biol* **10**, 194-201.

Toyoshima, H. and Hunter, T. (1994). p27, a novel inhibitor of G1 cyclin-Cdk protein kinase activity, is related to p21. *Cell* **78**, 67-74.

Triezenberg, S. J., Kingsbury, R. C. and McKnight, S. L. (1988). Functional dissection of VP16, the trans-activator of herpes simplex virus immediate early gene expression. *Genes Dev* **2**, 718-29.

Trougakos, I. P., Saridaki, A., Panayotou, G. and Gonos, E. S. (2006). Identification of differentially expressed proteins in senescent human embryonic fibroblasts. *Mech Ageing Dev* **127**, 88-92.

Tunnemann, G., Martin, R. M., Haupt, S., Patsch, C., Edenhofer, F. and Cardoso, M. C. (2006). Cargo-dependent mode of uptake and bioavailability of TAT-containing proteins and peptides in living cells. *FASEB J* **20**, 1775-84.

Tyagi, M., Rusnati, M., Presta, M. and Giacca, M. (2001). Internalization of HIV-1 tat requires cell surface heparan sulfate proteoglycans. *J Biol Chem* **276**, 3254-61.

Uchikawa, M., Kamachi, Y. and Kondoh, H. (1999). Two distinct subgroups of Group B Sox genes for transcriptional activators and repressors: their expression during embryonic organogenesis of the chicken. *Mech Dev* **84**, 103-20.

Utikal, J., Polo, J. M., Stadtfeld, M., Maherali, N., Kulalert, W., Walsh, R. M., Khalil, A., Rheinwald, J. G. and Hochedlinger, K. (2009). Immortalization eliminates a roadblock during cellular reprogramming into iPS cells. *Nature* **460**, 1145-8.

Uwanogho, D., Rex, M., Cartwright, E. J., Pearl, G., Healy, C., Scotting, P. J. and Sharpe, P. T. (1995). Embryonic expression of the chicken Sox2, Sox3 and Sox11 genes suggests an interactive role in neuronal development. *Mech Dev* **49**, 23-36.

Vallier, L., Alexander, M. and Pedersen, R. A. (2005). Activin/Nodal and FGF pathways cooperate to maintain pluripotency of human embryonic stem cells. *J Cell Sci* **118**, 4495-509.

Vallier, L., Mendjan, S., Brown, S., Chng, Z., Teo, A., Smithers, L. E., Trotter, M. W., Cho, C. H., Martinez, A., Rugg-Gunn, P. et al. (2009). Activin/Nodal signalling maintains pluripotency by controlling Nanog expression. *Development* **136**, 1339-49.

Vernallis, A. B., Hudson, K. R. and Heath, J. K. (1997). An antagonist for the leukemia inhibitory factor receptor inhibits leukemia inhibitory factor, cardiotrophin-1, ciliary neurotrophic factor, and oncostatin M. *J Biol Chem* **272**, 26947-52.

Wadia, J. S., Stan, R. V. and Dowdy, S. F. (2004). Transducible TAT-HA fusogenic peptide enhances escape of TAT-fusion proteins after lipid raft macropinocytosis. *Nat Med* **10**, 310-5.

Wakayama, T., Perry, A. C., Zuccotti, M., Johnson, K. R. and Yanagimachi, R. (1998). Full-term development of mice from enucleated oocytes injected with cumulus cell nuclei. *Nature* **394**, 369-74.

Wang, H., Mannava, S., Grachtchouk, V., Zhuang, D., Soengas, M. S., Gudkov, A. V., Prochownik, E. V. and Nikiforov, M. A. (2008a). c-Myc depletion inhibits proliferation of human tumor cells at various stages of the cell cycle. *Oncogene* **27**, 1905-15.

Wang, J., Levasseur, D. N. and Orkin, S. H. (2008b). Requirement of Nanog dimerization for stem cell self-renewal and pluripotency. *Proc Natl Acad Sci U S A* **105**, 6326-31.

Wang, J., Rao, S., Chu, J., Shen, X., Levasseur, D. N., Theunissen, T. W. and Orkin, S. H. (2006). A protein interaction network for pluripotency of embryonic stem cells. *Nature* **444**, 364-8.

Wang, L., Schulz, T. C., Sherrer, E. S., Dauphin, D. S., Shin, S., Nelson, A. M., Ware, C. B., Zhan, M., Song, C. Z., Chen, X. et al. (2007). Self-renewal of human embryonic stem cells requires insulin-like growth factor-1 receptor and ERBB2 receptor signaling. *Blood* **110**, 4111-9.

Wegner, M. (1999). From head to toes: the multiple facets of Sox proteins. *Nucleic Acids Res* **27**, 1409-20.

Wender, P. A., Mitchell, D. J., Pattabiraman, K., Pelkey, E. T., Steinman, L. and Rothbard, J. B. (2000). The design, synthesis, and evaluation of molecules that enable or enhance cellular uptake: peptoid molecular transporters. *Proc Natl Acad Sci U S A* **97**, 13003-8.

West, M. D., Pereira-Smith, O. M. and Smith, J. R. (1989). Replicative senescence of human skin fibroblasts correlates with a loss of regulation and overexpression of collagenase activity. *Exp Cell Res* **184**, 138-47.

Whitaker, N. J., Bryan, T. M., Bonnefin, P., Chang, A. C., Musgrove, E. A., Braithwaite, A. W. and Reddel, R. R. (1995). Involvement of RB-1, p53, p16INK4 and telomerase in immortalisation of human cells. *Oncogene* **11**, 971-6.

Wiles, M. V. and Keller, G. (1991). Multiple hematopoietic lineages develop from embryonic stem (ES) cells in culture. *Development* **111**, 259-67.

Williams, R. L., Hilton, D. J., Pease, S., Willson, T. A., Stewart, C. L., Gearing, D. P., Wagner, E. F., Metcalf, D., Nicola, N. A. and Gough, N. M. (1988). Myeloid leukaemia inhibitory factor maintains the developmental potential of embryonic stem cells. *Nature* **336**, 684-7.

Wilmut, I., Schnieke, A. E., McWhir, J., Kind, A. J. and Campbell, K. H. (1997). Viable offspring derived from fetal and adult mammalian cells. *Nature* **385**, 810-3.

Winnemöller, D. (2007). Untersuchungen zur Aktivität des Stammzellfaktors Nanog in embryonalen Stammzellen und somatischen Zellen. In *Institute of Reconstructive Neurobiology*, vol. PhD (ed. Bonn: University of Bonn.

Wobus, A. M., Guan, K., Yang, H. T. and Boheler, K. R. (2002). Embryonic stem cells as a model to study cardiac, skeletal muscle, and vascular smooth muscle cell differentiation. *Methods Mol Biol* **185**, 127-56.

Woltjen, K., Michael, I. P., Mohseni, P., Desai, R., Mileikovsky, M., Hamalainen, R., Cowling, R., Wang, W., Liu, P., Gertsenstein, M. et al. (2009). piggyBac transposition reprograms fibroblasts to induced pluripotent stem cells. *Nature* **458**, 766-70.

Wood, H. B. and Episkopou, V. (1999). Comparative expression of the mouse Sox1, Sox2 and Sox3 genes from pre-gastrulation to early somite stages. *Mech Dev* **86**, 197-201.

Wu, Q., Chen, X., Zhang, J., Loh, Y. H., Low, T. Y., Zhang, W., Sze, S. K., Lim, B. and Ng, H. H. (2006). Sall4 interacts with Nanog and co-occupies Nanog genomic sites in embryonic stem cells. *J Biol Chem* **281**, 24090-4.

Xu, R. H., Chen, X., Li, D. S., Li, R., Addicks, G. C., Glennon, C., Zwaka, T. P. and Thomson, J. A. (2002). BMP4 initiates human embryonic stem cell differentiation to trophoblast. *Nat Biotechnol* **20**, 1261-4.

Xu, R. H., Sampsell-Barron, T. L., Gu, F., Root, S., Peck, R. M., Pan, G., Yu, J., Antosiewicz-Bourget, J., Tian, S., Stewart, R. et al. (2008). NANOG is a direct target of TGFbeta/activin-mediated SMAD signaling in human ESCs. *Cell Stem Cell* **3**, 196-206.

Yeom, Y. I., Fuhrmann, G., Ovitt, C. E., Brehm, A., Ohbo, K., Gross, M., Hubner, K. and Scholer, H. R. (1996). Germline regulatory element of Oct-4 specific for the totipotent cycle of embryonal cells. *Development* **122**, 881-94.

Ying, Q. L., Nichols, J., Chambers, I. and Smith, A. (2003a). BMP induction of Id proteins suppresses differentiation and sustains embryonic stem cell self-renewal in collaboration with STAT3. *Cell* **115**, 281-92.

Ying, Q. L., Nichols, J., Evans, E. P. and Smith, A. G. (2002). Changing potency by spontaneous fusion. *Nature* **416**, 545-8.

Ying, Q. L., Stavridis, M., Griffiths, D., Li, M. and Smith, A. (2003b). Conversion of embryonic stem cells into neuroectodermal precursors in adherent monoculture. *Nat Biotechnol* **21**, 183-6.

Ying, Q. L., Wray, J., Nichols, J., Batlle-Morera, L., Doble, B., Woodgett, J., Cohen, P. and Smith, A. (2008). The ground state of embryonic stem cell self-renewal. *Nature* **453**, 519-23.

Yoon, I. K., Kim, H. K., Kim, Y. K., Song, I. H., Kim, W., Kim, S., Baek, S. H., Kim, J. H. and Kim, J. R. (2004). Exploration of replicative senescence-associated genes in human dermal fibroblasts by cDNA microarray technology. *Exp Gerontol* **39**, 1369-78.

Yoshida, Y., Takahashi, K., Okita, K., Ichisaka, T. and Yamanaka, S. (2009). Hypoxia enhances the generation of induced pluripotent stem cells. *Cell Stem Cell* **5**, 237-41.

Yu, J., Hu, K., Smuga-Otto, K., Tian, S., Stewart, R., Slukvin, II and Thomson, J. A. (2009). Human induced pluripotent stem cells free of vector and transgene sequences. *Science* **324**, 797-801.

Yu, J., Vodyanik, M. A., Smuga-Otto, K., Antosiewicz-Bourget, J., Frane, J. L., Tian, S., Nie, J., Jonsdottir, G. A., Ruotti, V., Stewart, R. et al. (2007). Induced pluripotent stem cell lines derived from human somatic cells. *Science* **318**, 1917-20.

Yuan, H., Corbi, N., Basilico, C. and Dailey, L. (1995). Developmental-specific activity of the FGF-4 enhancer requires the synergistic action of Sox2 and Oct-3. *Genes Dev* **9**, 2635-45.

Zappone, M. V., Galli, R., Catena, R., Meani, N., De Biasi, S., Mattei, E., Tiveron, C., Vescovi, A. L., Lovell-Badge, R., Ottolenghi, S. et al. (2000). Sox2 regulatory sequences direct expression of a (beta)-geo transgene to telencephalic neural stem cells and precursors of the mouse embryo, revealing regionalization of gene expression in CNS stem cells. *Development* **127**, 2367-82.

Zhang, J., Wang, X., Chen, B., Suo, G., Zhao, Y., Duan, Z. and Dai, J. (2005). Expression of Nanog gene promotes NIH3T3 cell proliferation. *Biochem Biophys Res Commun* **338**, 1098-102.

Zhang, S. C., Wernig, M., Duncan, I. D., Brustle, O. and Thomson, J. A. (2001). In vitro differentiation of transplantable neural precursors from human embryonic stem cells. *Nat Biotechnol* **19**, 1129-33.

Zhang, X., Neganova, I., Przyborski, S., Yang, C., Cooke, M., Atkinson, S. P., Anyfantis, G., Fenyk, S., Keith, W. N., Hoare, S. F. et al. (2009). A role for NANOG in G1 to S transition in human embryonic stem cells through direct binding of CDK6 and CDC25A. *J Cell Biol* **184**, 67-82.

Zhang, Y. B., Howitt, J., McCorkle, S., Lawrence, P., Springer, K. and Freimuth, P. (2004). Protein aggregation during overexpression limited by peptide extensions with large net negative charge. *Protein Expr Purif* **36**, 207-16.

Zhao, Y., Benita, Y., Lok, M., Kuipers, B., van der Ley, P., Jiskoot, W., Hennink, W. E., Crommelin, D. J. and Oosting, R. S. (2005). Multi-antigen immunization using IgG binding domain ZZ as carrier. *Vaccine* **23**, 5082-90.

Zhou, H., Wu, S., Joo, J. Y., Zhu, S., Han, D. W., Lin, T., Trauger, S., Bien, G., Yao, S., Zhu, Y. et al. (2009). Generation of induced pluripotent stem cells using recombinant proteins. *Cell Stem Cell* **4**, 381-4.

Zhu, J., Woods, D., McMahon, M. and Bishop, J. M. (1998). Senescence of human fibroblasts induced by oncogenic Raf. *Genes Dev* **12**, 2997-3007.

Zhuang, D., Mannava, S., Grachtchouk, V., Tang, W. H., Patil, S., Wawrzyniak, J. A., Berman, A. E., Giordano, T. J., Prochownik, E. V., Soengas, M. S. et al. (2008). C-MYC overexpression is required for continuous suppression of oncogene-induced senescence in melanoma cells. *Oncogene* **27**, 6623-34.